IMPROVED PROPAGATION LOSS PREDICTION FOR LAND MOBILE RADIO COMMUNICATIONS

JING CHEN

IMPROVED PROPAGATION LOSS PREDICTION FOR LAND MOBILE RADIO COMMUNICATIONS

By

© Jing Chen

A thesis submitted to the School of Graduate Studies

in partial fulfillment of the requirements for the degree of

Master of Engineering

Faculty of Engineering and Applied Science

Memorial University of Newfoundland

July, 1993

St. John's Newfoundland Canada

ISBN 0-315-86649-7

Canada

Abstract

In land mobile radio communications, it is well known that almost 95% of the radio links between transmitter and receiver are non-line-of-sight. The propagation loss between transmitter and receiver is heavily dependent on the terrain features. Hence, this thesis examines and improves the CRC propagation loss prediction in two main aspects.

One is to create a higher resolution and more accurate digital terrain data base based on the CRC data base. The developed procedure is as follows. For a given area of interest first the complete quadratic two-dimensional interpolation for elevations and the weighted vote method for surface codes are applied to augment the CRC data base from 500 meters spacing to 100 meters spacing. If the contour from the augmented data base is not checked with the topographic map, then the data of missed critical terrain features are taken directly from the topographic map and are used to correct the augmented data base. In this step, the triangular interpolation scheme is introduced to modify the elevations, and the weighted vote method is used to modify the surface codes. There are eight surface codes which indicate tree, bare ground, fresh water, suburban, marsh, seawater, urban core and unknown type. As the result of the modified data base, the evaluations of diffraction, reflection, tropospheric scattering, urban, and season losses are more accurate. Thus, the total propagation loss prediction is greatly improved.

As another major work in this thesis, the modified diffraction loss prediction model is proposed. It involves: (a) for the implementation of the de Assis method, the radius of curvature of rounded obstacles' crest is determined by least-squares

parabolic fitting; (b) the Deygout correction factor is first applied to deal with multiple rounded obstacles which are close to each other; (c) based on the availability of much more detailed information from the modified data base, all the defineable obstacles in a path profile are taken into account in the diffration loss prediction.

It is shown that our propagation loss prediction results are close to CRC results when the terrain is smooth; but in the irregular terrain, our results provide a substantial improvement.

Acknowledgements

I would like to express my deepest gratitude to my supervisor Dr. S. LeNgoc, for all his guidance, advice and assistance during the course of my graduate studies and the writing up of the thesis.

I am very much thankful to Novacom Inc. for providing their financial support and CRC computer program prediction system.

The financial support by Natural Sciences and Engineering Research Council of Canada, and by the Faculty of Engineering is gratefully acknowledged.

The last but not least, I would like to thank Mr. Ping Zhou for providing helpful discussions.

Contents

List of Figures

Chapter 1

Introduction

1.1 Statement of the Problem

Propagation loss prediction is the central problem in the planning of mobile radio services. It is also a very important aspect of the design and development of mobile radio systems and networks. The applications of propagation loss prediction include site selection of base station for the optimum signal coverage, or the prediction of cell sizes for cellular radio systems, finding the locations of possible radio drop-out (dead) zones, examining system performance as a function of transmitter power, receiver sensitivity, antenna types and heights, etc.

The propagation loss, or the transmission loss in communication systems, is the total reduction in the radiant power density which propagates from transmitting antenna to an equivalent loss-free receiving antenna. The transmission loss is affected by many factors such as operating frequency, distance between transmitter and receiver, antenna heights, curvature of the earth, atmospheric conditions, and specially for land mobile systems, the terrain features as hills, trees, buildings. In land mobile frequency bands propagation except in the local environment of receiver can be described by several modes as free space propagation, reflection from

the surface of the earth, diffractions over a smooth earth and over irregular terrain and man-made obstacles, refraction of the atmosphere, troposphere scattering, and superrefraction and ducting in coastal areas. These propagation effects result in the received signal with slow amplitude variations along the transmission path, referred to as slow fading. Within local environment of receiver, since the mobile antenna is located close to the ground and is usually in motion, most of the received signals are reflected from surrounding objects by multipath propagation. A small change in the location of the mobile antenna and /or any change in the surrounding environment can cause a large change in the received signal. This kind of rapid and large amplitude fluctuations is referred to as fast fading. Based on measurements, slow fading is found to be log normal distribution. The median value of this distribution is defined as median transmission loss, and the standard deviation of this distribution is called location variability which represents a specified environment.

Propagation loss prediction is the prediction of median transmission loss. Some prediction methods also include location variability evaluation. In land mobile radio communications median transmission loss, referred as propagation loss in this thesis, mainly consists of free space loss, diffraction loss, reflection loss, tropospheric scattering loss, urban loss, clutter loss, and season loss. Propagation loss is heavily dependent on the terrain features. There are basically two methods to predict propagation loss. One is empirical; the other is an analytical method. More recently, computer program prediction systems which combine analytical and empirical models have come into use. The Communications Research Centre (CRC) has developed the computer program prediction system which employs a digital terrain data base to provide terrain information.

The use of the CRC computer program prediction system in some cases does not provide desirable prediction results. One of the main factors accounting for this disagreement between prediction and experiments is that the path profiles from CRC data base are not close to the actual situations. Since CRC terrain data base has every point 500 m apart, it is always possible to miss some important terrain features. On the other hand, building a high resolution and accurate terrain data base by hand-scaling the large scale topographic maps is a very exhausting and time-consuming task. Therefore, the problem of obtaining a satisfactory data base at minimum effort still requires solution.

Since almost 95% of the mobile radio links between the transmitter and receiver is non-line-of-sight, diffraction is one of the major mechanisms in the propagation. It stands to reason that any effort made in the improvement of diffraction loss evaluation will result in more accurate prediction of propagation loss.

As the demand of mobile radio services increases rapidly such as in cellular radio systems, cell size is getting smaller and smaller to accommodate a large number of subscribers. This situation has made necessary a parallel development of more accurate and practical techniques for the propagation loss prediction.

1.2 Literature Review

In the area of propagation loss prediction, a variety of theoretically or experimentally based models have been developed since 1930's. Most of them are not specifically for application to land mobile channel and more in general perspective. As in land mobile radio communications, terrain features are the main parameter to the propagation loss prediction, a number of models reported in the literature

will be reviewed with emphasis on the degree to which they account for terrain characteristics, as regular or irregular terrain; urban, suburban, or open areas; or, hills, trees, buildings.

The basic theoretical model is the free space model which predicts propagation loss due to radial spreading in an ideal region without boundaries [1]. It is the function of the distance between transmitter and receiver, and the operating frequency. It is normally used as a reference for losses caused by various other propagation mechanisms.

In 1937, the plane earth model was derived [2] to give the median transmission loss as the function of distance, frequency, and antenna heights of transmitter and receiver. This model treats the earth as a plane surface with finite conductivity, and it does not include any effects of terrain features. In 1957, J. Egli applied this plane earth model with adding 'terrain factor' which is obtained from empirical formulas [3]. This terrain factor considers only quasismooth terrain and statistically uniform hilly terrain, and it does not distinguish rural or urban areas. In 1970, J.P. Murphy gave median transmission loss by summing the plane earth loss and median terrain factor [4]. He used empirical data from the plains and mountains of Colorado which is applicable for rural areas. It also does not apply to irregular hilly terrain. In 1977, still based on the plane earth model, K. Allsebrook and J.D. Parsons developed a model specifically for urban environments using data from three British cities [5]. This model can be continuously adjusted to take into account the losses due to buildings. It can also apply to statistically irregular hilly urban areas.

While the above models were developed by combining the plane earth model with empirical formulas of terrain factor, Y. Okumura gave the prediction curves

completely based on the extensive measurements made in Tokyo and surrounding suburbs in 1968 [6]. This prediction is specially for land mobile systems. In 1980, M. Hata added to Okumura's original work by deriving easily used formulas [7]. In this model, median field strength is given in function of frequency, distance, antenna heights of the base station and mobile station, and four types of regions as open area, suburban area, medium-small city, and large city. The definitions of environmental types are valid only for the buildings in Tokyo. This model became one of the most commonly used models and is more suitable for urban area. However, it does not take into account the diffraction loss due to irregular terrain.

For irregular terrain, one of the main problems is how to deal with the diffraction over the obstacles. From his publications in 1947 [8] and in 1977 [9], K. Bullington analytically dealt the smooth curved earth with three idealized types of terrain such as no obstruction, a single sharp ridge, and multiple hills. He treated hills which are well separated and of irregular height based on an approximate solution of diffraction over two knife edges. He replaced the terrain profile by an equivalent single knife-edge. This method seriously oversimplifies the situation when large numbers of hills are involved, and is not satisfactory for two or more nearby hills of relatively uniform height. In 1963, K. Furutsu gave the formulation in terms of an integral equation for diffraction past an arbitrary sequence of smooth rounded obstacles [10]. However, this formulation does not lend itself to numerical evaluation except for few special cases. Explicit solution for double knife-edge diffraction was given by G. Millington in terms of a double Fresnel integral that was evaluated using geometrical arguments [11]. For an arbitrary number of knife-edges, S.W. Lee achieved analytical solutions for the special case when transmitter, receiver, and

edges all lie in a common plane by using path integral methods [12]. J.H. Whitteker attempted to give a ray representation for multiple knife-edge diffraction in terms of a single modified line source above the preceding diffracting edge [13]. However, this simple ray model is only valid for a few edges. The problem of evaluating diffraction by irregular terrain is still required to be solved.

For propagation loss prediction, one of the most popular methods is Longley and Rice method. This method, as a form of computer program, gives long-term median transmission loss over irregular terrain. The computer programs have been revised several times from 1968 to 1985, and many modifications have been made [14], [15]. This method requires a series of input parameters as: frequency, polarization, path length, antenna heights above ground, surface refractivity, effective earth's radius, climate, ground conductivity and dielectric constant. It also requires detailed terrain profile in order to obtain other input parameters, such as effective antenna heights, horizon distances of the antennas, horizon elevation angles, the angular distance for a transhorizon path, and terrain irregularity of the path. The programs have two distinct parts, one is the prediction of median transmission loss, the other the prediction of signal variabilities. In median transmission loss prediction, it has the results which agree with Bullington model in line-of-sight mode and diffraction mode [16]. For diffraction by a knife-edge obstacle, however, it does not take into account the attenuation when the obstacle penetrates the first Fresnel zone below the central ray between the transmit and receive antennas. This is a deficiency since mobile propagation usually has first Fresnel zone penetration near the receiver. In signal variability prediction, A.G. Longley developed equations of location variability as a function of wavelength and the terrain irregularity

parameter [17]. The variabilities also depend upon the effective transmitting and receiving elevations. Longley-Rice computer programs include digital terrain data bases which have considerable effects on the accuracy of the predictions. Since the predictions are sensitive to the effective antenna height of the receiver which is determined from the ground elevation of the receiver, any small change in the surrounding terrain of the receiver causes sizeable change in median transmission loss. Also, small changes in terrain elevations near receiver may intercept the central ray between transmitter and receiver, so that cause a considerable change in median transmission loss. In addition to these effects, depending upon the accuracy of the digital terrain information used, whether an obstacle is present or absent may often be due to data base factors rather than due to actual physical situations. Moreover, in relatively smooth terrain area, large variations in signal variability may be because of digital data base factor.

There is another popular prediction method known as the terrain integrated rough earth model (TIREM) [18]. This computer program has several versions developed from 1983 to 1987. The method requires detailed terrain profile for a series of basic parameters as effective antenna heights, radio horizon distance, path angular distance, etc..., so that it also includes digital data bases. It has different definition of effective antenna height from that of Longley-Rice model, but has the same way for determining terrain irregularity. TIREM contains three modes for line-of-sight paths and nine modes for non-line-of-sight paths. It predicts median transmission loss using Longley-Reasoner empirical equation [19], or Longley-Rice method or weighted combination of these two, based on different frequency ranges. One problem with this model is that, for line-of-sight paths, it predicts a sizeable

region wherein changes of the transmitter height have no effect on the transmission loss. Another problem is that the Longley-Reasoner equation has very little dependance on path length. This does not agree with the results predicted by Bullington model and that measured by Okumura, because the equation is primarily for point-to-point communication paths. Since median transmission loss is dependent primarily on the effective receiver height, the method for determining this parameter has significant effect on the results. The method used in TIREM for determining this parameter is different from that in Longley-Rice model, so that the results are also different.

According to the comparison of prediction methods made by J.F. Aurand and R.E. Post [20], CRC (Communications Research Centre) method is the most accurate one, based on the degree to which one accounts for terrain characteristics. This method is the basis of the research work in this thesis. CRC method is in the form of a computer program system with digital terrain data base which covers most parts of Canada. It has been revised several times from 1981 to 1990 [21], [22]. This method includes two main models: a detailed model which is used when evaluating detailed terrain profiles, and irregular terrain model when only general features of the terrain are available. The detailed model consists of free space loss, diffraction loss or reflection loss, urban loss, tropospheric loss, clutter loss, and time variability. The irregular terrain model is Longley-Rice method reported in 1968, with adding clutter loss and time variability. The clutter loss takes into account buildings or trees which are close to either the transmitting or receiving antenna. Since this method uses the terrain profiles reconstructed from topographic data base, the problems about using digital terrain data base mentioned above also ex-

ist. Moreover, because CRC data base has every point 500 metres away from each other, important terrain features may be missed within this interval. This is one of the main factors which defeats the accuracy of prediction results. A modification by which more points are inserted in the data base, making elevation values more precice is very necessary.

As mobile communications are demanded more and more in high population areas, the treatment of buildings is one of the essential matters. In 1988, H.L. Betoni and J. Walfisch published one theoretical model for predicting the effect of buildings on the median transmission loss [23]. This model treats the buildings in urban and suburban areas with fairly uniform height and in rows with small separation between neighboring buildings. For the interior of multifloored buildings, in 1992 S.Y. Seidel and T.S. Rappaport provided experimentally based models to predict the effects of walls, office partitions, floors, and building layout on propagation loss at 914 MHz [24].

From literature reviewed, it is apparent that as personal and land mobile communications are increasing rapidly, the prediction of propagation loss is required to be more and more accurate. As the digital terrain data base is one of the important factors affecting the accuracy of propagation loss prediction, it is essential to have a more accurate terrain data base. More accurate calculations of diffraction loss, reflection loss, tropospherical scattering loss, and urban loss, etc., are also required for improving the prediction of median transmission loss.

1.3 Scope of the Work

In this thesis, various propagation modes related to land mobile radio communications and their loss models are reviewed. The propagation loss prediction is studied based on the CRC work. Since the digital terrain data base is the most important factor in determining the accuracy of propagation loss prediction, a major effort is devoted to obtain high resolution and accurate terrain data base and path profiles. A modification procedure to CRC terrain data base is developed which includes two steps. This modification employs complete quadratic interpolation, linear triangular interpolation, and weighted vote method. As diffraction mode is one of the main propagation modes, an effort is also made to improve diffraction loss evaluation in three aspects:

(i) determining the radius of curvature of obstacle's crest;

(ii) applying a new correction factor due to closeness of obstacles;

(iii) taking into account all the obstacles in a path profile.

By modifying CRC program system to accept the modified data base, to construct the path profiles, to evaluate all kinds of losses based on modified path profiles, and to implement the improved diffraction loss evaluation, the improved total propagation loss prediction is obtained.

1.4 Organization of the Thesis

This thesis is organized as follows:

Chapter 2 presents various propagation modes and their loss models, such as reflection loss, diffraction loss, tropospheric scattering loss, etc.

Chapter 3 briefly introduces CRC digital terrain data base, and describes in details the proposed procedure of the modification to the data base.

Chapter 4 describes the proposed modified diffraction loss prediction.

Chapter 5 contains a brief discussions of the total propagation loss prediction and the program flow charts. A number of the improved results are presented and compared with CRC results.

Chapter 6 gives the conclusion and the recommendations for future work.

Chapter 2

Propagation Loss Models

In land mobile radio communications, the propagation loss prediction involves the evaluations of free space loss, reflection loss from the earth surface, diffraction loss over irregular terrain, atmospheric refraction, tropospheric scattering loss, the losses due to terrain cover such as trees and buildings, and median transmission loss variation with time and location. In the following sections, these propagation losses will be briefly discussed with emphasis on the diffraction loss.

2.1 Free Space Loss

Models for radio propagation all begin with the concept of two point source antennas in free space separated by a distance d. Radiated from transmitter point antenna with source power P_t, the radio wave energy spreads out uniformly in all directions and the power at receiver point source antenna will be

$$P_r = A\frac{P_t}{4\pi d^2} \tag{2.1}$$

where A is the effective aperture of receiver point antenna and is expressed as

$$A = \frac{\lambda^2}{4\pi}, \tag{2.2}$$

λ is the wavelength of the operating signal.

The free space loss factor l_f is defined as:

$$l_f = \frac{P_t}{P_r} = (\frac{4\pi d}{\lambda})^2. \tag{2.3}$$

Usually the free space loss is presented in the logarithmic form:

$$L_f = 20\log(\frac{4\pi d}{\lambda}). \tag{2.4}$$

For convenience, L_f is also expressed by:

$$L_f = 32.45 + 20\log f(MHz) + 20\log d(Km) \tag{2.5}$$

where f is the operating frequency.

Generally, free space conditions can be deemed to prevail if the path between transmitter and receiver has no reflections from the surface of the earth or from hills, trees, buildings, etc, and no blocking, refraction, diffraction and absorption. These conditions are rarely encountered in land mobile communications; however, free space loss is used as reference for various other propagation losses.

2.2 Atmospheric Refraction

Radio wave signals radiated at angles above the horizon may be bent around the curvature of the earth and received at distances beyond the normal horizon, this phenomenon is known as atmospheric refraction. The amount of bending varies with atmospheric conditions such as temperature, pressure, and moisture content of the air. For describing the refraction of the atmosphere, the refractive index n is defined as the ratio of the radio wave speed in a vacuum to that in the atmosphere.

It can be measured directly with a refractormeter. For computational purpose, radio refractivity N_s is defined as

$$N_s = (n-1) * 10^6. \tag{2.6}$$

It can also be obtained from measured values of the physical parameters by [25]:

$$N_s = 77.6(\frac{C}{T}) + 3.73 * 10^5(\frac{e}{T^2}) \tag{2.7}$$

where C is the total atmospheric pressure in millibars, e is the partial pressure of water vapor in millibars, and T is the absolute temperature in degrees Kelvin. At the surface of the earth the radio refractivity is an average of about $N_s = 301$ and about 260 at 1 Km above the surface in temperate climates.

The effect of atmospheric refraction is taken into account by the effective earth radius which is the multiplication of the actual earth radius and the equivalent earth radius factor K. The K factor corresponding to an atmosphere with a linear gradient of refractive index dn/dh can be calculated from

$$K = \frac{1}{1 + \frac{a}{n} * \frac{dn}{dh}} \tag{2.8}$$

where a is the true radius of the earth, and dn/dh is the gradient of n with respect to height in the portion of the atmosphere affecting the radio path. The effective earth radius R_e can be obtained by $R_e = K * a$, or

$$\frac{1}{R_e} = \frac{1}{a} + \frac{\frac{dn}{dh}}{n}. \tag{2.9}$$

The propagation loss evaluations in the following sections are all based on the effective earth radius. By using this concept to draw path profiles, ray paths can be represented as straight lines, greatly simplifying ray tracing procedures. The

only restriction for using straight lines is that heights above the surface must be small compared with the earth's radius.

Since the equivalent earth radius factor K expresses the degree and direction of ray bending, any change in the atmosphere condition will cause a change in K and then the effective earth radius. The atmosphere conditions change in hours and seasons; however during the daytime hours from 1 or 2 hours after sunrise to 1 or 2 hours before sunset and during normal weather conditions, the refractive effect does not usually vary much in most areas. This condition is often referred to as standard and K=4/3. The peak values of K are usually higher in summer than in winter, while the least values are the same for both summer and winter. In practice, the best guide for the choice of K values is based on past history and experience in the field.

2.3 Reflections from the Earth Surface

In the prediction of propagation loss at land mobile frequency bands, one of the effects that may be taken into consideration is the reflection of radio waves from the ocean, lakes, or flat ground. At the point of reception, the reflected wave and the direct wave combine, and the resulting field strength depends on the amplitude of the reflected wave and on its phase relative to that of the direct wave. The method for finding the point of reflection from a spherical earth, obtaining the reflection coefficient and reflection loss will be described in the following subsections.

2.3.1 Finding the Point of Reflection

To find the reflection point, first consider the condition that the point must satisfy. In Fig. 2.1, the antennas are at A_1 and A_2, P is any point chosen on the reflecting surface. The broken line represents the plane tangent at P. h_1 and h_2 are the heights of the antennas above the spherical earth, where h_1' and h_2' are their heights above the tangent plane. Respected to the tangent plane, the curved surface can be represented as:

$$y = -\frac{(x - x_1)^2}{2R_e} \tag{2.10}$$

where $|x - x_1| \ll R_e$ and R_e is the effective radius of the earth. Then h_1' is expressed by

$$h_1' = h_1 - \frac{x_1^2}{2R_e}. \tag{2.11}$$

The angle between the incident ray and the tangent plane is approximated as

$$\psi_1 = \frac{h_1'}{x_1} = \frac{h_1}{x_1} - \frac{x_1}{2R_e} \tag{2.12}$$

and similarly,

$$\psi_2 = \frac{h_2'}{x_2} = \frac{h_2}{x_2} - \frac{x_2}{2R_e} \tag{2.13}$$

The condition for point P to be the reflection point is

$$\Delta\psi = \psi_2 - \psi_1 = \frac{h_2}{x_2} - \frac{h_1}{x_1} - \frac{x_2 - x_1}{2R_e} = 0 \tag{2.14}$$

with the constraint that $x_1 + x_2 = d$, which is the total path length. By solving the equation above, x_1 or x_2 (i.e. the location of point P) can be found. However, this solution is based on the ideal reflecting surface. For a real transmission path,

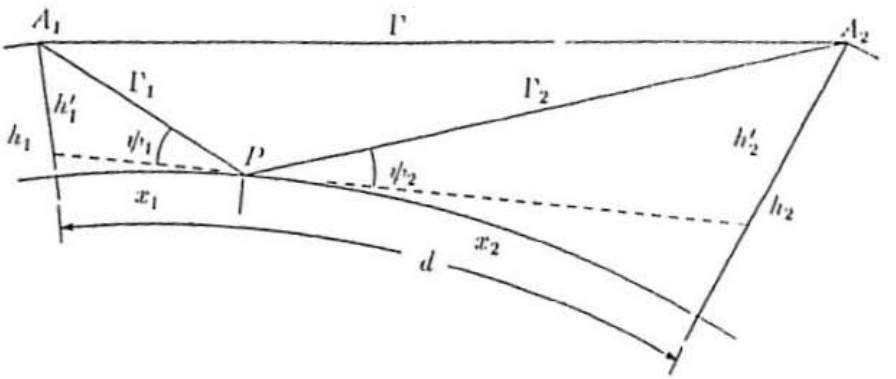

Figure 2.1: Reflection from a Spherical Earth

the treatment is using an average elevation over some part of the propagation path. Finding this region for average elevation will be discussed in the following.

To realize the portion of a path within which the point of reflection must exist, first consider some possible reflecting surfaces as shown in Fig. 2.2, where A_1 and A_2 are antennas separated in height by 200 m. For each surface the reflected ray is shown, and the broken line is the locus of all the reflection points. These surfaces are concentric about the centre of the earth, and to a sufficient approximation, they all have the same radius of curvature, the effective earth's radius. For each of these, the horizontal position of the point of reflection can be found. The diagrams show the locus of such points. The point of reflection is the point at which the path profile intersects this locus. The region which contains the point of reflection, is limited by the mid-point of the path, since the reflection must occur in the half of the path occupied by the lower antenna. The other limit is illustrated in Fig. 2.2, it is the point P_1 at which the direct ray is tangent to one of the hypothetical reflecting surfaces. The horizontal coordinate of this limit, measured from A_1, can be derived as:

$$x = \frac{d}{2} - \frac{R_e}{d} * (h_2 - h_1) \tag{2.15}$$

where d is the distance from one antenna to the other, h_1, h_2 are the heights of the antennas above sea level, and h_1 is the lower one. The portion of a path with these two limits is called initial region.

There is another fact must be considered: the specular reflection of waves does not take place at a point. Rather, it takes place, and requires a smooth surface, over a finite region for which ray path lengths do not vary by more than some fraction of a wavelength. If this fraction is $\lambda/2$, the region is known as the first

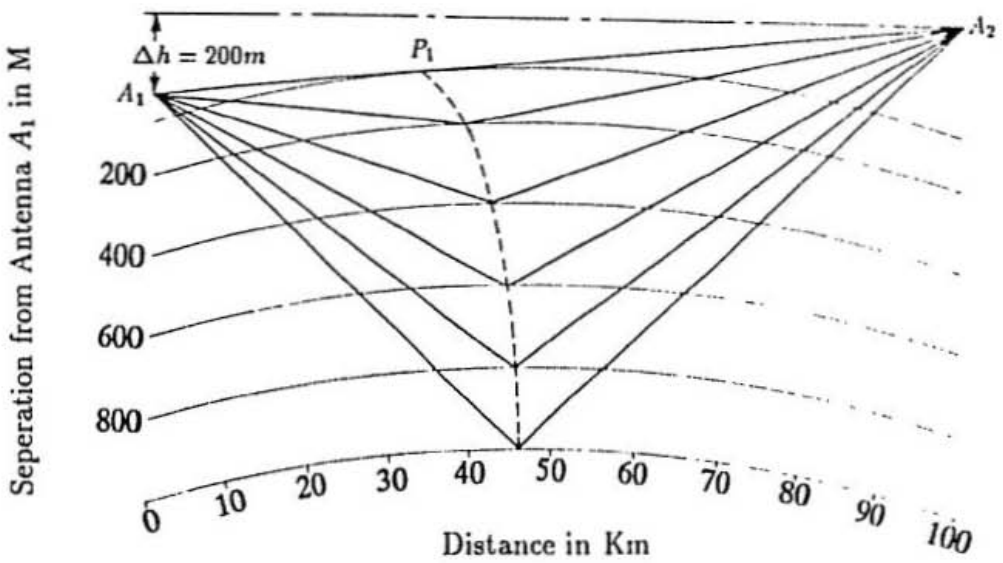

Figure 2.2: The locus of reflection points for a number of spherical reflecting surfaces

Fresnel zone. For low ray angles, the first Fresnel zone is much longer along the propagation path than perpendicular to it. Therefore, it is reasonable to suppose that a smooth surface extends for a sufficient distance perpendicular to the path, and to be concerned only about its extent along the path. It is concluded that the first Fresnel zone is unnecessarily large for representing the reflecting region, and a reflection zone is defined to be one bounded by [26]

$$\Delta\Gamma - \Delta\Gamma_o = 0.3\lambda \tag{2.16}$$

where

$$\Delta\Gamma = \Gamma_1 + \Gamma_2 - \Gamma, \tag{2.17}$$

and $\Delta\Gamma_o$ is the $\Delta\Gamma$ when $\psi_1 = \psi_2$ in Fig. 2.1.

In order to find the reflection point for a real transmission path, the procedure can be described as the following. First, find the initial region of the reflection point, average the elevations within this region, and calculate the location of the reflection point. Second, find the reflection zone of the point obtained, average the elevations within this zone, calculate the location of reflection point again based on the new average elevation. Third, iterate within reflection zone until the elevation at the reflection point is found equal to the average elevation of the corresponding reflection zone. Thus this point is the real reflection point. If the terrain profile is smooth enough in the appropriate region to support reflections, this procedure converges rapidly.

2.3.2 The Reflection Coefficient and Loss (Gain)

After the real point of reflection has been found, the reflection coefficient then can be obtained by [27].

$$\rho = \frac{\varrho \sin\psi - (n_g^2 - \cos^2\psi)^{\frac{1}{2}}}{\varrho \sin\psi - (n_g^2 - \cos^2\psi)^{\frac{1}{2}}} \tag{2.18}$$

where n_g is the refractive index of the ground, and expressed in the complex form by

$$n_g^2 = \varepsilon_r + i60\sigma\lambda \tag{2.19}$$

ε_r is the ratio of the average permittivity of the ground to that of air, σ is the average ground conductivity, and $i = \sqrt{-1}$.

ψ is the angle between the ray and the surface. $\varrho = n_g^2$ for vertical polarization, $\varrho = 1$ for horizontal polarization.

The amplitude of the reflection coefficient is also reduced by the following factors.

(i). Since trees and buildings are expected to be too rough to support reflections, the fraction of the surface (f_s) that can reflect waves within the reflection zone is one of the reduction factors.

(ii). A rough surface reflects less well than a smooth one, then the terrain roughness factor (f_r) can be expressed as [28]:

$$f_r = \exp\{-\frac{1}{2}[4\pi\sigma_h \sin(\frac{\psi}{\lambda})]^2\} \tag{2.20}$$

where σ_h is the *rms* elevation variation within the reflection zone.

(iii). The amplitude of the reflected wave is reduced by divergence due to reflection from a convex mirror. National Bureau of Standards Technical Note 101

[29] gives the divergence factor as

$$f_d = (1 + \frac{2x_1x_2}{dR_c \tan\psi})^{-\frac{1}{2}} \tag{2.21}$$

where x_1, x_2 are the distances from the antennas to the point of reflection.

(iv). If the reflected ray is blocked by obstacles, the diffraction attenuation factor (f_a) should be considered. Diffraction will be discussed in detail in section 2.4.

Therefore, the amplitude of the reflected wave relative to the direct wave, is obtained as:

$$A_m = |\rho| * f_s * f_r * f_d * f_a. \tag{2.22}$$

The phase of the reflected wave relative to that of the direct wave is also estimated by:

$$\Phi = \angle\rho + \frac{2\pi\Delta\Gamma_o}{\lambda}. \tag{2.23}$$

Then the power of transmitted signal available at the receiver antenna is:

$$P_r = 1 + A_m^2 + 2A_m \cos\Phi. \tag{2.24}$$

Finally, the path loss or gain due to the reflection from the surface of the earth can be obtained as

$$L_r(dB) = -10 \log P_r. \tag{2.25}$$

2.4 Diffraction over Irregular Terrain

2.4.1 Diffraction over a Single Knife Edge

Propagation over hilly terrain is often adversely affected by obstructions such as hill tops. Kirchhoff's theory on diffraction has been found useful for predicting path

loss along a transmission path containing mountain ridges and similar obstructions. The hills can be approximately replaced by knife edges.

In classic electromagnetic theory applications, the field strength of a diffracted radio wave associated with a knife edge E can be expressed as [1]

$$\frac{E}{E_o} = Fe^{j\Delta\phi} \tag{2.26}$$

where E_o is the free space wave field with no knife-edge diffraction present, F is the diffraction coefficient, and $\Delta\phi$ is the phase difference with respect to the path of the direct wave. The loss due to diffraction is

$$L_d = 20 \log F \tag{2.27}$$

where F is given as

$$F = \frac{S + 0.5}{\sqrt{2}\sin(\Delta\phi + \frac{\pi}{4})} \tag{2.28}$$

$$\Delta\phi = \tan^{-1}(\frac{S + 0.5}{C + 0.5}) - \frac{\pi}{4} \tag{2.29}$$

and C and S are the Fresnel integrals, expressed as

$$C = \int_0^v \cos(\frac{\pi}{2}x^2)dx \tag{2.30}$$

$$S = \int_0^v \sin(\frac{\pi}{2}x^2)dx \tag{2.31}$$

where v is a dimensionless parameter, defined:

$$v = -H\sqrt{\frac{2}{\lambda}(\frac{1}{x_1} + \frac{1}{x_2})} \tag{2.32}$$

Here, x_1 and x_2 are the separation distances, and H is the height of the knife-edge relative to line of sight as shown in Fig. 2.3. The exact solution for Eq. (2.28) is shown graphically in Fig. 2.4. Usually approximate solutions are used.

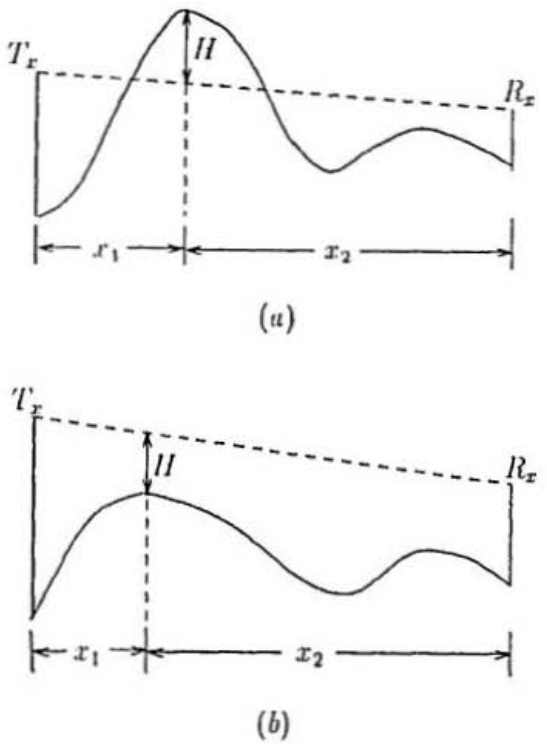

Figure 2.3: Effects of knife-edge obstructions on transmitted radio waves. (a). The knife edge is above the line of sight. (b). The knife edge is below the line of sight.

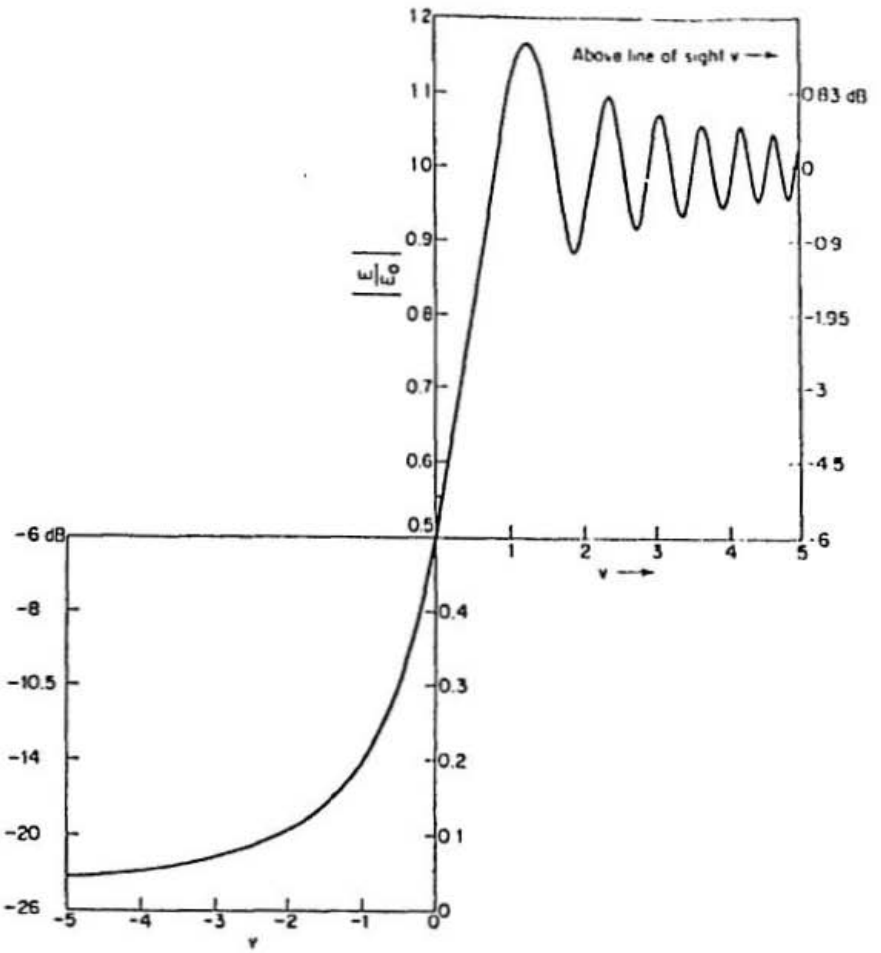

Figure 2.4: Magnitude of relative field strength E/E_o due to diffraction loss (from Ref. [1])

2.4.2 Diffraction over a Single Rounded Obstacle

Objects which are encountered in the physical world frequently have large thicknesses compared to the wavelength of transmission, e.g. mountains or trees. In these cases, it is necessary to account for effects other than knife-edge diffraction.

The treatment normally given to the problem of a rounded obstacle is to replace it by a conducting cylinder of equal radius to the crest. A solution can be obtained by defining a dimensionless parameter ζ as

$$\zeta = (\frac{\lambda}{\pi})^{\frac{1}{6}} r^{\frac{1}{3}} (\frac{d}{x_1 x_2})^{\frac{1}{2}} \tag{2.33}$$

where λ is wavelength, r the radius of the crest, d the distance between transmitter and receiver, and x_1, x_2 are the distances from the obstacle to transmitter and receiver. The diffraction loss may then be represented by a two dimensional quantity as:

$$L_d(u,\zeta) = L_d(u,0) + L_d(0,\zeta) + L_d(u\zeta) \tag{2.34}$$

where $L_d(u,0)$ is the knife-edge diffraction loss, $u = -v$ as in Eq. (2.32). And $L_d(0,\zeta)$ is 'curvature loss' which takes account the effect of obstacle's thickness, $L_d(u\zeta)$ is a correction factor. There are a number of ways by which improvements can be made. CCIR (International Radio Consultative Committee) method is one of them.

In CCIR method, diffraction loss is the function of the parameters as obstacle height above the line of sight H, first Fresnel zone radius R of the obstacle, factor of rounded obstacle α, and minimum effective antenna height h_m, i.e.

$$L_d = F(H/R, \alpha, h_{mt}, h_{mr})$$

where h_{mt}, h_{mr} are h_m for transmitter and receiver. These parameters are given by [30]:

$$R = \sqrt{\frac{\lambda x_1 x_2}{d}} \tag{2.35}$$

$$\alpha = \frac{1}{R}\exp[0.7675\log(r\lambda^2)] \tag{2.36}$$

where r is the radius of crest of the rounded obstacle, x_1, x_2, and d are the same as above.

$$h_m = \sqrt{h_a^2 + h_{min}^2} \tag{2.37}$$

where h_a is the antenna height above ground, and

$$h_{min} = \begin{cases} \frac{\lambda}{6.28318} * A_h & \text{for horizontal polarization} \\ \frac{\lambda}{6.28318} * A_v & \text{for vertical polarization} \end{cases} \tag{2.38}$$

here

$$A_h = \frac{1}{[(\varepsilon_g - 1)^2 + (60\lambda\sigma_g)^2]^{1/4}} \tag{2.39}$$

$$A_v = [(\varepsilon_g + 1)^2 + (60\lambda\sigma_g)^2]^{1/4} \tag{2.40}$$

and ε_g, σ_g are the permittivity and conductivity of the ground under the transmitter or the receiver.

For diffraction loss calculations, an approximate expression of CCIR curves is shown below [30].

(i). If $H/R < -0.6$, $L_d = 0$. This is the clear case.

(ii). If - $0.6 \leq H/R < 0$, it is not clear but still line-of-sight .

When $I \geq 2$, then

$$L_d = a_1 * exp(-0.015J) + a_2 * [1 - exp(-0.015J)] \tag{2.41}$$

when $I < 2$, then

$$L_d = 0.5I\{a_1 * exp(-0.015J) + a_2 * [1 - exp(-0.015J)]\} + 0.5a_3(2 - I) \tag{2.42}$$

where

$$I = \min\{h_{mt}, h_{mr}\} \tag{2.43}$$

$$J = \max\{\frac{h_{mt}}{h_{mr}}, \frac{h_{mr}}{h_{mt}}\} \tag{2.44}$$

$$a_1 = 6.98 * 2^{\alpha}\{1 - exp[\frac{5.3}{2^{\alpha}} * (\log(-H/R) + 0.2218)]\} \tag{2.45}$$

$$a_2 = 12.33 * 1.5^{\alpha}\{1 - exp[\frac{3}{1.5^{\alpha}} * (\log(-H/R) + 0.2218)]\} \tag{2.46}$$

$$a_3 = 34 - 20\log[7 - 71.85 * (H/R)] \tag{2.47}$$

(iii). If $H/R \geq 0$ (when H/R=0, let H/R=0.001), it is non-line-of-sight. In this case, diffraction loss is still calculated by Eq. (2.41) or Eq. (2.42), but parameters $a_i (i = 1,2,3)$ have different expressions and are different values for different α ranges.

$$a_i = -b_i + \sqrt{b_i^2 - c_i} + d_i \tag{2.48}$$

where

$$b_i = 0.5 * [40\log(H/R) + f_i] * \tan(\frac{e_i}{57.3}) \tag{2.49}$$

$$c_i = \frac{g_i^2[1 + \cos(f_i/57.3)]}{2\cos(f_i/57.3)} \tag{2.50}$$

and d_i, e_i, f_i, g_i are expressed based on different α ranges.

When $\alpha \leq 1$

$$\begin{array}{ll} d_1 = 5 + 4\alpha & e_1 = 150 - 53\alpha \\ d_2 = 5 + 10\alpha & e_2 = 150 - 40\alpha \\ d_3 = 5 + 11\alpha & e_3 = 150 - 25\alpha \\ f_1 = 16 - 22\alpha & g_1 = 19.8 * exp(0.269\alpha) \\ f_2 = 14 - 4\alpha & g_2 = 14 \\ f_3 = 16 + 40\alpha & g_3 = 7 * exp(0.827\alpha) \end{array} \tag{2.51}$$

When $1 < \alpha < 2$

$$\begin{array}{ll} d_1 = -6 + 15\alpha & e_1 = 103.36 - 6.36\alpha \\ d_2 = -20 + 35\sqrt{\alpha} & e_2 = 115 - 5\alpha \\ d_3 = 5 + 11\alpha & e_3 = 125 \\ f_1 = -35 + 29\alpha & g_1 = 46 * exp(-0.5\alpha) \\ f_2 = -29 + 55\sqrt{\alpha - 0.5} & g_2 = 16 * exp(-0.112\alpha) \\ f_3 = 46 + 10\alpha & g_3 = 21 * exp(-0.29\alpha) \end{array} \tag{2.52}$$

When $\alpha \geq 2$

$$e_1 = 90.53 \quad e_2 = 105 \quad e_3 = 125 \tag{2.53}$$

and d_i, f_i, g_i are the same as those in the case of $1 < \alpha < 2$.

This method of calculating diffraction loss over single rounded obstacle is the basis for multiple obstacle case. In order to see clearly the effects of each parameter on diffraction loss over single rounded obstacle, their relationships are graphically shown in the following. Fig. 2.5 shows that with the other parameters fixed, when H/R increases the diffraction loss increases. The diffraction loss versus frequency is given in Fig. 2.6. When f changes, R, α, h_{mt} and h_{mr} all change, so L_d changes. The basic parameters like H, x_1, x_2, r, etc. are fixed as shown in this figure, where h_{at}, h_{ar} are the transmitter and receiver antenna heights above ground. Regarding to the effect of the obstacle's location, when x_1 changes, R changes, and then L_d changes. Fig. 2.7 demonstrates their relationships. It can be seen that if the obstacle is close to the transmitter or the receiver, the diffraction loss increases very rapidly. About the effect of the radius of the obstacle crest, Fig. 2.8 shows the diffraction loss versus r. r increases, L_d increases. If transmitter antenna height or receiver antenna height increases, H will decrease, and L_d will decrease. Fig. 2.9 and Fig. 2.10 present the diffraction loss against antenna heights. Around 160 m in Fig. 2.9 and around 525 m in Fig. 2.10, there are irregular portions. These

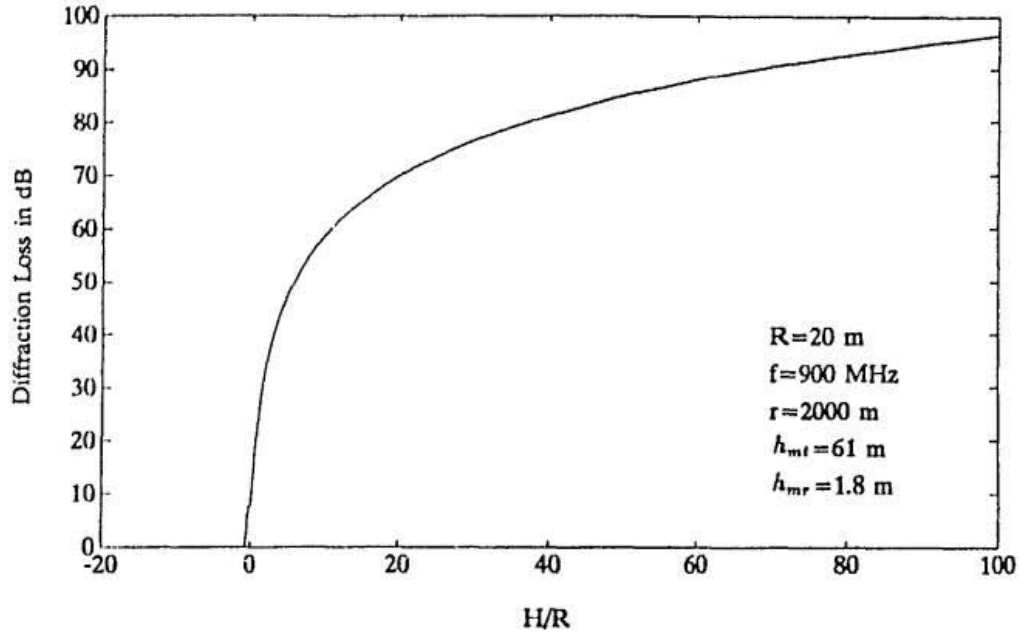

Figure 2.5: The Effect of H/R on Diffraction Loss

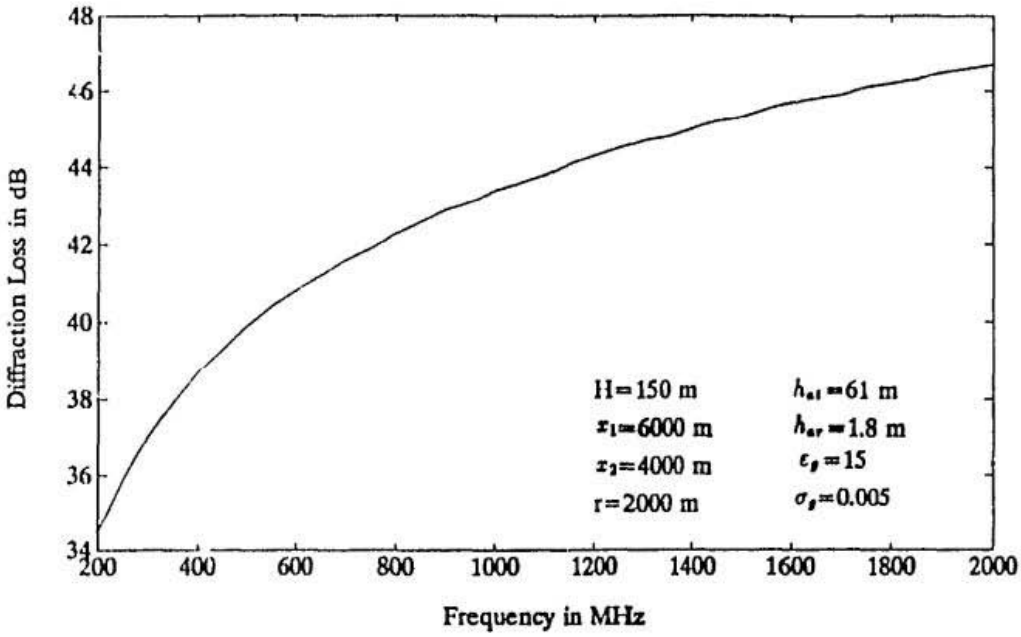

Figure 2.6: The Effect of Frequency on Diffraction Loss

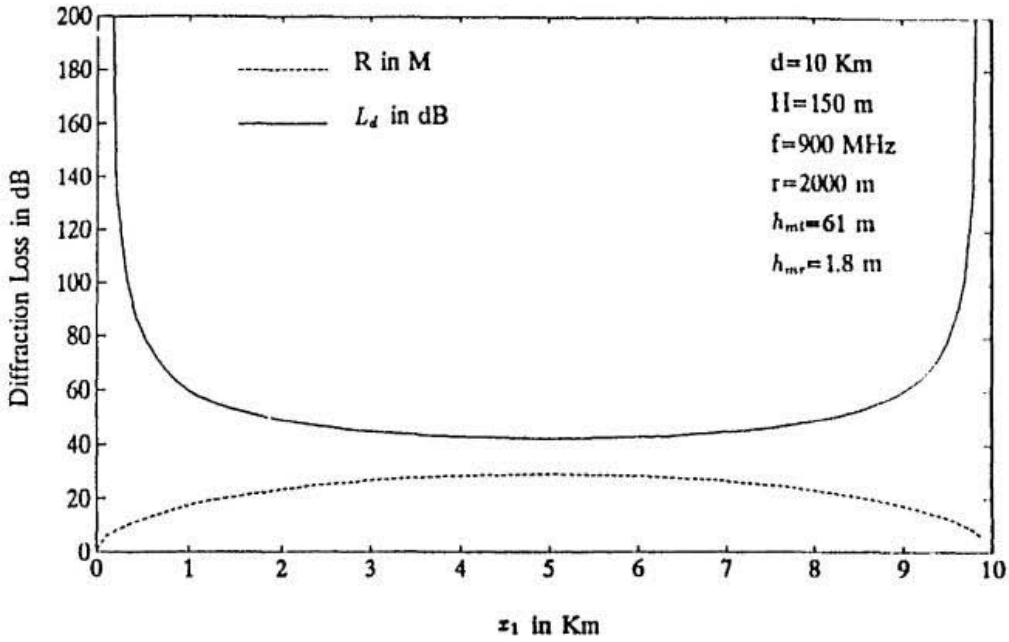

Figure 2.7: The Effect of the Obstacle's Location on Diffraction Loss

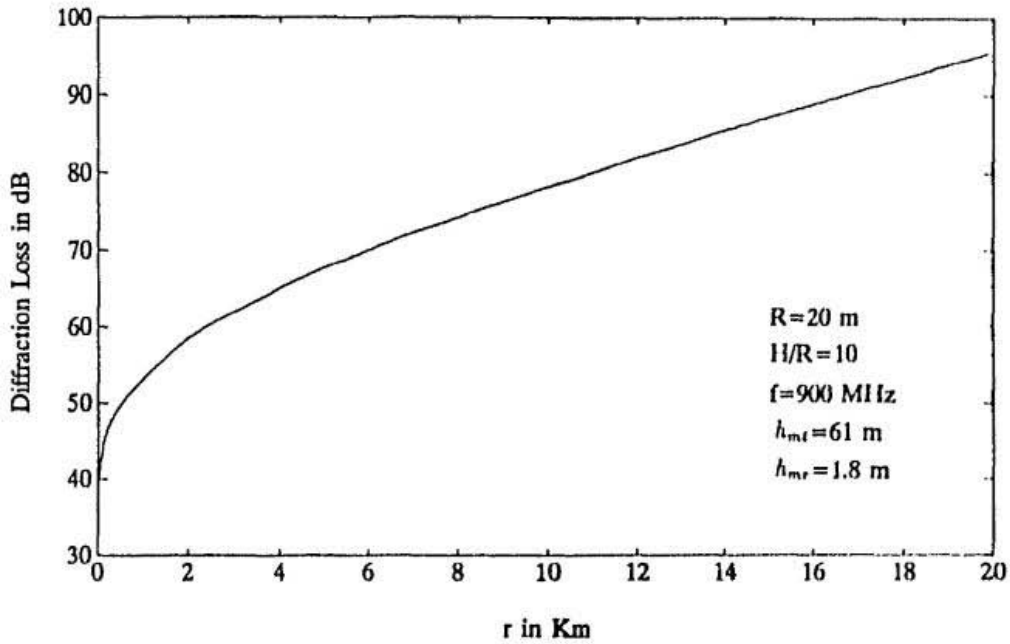

Figure 2.8: The Effect of r on Diffraction Loss

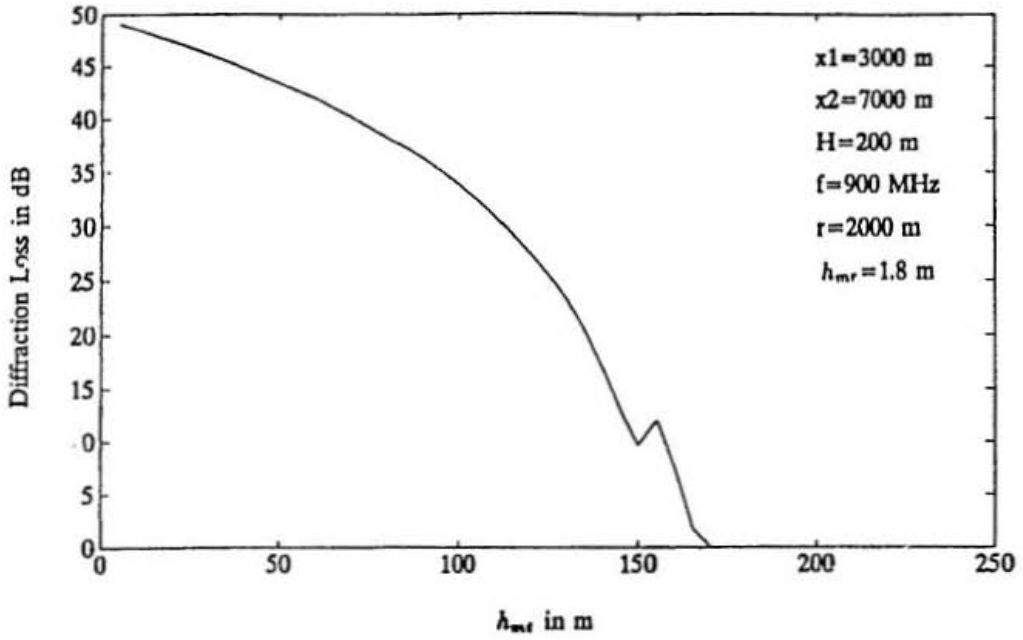

Figure 2.9: The Effect of h_{at} on Diffraction Loss

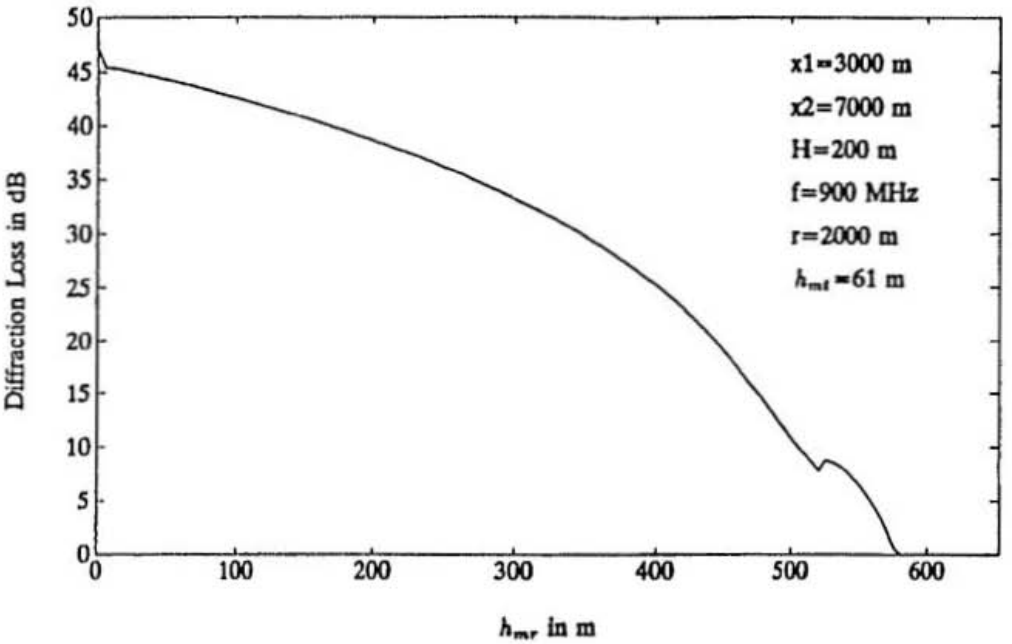

Figure 2.10: The Effect of h_{ar} on Diffraction Loss

are due to the approximation that if H/R=0, set it to 0.001, since in Eqs. (2.45), (2.46), and (2.49) H/R must be greater than 0.

2.4.3 Diffraction over Multiple Obstacles

The extension of the single knife-edge diffraction theory to two or more knife edges involves considerable mathematical complexity. The length and mathematical intricacy of the exact solution has made the use of approximations favourable, especially for more than two edges.

There are a number of approximate methods for diffraction over multiple knife edges. An early proposal was given by Bullington in 1947 [8]. This involves the replacement of the real terrain by only one single equivalent knife edge at the point of intersection of the optical paths made by each terminal and its horizon as shown in Fig. 2.11. The diffraction loss of this equivalent knife edge is computed as representing the loss of the original real terrain situation. This method oversimplifies the situation when large numbers of obstacles are involved.

The Epstein-Peterson method [31] calculates the diffraction loss by adding the attenuations produced by each knife edge in turn. Fig. 2.12 shows the two obstacle case in which the loss is evaluated as the sum of the diffraction losses for paths $T_x - M_1 - M_2$ and $M_1 - M_2 - R_x$. This method has large errors when the two obstacles are closely spaced.

The Japanese Atlas method [32] is shown in Fig. 2.13. The total loss is the sum of losses for paths $T_x - M_1 - M_2$ and $T_x' - M_2 - R_x$. T_x' is the projection of the horizon ray $M_1 - M_2$ onto the plane of T_x.

The Deygout method [33] is often called the 'main-edge' method. Compared

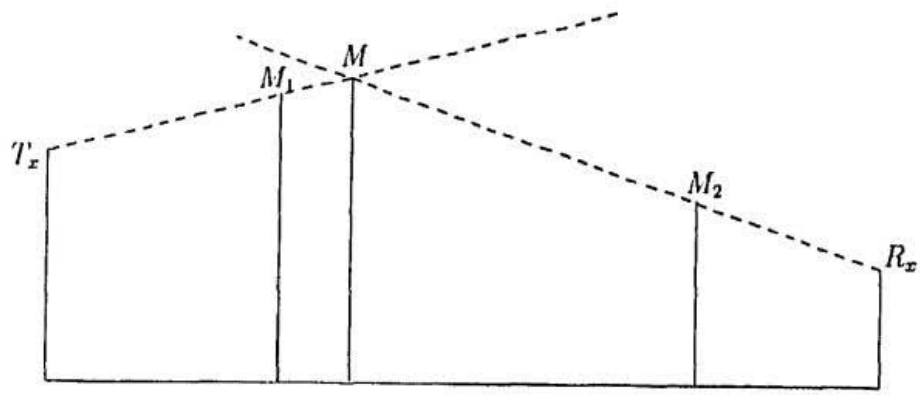

Figure 2.11: Bullington method for diffraction over multiple knife edges

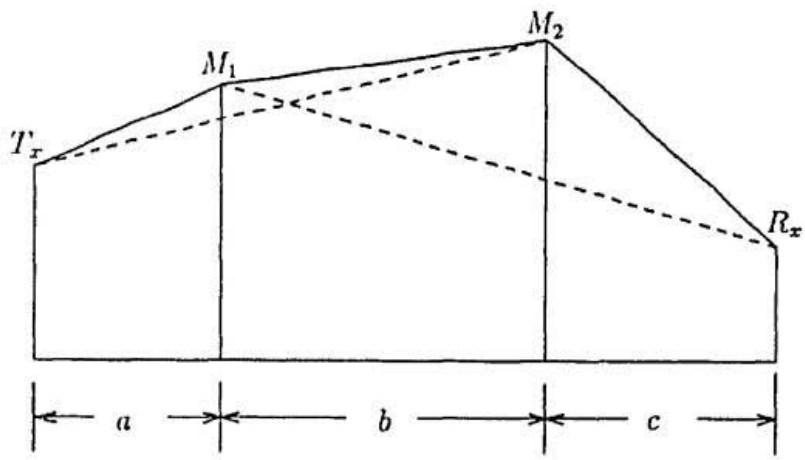

Figure 2.12: Epstein-Peterson method for diffraction over multiple knife edges

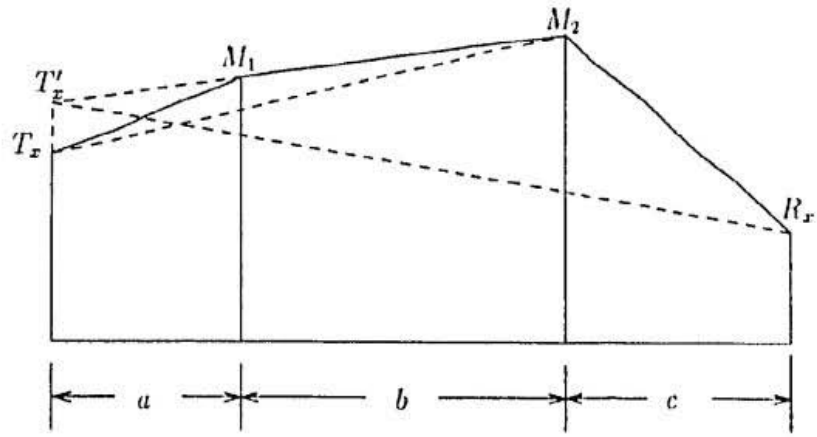

Figure 2.13: Japanese Atlas method for diffraction over multiple knife edges

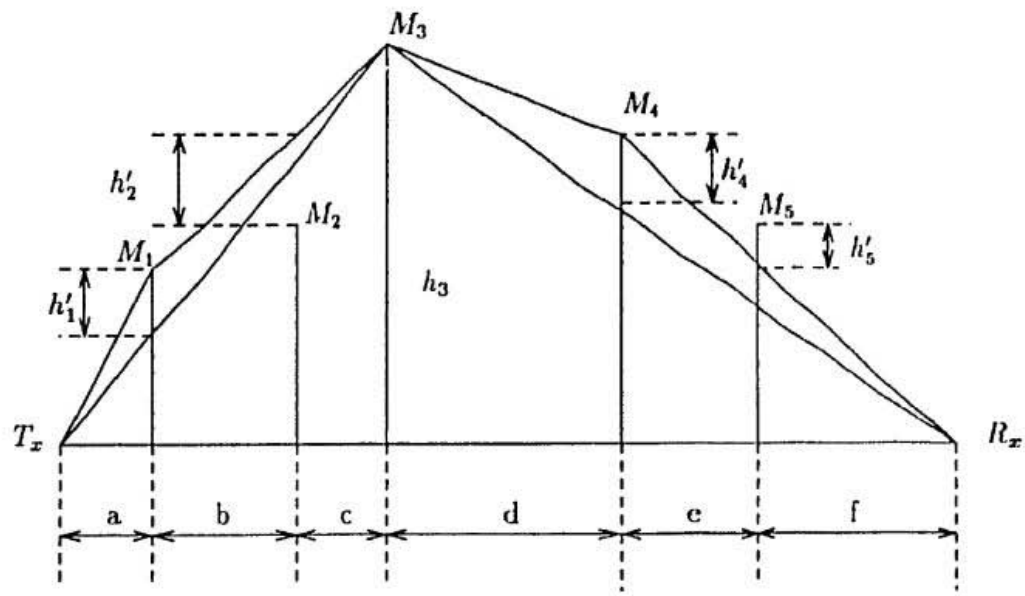

Figure 2.14: Deygout method for diffraction over multiple knife edges

with the methods above, Deygout method has been demonstrated to give increased accuracy for highly irregular terrain [34]. This method will be given detailed description by a following example.

Fig. 2.14 shows five knife-edge case. The first step is to calculate the value of H/R for each edge in the absence of the others. The edge M_3 with largest H/R is termed as the 'main edge' and its diffraction loss is calculated for the path $T_x - M_3 - R_x$ without the onsideration of other edges. The second step is to consider two sides of the main edge separately. For edges on the left of M_3, M_3 is treated as a receiver, and the H/R for M_1, M_2 are calculated based on the line of sight T_xM_3. The edge with larger H/R (M_1) is termed as the 'secondary edge' and its loss is calculated for the path $T_x - M_1 - M_3$ in the absence of M_2. The parameters for the calculation is shown in Table 2.1. Similarly, on the right side of M_3, M_3 represents the transmitter, and the loss of the secondary edge M_4 is calculated for the path M_3-M_4-R_x. In the same way, M_2 is the third edge on the right of M_1 and its diffraction loss is calculated for the path $M_1 - M_2 - M_3$. The diffraction loss of M_5 is calculated for the path $M_4 - M_5 - R_x$. Each of these individual losses is calculated based on single knife-edge formulas and all the parameters are given in Table 2.1. Finally, the total diffraction loss is evaluated as the sum of these five individual losses.

Table 2.1 : Parameters for Deygout Method

Parameters	M_1	M_2	M_3	M_4	M_5
H	h_1'	h_2'	h_3	h_4'	h_5'
x_1	a	b	a+b+c	d	e
x_2	b+c	c	d+e+f	e+f	f

For the case that the main edge is below line of sight, this method will cause more losses for other edges than they should be, so reduction should be made for edges except the main one. One way is to take half of their individual losses for the sum.

The Deygout method was developed in 1966 and more suitable for the multiple knife edges which are separated enough. When two edges are close to each other, this method gives excess diffraction loss, therefore the correction should be considered. Deygout correction factor for multiple knife edges will be discussed in Chapter 4.

All the methods stated above are for knife edges. In 1971, de Assis applied the Deygout method to rounded obstacles and found it satisfactory [35]. In the de Assis method, all the individual losses are calculated based on the diffraction loss by single rounded obstacle. The de Assis method, which is considered to be among the most useful method, is applied in this thesis.

2.5 Tropospheric Scattering Loss

When radio waves propagate through tropospheric path, the radio energy is scattered at random over a particle, a surface or through a space or substance, this is known as scattering. For long tropospheric paths, the propagation mechanism is usually forward scatter, especially during times of day and seasons of the year when ducts and elevated layers are rare. Often, for other periods of time, as scattering becomes more coherent it is more properly called reflection. Sometimes no distinction can be made between 'forward scatter' from a turbulent atmosphere and 'incoherent reflections' from patchy elevated layers.

In most theories of forward scatter from clouds, precipitation, refractive index, turbulence, layers, or feuillets, there are at least three distinguishing features. A calculation is first made of the expected or average forward scattering pattern, reradiation pattern, or diffraction pattern of a scatterer or a group of scatterers, usually located in free space, and usually assuming an incident plane wave and a distant receiver. Second, a decision is made that the relative phases of waves scattered from individual raindrops or subvolumes of refractivity turbulence or feuillets are random, so that the total power scattered may be obtained by adding the power contributions from these elements and ignore the phases. This is an essential feature of a random scatter theory. And third, some way is found to relate the actual terrain, atmosphere, and antenna parameters to the theoretical model so that a comparison may be made between data and theory.

By combining the forward scatter theory and the available long-term median transmission loss data, P.L. Rice, A.G. Longley, K.A. Norton, and A.P. Barsis [29] has developed the model for median tropospheric scattering transmission loss. In this model, the basic forward scattering loss is represented as:

$$L_{bs}(dB) = 30 \log f - 20 \log d + F(\theta d) - F_o + H_o + A_a \qquad (2.54)$$

where, f is the radio frequency in MHz, d is the distance in Km between transmitter and receiver. $F(\theta d)$ is the attenuation function, where θd is the multiplication of θ and d, θ is the angular distance in radians. F_o is the scattering efficiency, H_o is the frequency gain function, and A_a is atmospheric absorption. For most applications the first three terms of Eq. (2.54) are sufficient for calculating L_{bs}. $F(\theta d)$ will be briefly discussed in the following.

The attenuation function $F(\theta d)$ depends upon the most important features of

the propagation path and upon the surface refractivity N_s. The function includes a small empirical adjustment to data available in the frequency range from 100 to 1000 MHz. Fig. 2.15 shows some geometric parameters of the transmission path. The angular distance θ is the angle between horizon rays in the great circle plane, and $\theta = \alpha_o + \beta_o$. The parameter $s = \alpha_o/\beta_o$ describes the path asymmetry. When a path is highly asymmetrical (s small), the attenuation for a given value of θd is less than that would be for a symmetrical path. For values of $\theta d \leq 10$, the effect of asymmetry is negligible, but increases with increasing θd, particularly when $s < 0.5$. For the great majority of transhorizon paths, s is within the range $0.75 \leq s \leq 1$. The analytical functions of $F(\theta d)$ for $0.75 \leq s \leq 1$ may be expressed as follows [29]:

for $0.01 \leq \theta d < 10$,

$$F(\theta d) = Q(N_s) + 0.34\theta d + 30\log(\theta d) \tag{2.55}$$

where

$$Q(N_s) = 139.5 + 0.06N_s - 2.4 * 10^{-4}N_s^2 \tag{2.56}$$

for $10 \leq \theta d < 70$,

$$F(\theta d) = Q_o(N_s) + Q_1(N_s)\theta d + Q_2(N_s)\log(\theta d) \tag{2.57}$$

where

$$Q_o(N_s) = 140.7 + 0.06N_s - 3.2 * 10^{-4}N_s^2 \tag{2.58}$$

$$Q_1(N_s) = 3.925 + 3.3 * 10^{-3}N_s - 1.9\log N_s \tag{2.59}$$

$$Q_2(N_s) = 22.5 + 0.05N_s \tag{2.60}$$

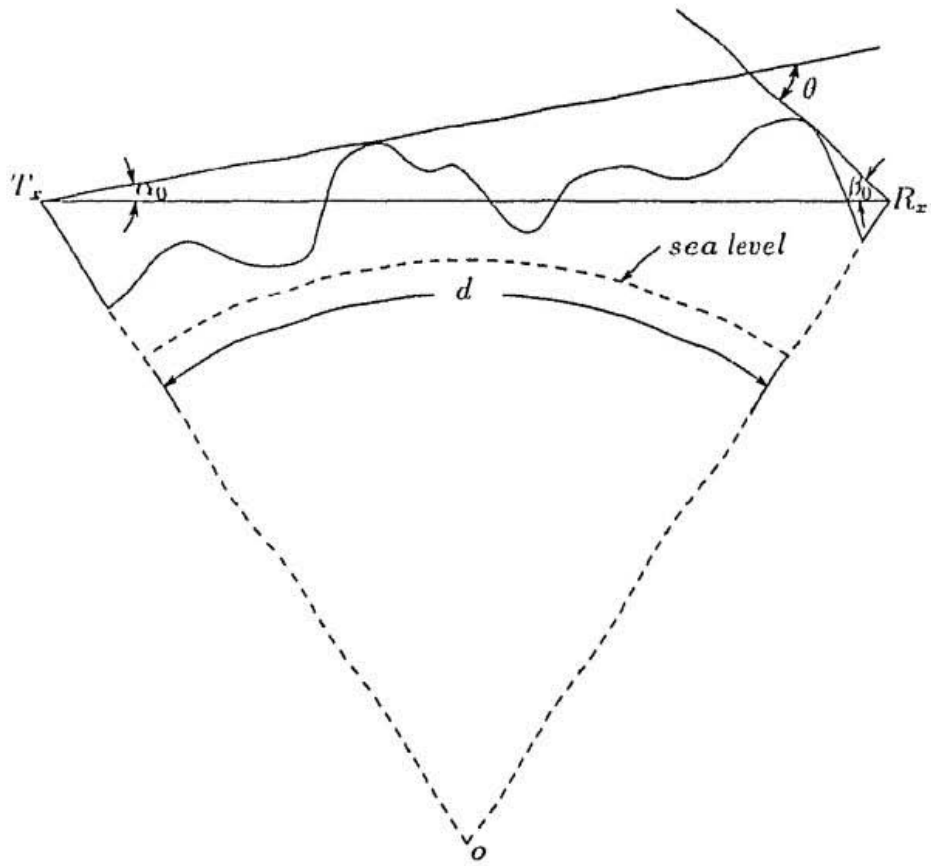

Figure 2.15: Geometric Parameters of Transmission Path

for $\theta d \geq 70$,

$$F(\theta d) = K(N_s) + 0.158\theta d + 44\log(\theta d) \tag{2.61}$$

where

$$Q(N) = 123.6 - 0.008N_s. \tag{2.62}$$

From the formulas above, it can be generally described that when θd increases, $F(\theta d)$ increases, and when N_s increases, $F(\theta d)$ decreases.

If the basic forward scatter transmission loss is added by an antenna to medium coupling loss L_{gp} and a climatic correction factor F_c, it forms the median forward scatter transmission loss L_s, i.e.

$$L_s = L_{bs} + L_{gp} - F_c \tag{2.63}$$

L_{gp} represents a statistical average effect of phase incoherence of the forward scattered fields. It can be computed as [30]:

$$L_{gp} = 0.07\exp[0.055(G_t + G_r)] \tag{2.64}$$

where G_t and G_r are transmitter and receiver free space antenna gains in decibels relative to an isotropic radiator, respectively.

Since the median forward scatter transmission loss varies with different climatic regions, F_c correction factor is provided for this variation based on experimental data.

In National Bureau of Standards Technical Note 101, P.L. Rice *et al*, gave the extensive investigation in transmission loss for tropospheric communications. It is considered as one of the most useful references for the tropospheric scattering loss evaluations.

2.6 The Losses due to Terrain Cover

The terrain cover is mainly concerned about trees and buildings along transmission paths. The high density of buildings in urban area cause urban loss. The trees and buildings near transmitter or receiver but not in urban area will bring additional loss which is called clutter loss. For the trees and buildings neither concerned in urban loss nor in clutter loss, they will be considered by diffraction loss. The following subsections will discuss these losses.

2.6.1 Urban and Suburban Losses

For transmission paths through or within urban or suburban area, one main effect on the transmission loss is buildings. The effect of buildings in these areas has been investigating by many theoretical and experimental methods. Based on the comparative study made at Laval University, and also proposed by CCIR report 567-1, Hata method [7] is adopted for estimating the transmission loss due to buildings in urban area and suburban area.

Hata model is developed from Okumura's work [6]. Y. Okumura gave the results of extensive propagation tests for land mobile radio service over various situations of irregular terrain and environmental clutter. The results are analyzed statistically to determine the distance and frequency dependences of the median field strength, location variabilities, and antenna height gain factors for the transmitter and receiver in urban, suburban, quasi-open and open areas over quasi-smooth terrain. M. Hata derived the equations of median transmission loss from Okumura's curves in order to make the use of them simpler. With computation simplicity, however, also come some restrictions. Hata's model is applicable to VHF/UHF land mobile

radio services under the conditions: frequency range 100-1500 MHz, distance 1-20 km, base station antenna height 30-200 m, mobile antenna height 1-10 m. For urban area, the formulas are [7]:

$$L_p(dB) = 69.55 + 26.16 \log f - 13.82 \log h_{at} - a(h_{ar}) + (44.9 - 6.55 \log h_{at}) \log d \tag{2.65}$$

where L_p is the propagation loss in urban area, f is frequency in MHz, h_{at} and h_{ar} are base station antenna height and mobile antenna height in metre above their ground, d distance in km. $a(h_{ar})$ is the correct factor for mobile antenna height and is expressed as:

for medium-small city,

$$a(h_{ar}) = (1.1 \log f - 0.7)h_{ar} - (1.56 \log f - 0.8) \tag{2.66}$$

for large city,

$$a(h_{ar}) = \begin{cases} 8.29(\log 1.54h_{ar})^2 - 1.1 & f \leq 200MHz \\ 3.2(\log 11.75h_{ar})^2 - 4.97 & f \geq 400MHz \end{cases} \tag{2.67}$$

For suburban area,

$$L_{ps} = L_p - 2(\log \frac{f}{28})^2 - 5.4 \tag{2.68}$$

Since the experimental data were taken in Japan, the definition of city size is different from that in Northern America. For the use of Hata's model in Canada, CRC has modified it as the follows. The propagation loss in urban area L_u is taken as L_p in the large city case in the above equations, and for frequency range $200 < f < 400MHz$ an linear interpolation is made. For suburban area, L_{su} is taken as the combination of L_p in medium-small city case and the loss in suburban area L_{ps}. The formulas [30] are shown in the following.

For urban area, if $f \leq 200MHz$,

$$\begin{aligned} L_{u'} &= 69.55 + 26.16\log f - 13.82\log h_{at} + (44.9 - 6.55\log h_{at})\log d \\ &\quad -\{8.29[\log(1.54h_{ar})]^2 - 1.1\} \end{aligned} \tag{2.69}$$

if $200 < f < 400MHz$,

$$\begin{aligned} L_{u'} &= 69.55 + 26.16\log f - 13.82\log h_{at} + (44.9 - 6.55\log h_{at})\log d \\ &\quad -\{8.29[\log(1.54h_{ar})]^2 - 1.1 + \frac{(f-200)}{200}[3.2(\log(11.75h_{ar}))^2 \\ &\quad -8.29(\log(1.54h_{ar}))^2 - 3.87]\} \end{aligned} \tag{2.70}$$

if $f \geq 400MHz$,

$$\begin{aligned} L_{u'} &= 69.55 + 26.16\log f - 13.82\log h_{at} + (44.9 - 6.55\log h_{at})\log d \\ &\quad -\{3.2[\log(11.75h_{ar})]^2 - 4.97\}. \end{aligned} \tag{2.71}$$

Finally, the urban loss L_u is:

$$L_u(dB) = \max(L_{u'}, L_f) \tag{2.72}$$

where L_f is the free space loss.

For suburban area,

$$\begin{aligned} L_{su'} &= 69.55 + 26.16\log f - 13.82\log h_{at} + (44.9 - 6.55\log h_{at})\log d \\ &\quad -[(1.1\log f - 0.7)h_{ar} - (1.56\log f - 0.8)] - 2(\log\frac{f}{28})^2 \\ &\quad -5.4 \end{aligned} \tag{2.73}$$

And finally, the suburban loss L_{su} is:

$$L_{su}(dB) = \max(L_{su'}, L_f). \tag{2.74}$$

This model is used when transmitter or/and receiver is in urban or suburban area, and its antenna is less than 10 m.

2.6.2 Clutter Loss

The clutter is denoted as trees or buildings in the immediate vicinity of the transmitting or receiving antennas but not in urban or suburban area. The effect of this kind of clutter should be considered in the transmission loss. A lot of work has been done in investigation of the effects of vegetation and building on VHF/UHF propagation. P.L. Rice made a composite of material collected from CCIR and other reports in paper [36]. The clutter loss is computed based on this paper and CRC method [30].

For the propagation attenuation through trees, it has the empirical relationship as [36]:

$$A_W(dB) = \gamma dw \tag{2.75}$$

where A_W is the absorption in decibels through dw metres of trees, And γ is γ_V for vertical polarization, or γ_H for horizontal polarization. They have the following empirical expressions:

$$\gamma_V(dB/m) = 1637\sigma_1 + 2717\exp(-\frac{90}{f})\log(1+\frac{f}{100}) \tag{2.76}$$

$$\gamma_H(dB/m) = 1637\sigma_1 + 4027\exp(-\frac{210}{f})\log(1+\frac{f}{200}) \tag{2.77}$$

where σ_1 is the effective conductivity. σ_1 can be obtained from empirical data in Table 2.2 which is used in CRC method.

Table 2.2 : The effect of trees on σ_1 (mhos/m)

	dry	wet
bare tree	$7 * 10^{-6}$	$1.4 * 10^{-5}$
leaf	$1 * 10^{-5}$	$2 * 10^{-5}$
evergreen	$3 * 10^{-5}$	$6 * 10^{-5}$
forest	$2 * 10^{-4}$	$4 * 10^{-4}$

It has been found that when a reflecting ionosphere is present, the radiated field consists primarily of two seperate waves, a lateral wave that skims along the tree tops, and a sky wave produced by a signal-hop reflection at the ionospheric layer, and that the lateral wave often plays a major role in the field variation, path loss, etc. When the trees are higher than the antenna, the attenuation due to lateral wave will be [36]:

$$A_L(dB) = l_a[1 - exp(-\frac{h}{10})] \tag{2.78}$$

where h in metres is the height of tree above the ground level at the antenna nearby. The parameter l_a is determined by:

$$l_a = \begin{cases} 12, & \sigma_1 < 1 * 10^{-5} \\ 30, & 1 * 10^{-5} \leq \sigma_1 < 2 * 10^{-4} \\ 40, & \sigma_1 \geq 2 * 10^{-4} \end{cases} \tag{2.79}$$

For the attenuation through buildings, it can be computed as [30]:

$$A_B(dB) = \frac{E_m}{15} d_b \tag{2.80}$$

where A_B is the absorption through the building and d_b is the building depth along line of sight. 15 means 15-metre-thick building. Coefficient E_m can be obtained in Table 2.3.

Table 2.3 : The coefficient E_m

wood	15
brick	30
concrete	30
metal	45
other kinds of materials	30

It has been shown that sometimes the reflection effects of building predominate over actual absorption of energy in the materials [37]. The interference effects of

reflections from various paths of a wall will result in large variations of field strength over short distance. This multipath attenuation may be computed by [30]:

$$A_M(dB) = 20 \log f(MHz). \tag{2.81}$$

There is a case that the clutter may be treated as opaque objects around which diffraction takes place, such as very dense stone buildings or groups of trees. In this case, the attenuation of diffraction over the top of clutter can be calculated by the approximation of knife-edge diffraction loss as [36]:

$$A_D(dB) = \begin{cases} 0 & \Delta h \leq 0 \\ 11 + 20 \log v & v > 3 \\ 40 & v \leq 3 \end{cases} \tag{2.82}$$

$$v = 0.082\sqrt{\frac{\Delta h^2 f}{d_c}} \tag{2.83}$$

where Δh is the height of clutter above the antenna nearby, d_c is the distance from the antenna to its clutter in metres.

There are several cases of attenuations regarding to the clutter as stated above. The case with least loss is considered as the clutter attenuation, i.e. for trees,

$$A_c = \min(A_W, A_L, A_D) \tag{2.84}$$

for buildings,

$$A_c = \min(A_B, A_M, A_D). \tag{2.85}$$

Finally, the extent of clutter across line of sight E_c (in metres), has the effect on A_c as [30]:

$$L_c(dB) = A_c[1 - exp(-\frac{2E_c}{d_c})]. \tag{2.86}$$

L_c is the clutter loss which contributes to the total median transmission loss. Since the attenuation due to trees and buildings can vary a great deal, the result of L_c is regarded as rough estimates.

2.6.3 The Effects of Trees and Buildings other than Clutter

For the trees and/or buildings which are along the transmission path but do not belong to clutter, and the buildings are also not in urban or suburban area, their effects in propagation are treated as obstacles like hills along the path. This treatment is derived from [36]. It can be implemented by the path profile which combines the terrain elevations and the effective heights of trees or buildings.

For trees, their effective heights are computed by empirical equation as [30]:

$$H_t = 10 + 10[0.5 + \frac{1}{\pi}\arctan(\frac{f - f_{mid}}{\Delta f})] \tag{2.87}$$

where H_t is in metres, f in MHz, and

$$f_{mid}(MHz) = \begin{cases} 140 & \text{horizontal polarization} \\ 100 & \text{vertical polarization} \end{cases} \tag{2.88}$$

$$\Delta f(MHz) = \begin{cases} 40 & \text{horizontal polarization} \\ 30 & \text{vertical polarization} \end{cases} \tag{2.89}$$

Add H_t to the terrain heights above mean sea level where the trees are.

For buildings not treated in urban or suburban model in subsection 2.6.1, also not treated in clutter model in subsection 2.6.2, the heights are estimated for computer program as

$$H_b(m) = \begin{cases} 30 & \text{in urban} \\ 7.5 & \text{in suburban} \end{cases} \tag{2.90}$$

Add H_b to the terrain heights above mean sea level where the buildings stand. Therefore, the effects of this kind of trees and buildings are taken as diffraction loss if they become the obstacle for the transmission path.

2.7 Variations of Propagation Loss

In land mobile communications, time variability is not as significant as location variability. However the fact that the transmission loss varied from season to season should be considered. This variation is denoted as season loss in this thesis. Season loss and location variability will be briefly discussed in the following subsections.

2.7.1 Variations with Time (Season Loss)

The variability of median transmission loss is usually due to slow changes in average atmospheric refraction, in the degree of atmospheric stratification, or in the intensity of refractive index turbulence. In land mobile systems, measurements of transmission loss between base station and mobile antennas, made as the mobile position varies, form a statistical distribution. The median value of this distribution for a given sector (a small area of up to 20 wavelength) is called the sector transmission loss and found it has variations from season to season. CRC developed a model to describe the deviation from the long-term median transmission loss at a particular month of the year and hour of the day for Canadian area [30].

Based on a large number of measurements, the annual and diurnal variations have been found to be the function of climatic region, effective distance, and time factor. Climatic regions include continental, maritime overland, maritime oversea, and great lakes. If M (1 to 12) denotes the month concerned, and H (1 to 24) for the hour, then the time factor for annual variation is [38]:

$$C_a = \begin{cases} \cos\frac{(M-1)\pi}{3} + \sin\frac{(M-1)\pi}{6} & \text{if great lakes} \\ \cos\frac{(M-1)\pi}{6} & \text{otherwise} \end{cases} \tag{2.91}$$

And the time factor for diurnal variation is:

$$C_d = \cos\frac{(H-14)\pi}{12}. \tag{2.92}$$

The effective distance d_e is defined as [30]:

$$d_e = \begin{cases} 130d/d_{ref} & d \le d_{ref} \\ 130 + d - d_{ref} & d > d_{ref} \end{cases} \tag{2.93}$$

where d is the distance between transmitter and receiver, d_{ref} is:

$$d_{ref} = 10^{-3} * (\sqrt{2R_e h_{tav}} + \sqrt{2R_e h_{rav}}) + \frac{300}{f^{1/3}} \tag{2.94}$$

and h_{tav}, h_{rav} are the transmitter and receiver antenna heights above average elevations near the transmitter and receiver. Let F_1, F_2 be the distance factors for annual and diurnal variations, then they are described by:

$$F_1 = 1 - \exp[-(\frac{d_e}{120})^4], \tag{2.95}$$

$$F_2 = (\frac{d_e}{120})^3 \exp[3(1 - \frac{d_e}{120})]. \tag{2.96}$$

Then, the season loss L_{se} in dB, is found to be:

$$L_{se} = C_a F_1 A(k,1) + C_d F_2[A(k,2) - C_a A(k,3)] \tag{2.97}$$

where $k = 1, 2, 3, 4$ denote to the climatic regions as continental, maritime overland, maritime oversea, and great lakes, respectively. And $A(k,1)$, $A(k,2)$, $A(k,3)$ are coefficients for annual and diurnal variations in the four climatic regions. They are

$$A(1,1) = 3.8 \quad A(1,2) = 4.3 \quad A(1,3) = 2.8$$

$$A(2,1) = 5.0 \quad A(2,2) = 2.0 \quad A(2,3) = 1.5$$

$$A(3,1) = 8.0 \quad A(3,2) = 0.0 \quad A(3.3) = 0.0$$

$$A(4,1) = 4.0 \quad A(4,2) = 1.5 \quad A(4,3) = 0.0$$

These empirical data are taken from the measurements in the reference [38].

2.7.2 Location Variability

In land mobile communications, the signal received by a mobile antenna varies because the obstructions to propagation change. Within a sector, the transmission loss can be described by Weibull distribution. For a set of sectors located in similar environments and at equal distance from the base station, their sector transmission losses form a log normal distribution. The standard deviation of this distribution is defined as location variability. Location variability describes the slow fading of transmission loss varying from sector to sector which is the result of shadowing and/or reflections by terrain features or man made propagation obstructions, etc.. A.G. Longley gave the formula for calculating location variability of transmission loss [39]. The similar formular appears in CCIR report [40].

To evaluate location variability, the detailed terrain profile is needed. In order to describe the terrain roughness, a least-squares line is fitted to the path profile. The distribution of terrain heights above and below the fitted line is assumed as Gaussian distribution. The difference between 10 and 90 percentile points of the distribution DH represents the terrain roughness. The variability due to terrain roughness is:

$$V_t(dB) = 1 + 0.55\sqrt{\frac{DH}{\lambda}} - 0.004\frac{DH}{\lambda} \tag{2.98}$$

This is CRC method [30] where the leading term 1 dB replaces the 6 dB in Longley's formula. Longley's formula refers to all paths of a given length, whereas here it requires the variability of paths terminating in an area small enough that the predicted path loss is constant.

As receiving antenna height h_r becomes large with respect to DH, the variability

will decrease.

$$V_a(dB) \cdot \cdot 1 + V_t \exp(-0.1\frac{h_r}{DH}). \tag{2.99}$$

Except terrain roughness, local clutter also contributes to the variability, say V_c. If terrain surface at the receiver is lake or sea, V_c=1 dB. For other kinds of surfaces, it is [30]:

$$V_c = (S \log f - 4.22) \exp(-0.1\frac{h_r}{h_c}) \tag{2.100}$$

where h_c is the height of clutter (m), and when the surface is bare ground or marsh,

$$S = 3 \quad h_c = 10;$$

when the surface is urban area,

$$S = 5.47 \quad h_c = 50;$$

and if the surface is any other type,

$$S = 3.5 \quad h_c = 10.$$

Combining terrain roughness and local clutter, the location variability will be:

$$L_{lv}(dB) = \sqrt{V_a^2 + V_c^2}. \tag{2.101}$$

The location variability can be used to aid some field experience and judgement in estimating a suitable reliability margin for mobile radio systems.

Chapter 3

Modification of the Terrain Data Base

3.1 Brief Introduction of CRC Data Base

CRC digital terrain data base is designed mainly for predictions of radio-wave field strengths at VHF and UHF bands. It provides path profiles for the predictions. It also can be used for preliminary surveys of line-of-sight paths for microwave links and sites proposed for satellite earth stations [41].

As of November 1990, the data base covers all of British Columbia and Alberta up to 55° latitude, all of Ontario up to about 49° latitude, much of southern Quebec, and all of the Atlantic provinces except for Labrador [42]. Fig. 3.1 shows the data base coverage. The data base has totally about 10 million points taken from 1:50,000 scale topographic maps. An elevation above mean sea level and a surface code for types such as tree, bare ground, fresh water, suburban, marsh, seawater, urban core, and unknown type, are stored for each point in a square array with 500 metre spacing. On these topographic maps, the contour interval is 25 feet where the terrain is not too rough and 50 feet where it is rough. Therefore an elevation

Figure 3.1: CRC Data Base Coverage (From Ref. [42])

can be uncertain by as much as 50 feet (15 m). However, in reasonable shaped terrain, the data base values, which are interpolated from the contour lines, are likely to be more precise than that. The other limitation on the precision is the fact that in the data base, elevations are stored at points 500 m apart. It is always possible for some hills to be missed in between these points.

The terrain data base is organized by files, pages and words. Each file represents a region of 4° latitude by 6° longitude and contains 3000 pages. Each page covers an area of 7.5 Km X 15 Km, and has 512 (i.e. 16 x 32) words with the columns and rows of words on the edges of the page duplicated from their adjacent pages. Each word is 16 bits, the first 3 bits are used to record the surface code and the rest 13 bits are for the elevation. The surface codes represent eight types of surfaces mentioned above. The greatest elevation that can be represented is 8191 metres above sea level. Since it is not possible in this scheme to represent areas below sea level, some pages do not exist; these can be indicated in the index records of each file.

The data base is simply a long string of numbers on a set of disk files. An index is required to relate geographic location to position in this string. The Universal Transverse Mercator (UTM) system of coordinates is used for creating and indexing the data base. The primary reason for this is that a UTM reference grid is printed on all large-scale topographic maps in Canada, so that maps can be scaled much more easily using UTM coordinates than using latitude and longitude. If a point is located by latitude and longitude, it will be transformed to UTM coordinates, and by using an index subroutine, its corresponding file name, the page number and the word number within the page will be found.

It is sometime useful to be able to determine whether a point or a path is in the data base area without actually accessing the data base. The data base has points from 41.75° latitude to 55° latitude. This range is divided into 53 strips with 0.25° of latitude each. Based on the shape of the data base coverage, there are 118 segments for all strips. Each segment has its west longitude and east longitude boundaries. To determine whether a given point or a path is in the data base area, just check whether it is within those segment boundaries.

CRC data base will be developed to cover more areas in the future.

3.2 Modification to the Terrain Data Base

CRC data base contains elevations and surface codes at points 500 m apart. In terrain that is not too rough, the resolution of 500 m spacing may be adequate. However, in rough terrain this spacing is very likely causing loss of important details, especially missing hills which are essential to propagation paths. This can have considerable effects on the accuracy of the prediction results, especially for cellular radio systems in which the cell sizes become smaller and smaller. To solve this problem, the most reliable way is to build a data base with desired small spacing by hand-scaling the large scale topographic maps. However, this is a very exhausting and time consuming task. In order to obtain a higher resolution and accurate data base economically, a procedure which includes two steps is proposed. First, increase more points with 100 m spacing by pure interpolations. Second, use correct data taken from topographic maps to interpolate again.

3.2.1 Augmentation of the Terrain Data Base

To obtain a more precise terrain data base, the first step in the proposed procedure is to add more points in CRC data base by pure interpolations. Regard to how small a spacing is adequate, according to the fact that in cellular system the smallest cell now is about 2 Km, a terrain data base with 100 m spacing seems reasonable. Hence, the spacing of 100 m is used in this thesis, but the proposed procedure can be used for any desired spacing.

In choosing interpolation methods for obtaining more points, a two-dimensional polynomial is considered for fitting each local irregular terrain surface, since a polynomial is easy to handle mathematically. In addition, a polynomial of arbitrarily high order permits a recognizable approximation to the true terrain. However, for practical purposes it is limited to one of finite orders. By truncating an infinite polynomial at different orders, it can easily vary the degree of approximation. The greater the number of terms included in the approximation, the more closely the true terrain is represented. This does not suggest that higher order polynomial should be always favoured over lower order one. By trading off the accuracy of approximation to a local terrain and the complexity of mathematical models or computational effort, a quadratic two-dimensional polynomial is selected for the interpolation of CRC data base. Based on the practical experience in interpolation, a quadratic polynomial is generally proper for approximating normal irregular terrain surface. For some particular areas where the terrain shapes change abruptly, or some hills and valleys are completely missed in CRC data base, a second step of interpolation will be provided. This will be discussed in the next subsection.

There are two quadratic two-dimensional polynomials which can be used. One

is called complete quadratic (nine points) interpolation and expressed as:

$$\begin{aligned} Z &= a_0 + a_1 x + a_2 y + a_3 x^2 + a_4 xy + a_5 y^2 \\ &\quad + a_6 x^2 y + a_7 x y^2 + a_8 x^2 y^2. \end{aligned} \tag{3.1}$$

The other is incomplete quadratic (eight points) interpolation and given as:

$$\begin{aligned} Z &= a_0 + a_1 x + a_2 y + a_3 x^2 + a_4 xy + a_5 y^2 \\ &\quad + a_6 x^2 y + a_7 x y^2. \end{aligned} \tag{3.2}$$

Since CRC data base takes every point with equal spacing, using complete quadratic interpolation is suitable and more accuate (one point more). In equation 3.1, let Z represents the elevation of a point, (x, y) is its coordinates in a reference coordinate system. Let the 500 m spacing of the points in CRC data base be normalized to unity, then Fig. 3.2 shows the geometric diagram for complete quadratic interpolation. Let $Z_1, Z_2, ..., Z_9$ be the elevations of points 1, 2, ..., 9 in CRC data base. By substituting these nine points into Eq. (3.1) respectively, and solving these nine equations, the coefficients $a_0, a_1, ..., a_8$ can be obtained and the interpolation polynomial for this local terrain surface is therefore determined.

The interpolation polynomial can be further expressed by shape function which is more convenient for practical interpolations and provides geometric meanings in broad sense. In order to avoid tedious algebraic manipulations, here only presents the final form to be applied in the interpolation implementation. This manipulation process can be appreciable by the relatively simple triangular interpolation in the following subsection. Let G_i (i=1, 2, ..., 9) be the shape function. According to the geometry in Fig. 3.2, for any point (x, y) within the area surrounded by these

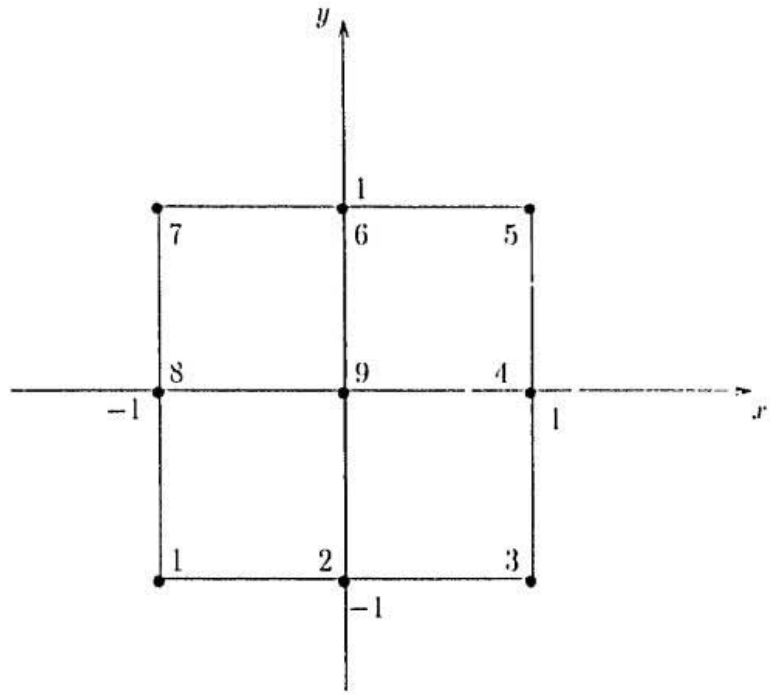

Figure 3.2: Complete Quadratic Interpolation

nine points, G_i is derived as:

$$G_1 = \frac{(1-x)(1-y)xy}{4} \tag{3.3}$$

$$G_2 = \frac{-(1-x^2)(1-y)y}{2} \tag{3.4}$$

$$G_3 = \frac{-(1+x)(1-y)xy}{4} \tag{3.5}$$

$$G_4 = \frac{(1+x)(1-y^2)x}{2} \tag{3.6}$$

$$G_5 = \frac{(1+x)(1+y)xy}{4} \tag{3.7}$$

$$G_6 = \frac{(1-x^2)(1+y)y}{2} \tag{3.8}$$

$$G_7 = \frac{-(1-x)(1+y)xy}{4} \tag{3.9}$$

$$G_8 = \frac{-(1-x)(1-y^2)x}{2} \tag{3.10}$$

$$G_9 = (1-x^2)(1-y^2) \tag{3.11}$$

Then the elevation of point (x,y) can be obtained by

$$Z = \sum_{i=1}^{9} G_i Z_i. \tag{3.12}$$

Usually the elevation of any point within an area surrounded by nine interpolating points can be interpolated. In this thesis, the consideration is always to use the closest nine points to interpolate, so the points in the small square area around the centre interpolating point are interpolated. As shown in Fig. 3.3, $D_1, D_2, ..., D_{16}$ are points in CRC data base. Only the 24 points around D_6 with 100 m spacing are interpolated by D_1, D_2, D_3, D_5, D_6, D_7, D_9, D_{10}, D_{11}. For the points in area A, instead of using these nine points, they are interpolated by using the points D_6, D_7, D_8, D_{10}, D_{11}, D_{12}, D_{14}, D_{15}, D_{16}, and they are more reliable than interpolated

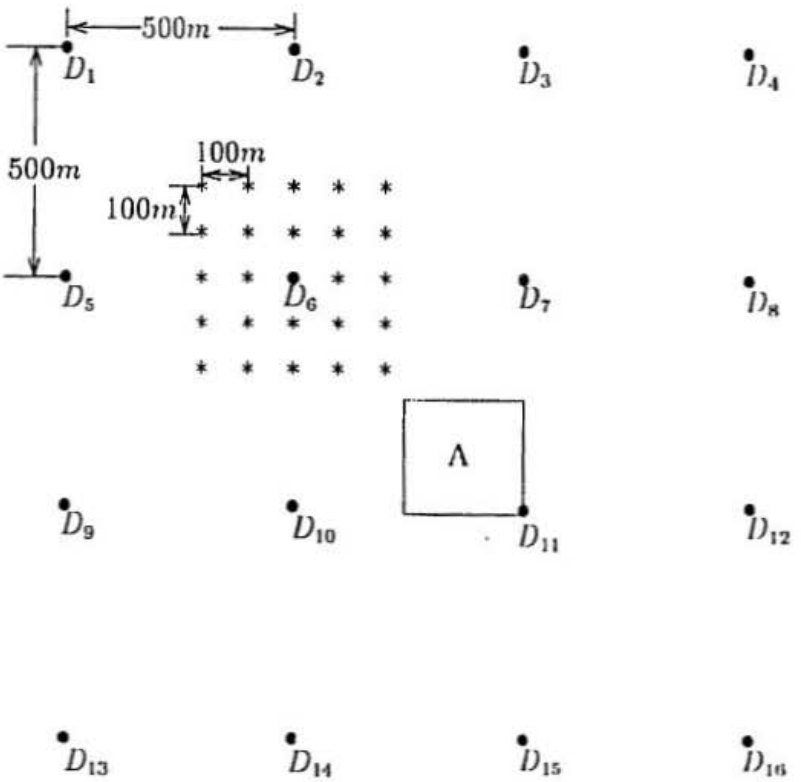

Figure 3.3: The First Step of Interpolation

by the last nine points. In augmenting CRC data base for an area of interest, the interpolation is implemented page by page with every point 100 m apart in northing and easting grids. Within a page, points in the areas near the edges are interpolated by taking some interpolating points from their adjacent pages. After the augmentation, each page has 12,800 points (i.e. 80 x 160, in CRC data base it is 16 x 32) with two columns or two rows on each edge duplicated from their adjoined pages. The duplication is because of the necessity for constructing path profiles which will be discussed in the next section, and also because of the simplicy of the implementation process.

By complete quadratic interpolation, elevations of interpolated points are obtained. For a terrain data base, a secondary but sometimes important piece of information which should be provided is the nature of the ground and ground cover. Therefore, surface codes of interpolated points need to be determined. Considering Eq. (3.12), it can be understood that G_i acts as a weight for its corresponding elevation. In obtaining surface codes, G_i also can be the weight for its corresponding code. In CRC data base, eight types of terrain surface are represented by eight codes (3 bits). Since the surface codes are finite and discrete numbers, for determining the code of a point, weighted vote method is used. This method can be described as following.

Let C_j (j=1,2,...,8) be the eight surface codes, and V_i (i=1,...,m) be the code of each interpolating point, while m=9 for the complete quadratic interpolation. By defining:

$$V_i * C_j = \begin{cases} 1 & V_i = C_j \\ 0 & V_i \neq C_j, \end{cases} \tag{3.13}$$

the weight of the ith interpolating point voted to the jth surface code C_j can be

expressed as:

$$w_{ij} = G_i(V_i * C_j) \tag{3.14}$$

while G_i is the shape function, for complete quadratic interpolation it is given by Eq. (3.3) to Eq. (3.11). Then the accumulated weight W_j which is voted to the jth surface code by all the interpolating points is:

$$W_j = \sum_{i=1}^{m} w_{ij}. \tag{3.15}$$

Among the eight surface codes, the maximum accumulated weight W_k is

$$W_k = \max(W_1, W_2, ..., W_8) \tag{3.16}$$

while the subscript k is equal to the index of the surface code with the maximum accumulated weight. Finally the code of the interpolated point, V, is obtained by

$$V = C_k. \tag{3.17}$$

The first step in the proposed procedure is to employ complete quadratic interpolation and weighted vote method to augment CRC data base with 100 m spacing for interested areas. For the regular terrain, after this step the augmented data base may be accurate enough. However, for the terrain which changes rapidly, some hills may be completely missed within 500 m spacing in CRC data base, and they may also be missed in the augmented data base. Therefore, the second step for making up missed important terrain features and correcting the augmented data base is necessary.

3.2.2 Correction of the Augmented Data Base

In order to see if there is any important terrain feature missed, the second step in proposed procedure starts with drawing out contour maps from augmented data

base. By checking these contour maps with large scale topographic maps (1:50,000 or 1:25,000), if it is found that some hills and valleys are missed or some areas are very different, then the augmented data base needs to be corrected. It would be time consuming if one inserts all the points related to missed hills or valleys into the augmented data by reading them from topographic maps in 100 m spacing. One way to solve this problem is to take the critical points such as the point on the top of missed hill or the bottom of missed valley from topographic maps, and use them with their closest points in CRC data base to interpolate again. Since the points of tops or bottoms of missed hills or valleys have random spacing with the points in CRC data base, triangular interpolations are suitable in this case. There are two method which can be applied. One is linear triangular interpolation, the other is complete cubic interpolation. Since the latter is much more complicated than the former, and also because the interpolation will be carried out in a small area which is less than $0.125\ Km^2$ (half of 0.5 Km x 0.5 Km), therefore linear triangular method is chosen for the second step of interpolation.

The linear triangular interpolation can be described as follows. The interpolation polynomial is

$$Z = a_0 + a_1 x + a_2 y. \tag{3.18}$$

Fig. 3.4 shows a triangle formed by three interpolating points 1, 2, 3. Let (x_1, y_1), (x_2, y_2), (x_3, y_3) be the coordinates of points 1, 2, 3, and Z_1, Z_2, Z_3 be their elevations, respectively. Substituting these three points into Eq. (3.18), we have:

$$\begin{pmatrix} Z_1 \\ Z_2 \\ Z_3 \end{pmatrix} = \begin{pmatrix} 1 & x_1 & y_1 \\ 1 & x_2 & y_2 \\ 1 & x_3 & y_3 \end{pmatrix} \begin{pmatrix} a_0 \\ a_1 \\ a_2 \end{pmatrix}. \tag{3.19}$$

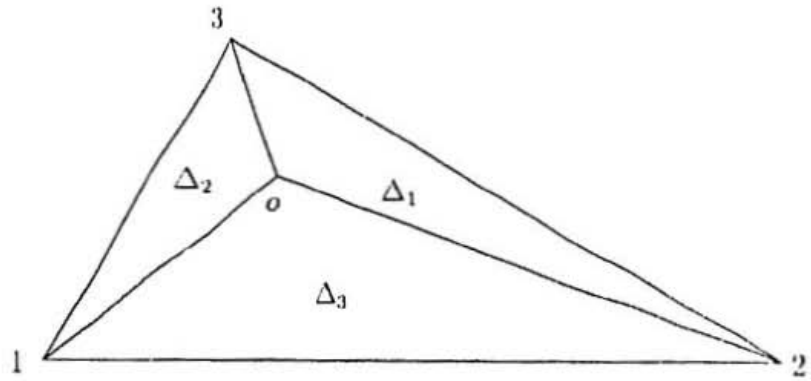

Figure 3.4: Linear Triangular Interpolation

For convenience, Eq. (3.19) can be represented as:

$$\mathbf{Z_n} = \mathbf{CA} \tag{3.20}$$

where

$$\mathbf{Z_n} = \begin{pmatrix} Z_1 \\ Z_2 \\ Z_3 \end{pmatrix}, \tag{3.21}$$

$$\mathbf{C} = \begin{pmatrix} 1 & x_1 & y_1 \\ 1 & x_2 & y_2 \\ 1 & x_3 & y_3 \end{pmatrix}, \tag{3.22}$$

$$\mathbf{A} = \begin{pmatrix} a_0 \\ a_1 \\ a_2 \end{pmatrix}. \tag{3.23}$$

Then the coefficients can be obtained by:

$$\mathbf{A} = \mathbf{C}^{-1}\mathbf{Z_n}. \tag{3.24}$$

So, the interpolation polynomial is determined and can be represented as:

$$Z = \begin{pmatrix} 1 & x & y \end{pmatrix} \mathbf{A} = \begin{pmatrix} 1 & x & y \end{pmatrix} \mathbf{C}^{-1}\mathbf{Z_n} = \mathbf{G}\mathbf{Z_n} \tag{3.25}$$

where

$$\mathbf{G} = \begin{pmatrix} G_1 & G_2 & G_3 \end{pmatrix} = \begin{pmatrix} 1 & x & y \end{pmatrix} \mathbf{C}^{-1}. \tag{3.26}$$

G_1, G_2, G_3 are called shape function. By manipulating Eq. (3.26), they can be expressed by:

$$G_1 = \frac{\begin{vmatrix} 1 & x & y \\ 1 & x_2 & y_2 \\ 1 & x_3 & y_3 \end{vmatrix}}{\begin{vmatrix} 1 & x_1 & y_1 \\ 1 & x_2 & y_2 \\ 1 & x_3 & y_3 \end{vmatrix}} = \frac{\Delta_1}{\Delta} \tag{3.27}$$

$$G_2 = \frac{\begin{vmatrix} 1 & x & y \\ 1 & x_3 & y_3 \\ 1 & x_1 & y_1 \end{vmatrix}}{\begin{vmatrix} 1 & x_1 & y_1 \\ 1 & x_2 & y_2 \\ 1 & x_3 & y_3 \end{vmatrix}} = \frac{\Delta_2}{\Delta} \tag{3.28}$$

$$G_3 = \frac{\begin{vmatrix} 1 & x & y \\ 1 & x_1 & y_1 \\ 1 & x_2 & y_2 \end{vmatrix}}{\begin{vmatrix} 1 & x_1 & y_1 \\ 1 & x_2 & y_2 \\ 1 & x_3 & y_3 \end{vmatrix}} = \frac{\Delta_3}{\Delta} \tag{3.29}$$

where Δ is the area of the triangle 1-2-3, and Δ_1, Δ_2, Δ_3 are the areas of the triangles o-2-3, o-1-3, and o-1-2 in Fig. 3.4, respectively. Point o (x, y) is any point within the triangle 1-2-3. So, the elevation of point o can be obtained as:

$$Z = \sum_{i=1}^{3} G_i Z_i. \tag{3.30}$$

This equation is similar to Eq. (3.12). About the surface code of point o, it can also be determined by the weighted vote method as stated in last subsection, except that m=3 in this case and G_i is defined as in Eq. (3.27), Eq. (3.28), and Eq. (3.29).

In the implementation of the second step of proposed procedure, first read from a topographic map the latitude, longitude, elevation, surface type of a point on the top or the bottom of a missed hill or a valley, or any point which is needed to insert its information into the augmented data base. According to the latitude, longitude, use the index routine to find its closest four points in CRC data base. Fig. 3.5 is the diagram, where bullets are the points in CRC data base, circle is the point read from a topographic map. By forming four triangles, the linear triangular interpolation is carried out for each of them respectively. The interpolated points in these four triangles are all 100 m spacing, and they are taken to replace the

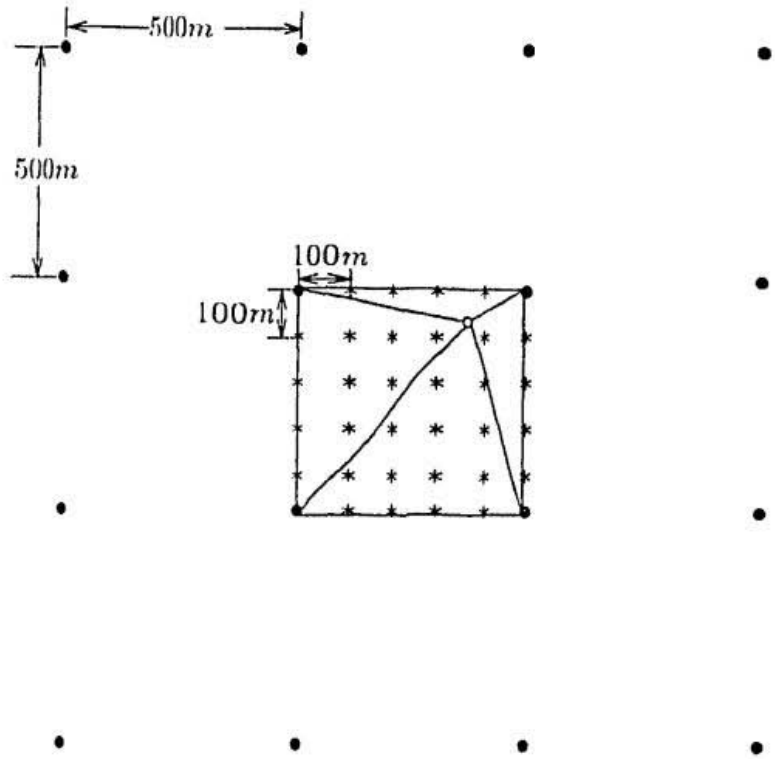

Figure 3.5: The Second Step of Interpolation

corresponding points in augmented data base. Therefore, the augmented data base is corrected and called modified data base. If a point read from a topographic map happens to be right on the 100 m spacing point, it will stay in the modified data base, otherwise only its interpolated points are in the data base to reflect its information. For any area of interest, the process of correcting the augmented data base is repeated until the modified data base agrees with the topographic maps. The modified data base has 12,800 points (i.e. 80 x 160) in every page.

3.2.3 Summary

The proposed procedure for modifying CRC data base consists of two steps. The first step is to use complete quadratic method and weighted vote method to interpolate elevations and surface codes from CRC data base and obtain augmented data base with points of 100 m spacing. The second step is to take the critical points from topographic maps which represent important terrain features but are missed in CRC and augmented data base, then by applying linear triangular interpolation for elevations and weighted vote method for surface codes to obtain the points with 100 m spacing and replace their corresponding points in augmented data base. After these two steps, the higher resolution and accurate data base is obtained. This procedure can be applied to any interested area.

The following is an example to show the results of the modification to CRC data base. In Fig. 3.6, it is a contour with the interval of 25 feet elevation drawn out from the points read directly from the topographic map (1:25,000) with 100 m spacing. It is a 2 Km x 2 Km area (latitude 47°36'31" to 47°37'36", longitude 52°57'23" to 52°58'59") in Bell island near St. John's, Newfoundland. This contour

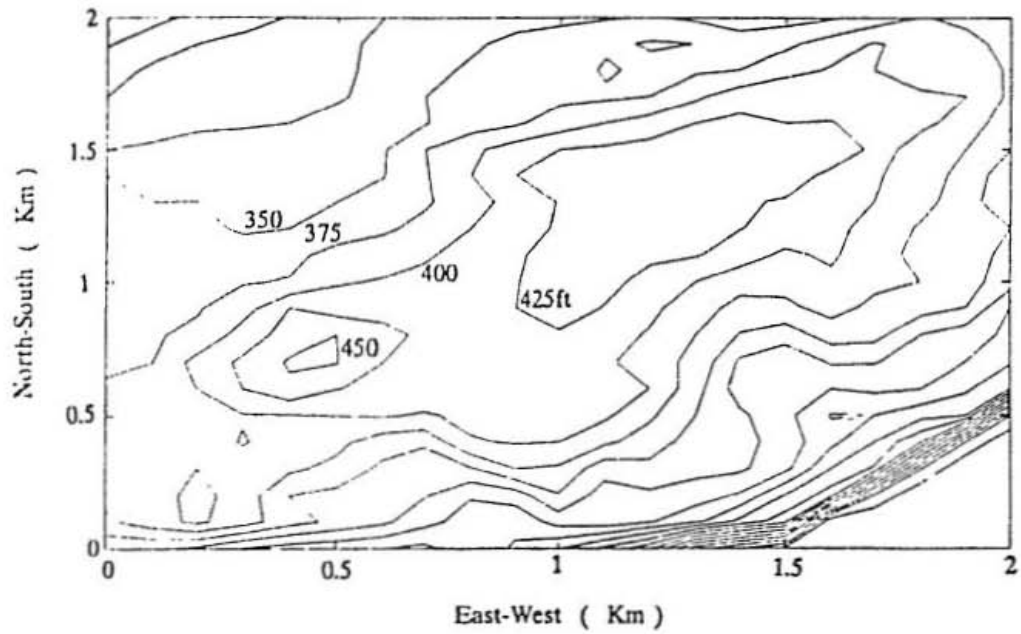

Figure 3.6: Contour from Topographic Map

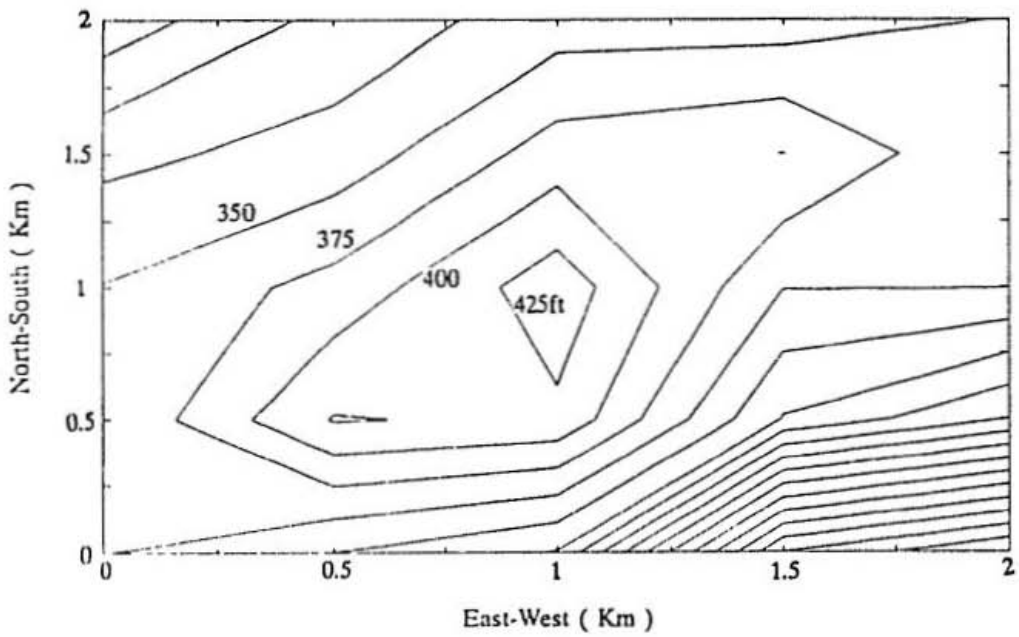

Figure 3.7: Contour from CRC Data Base

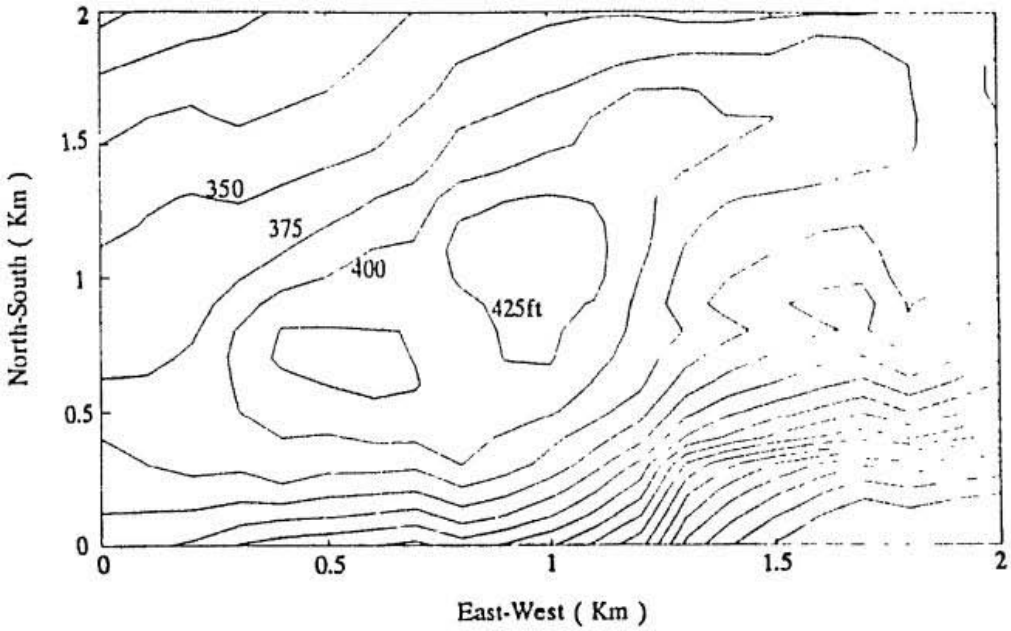

Figure 3.8: Contour from Augmented Data Base

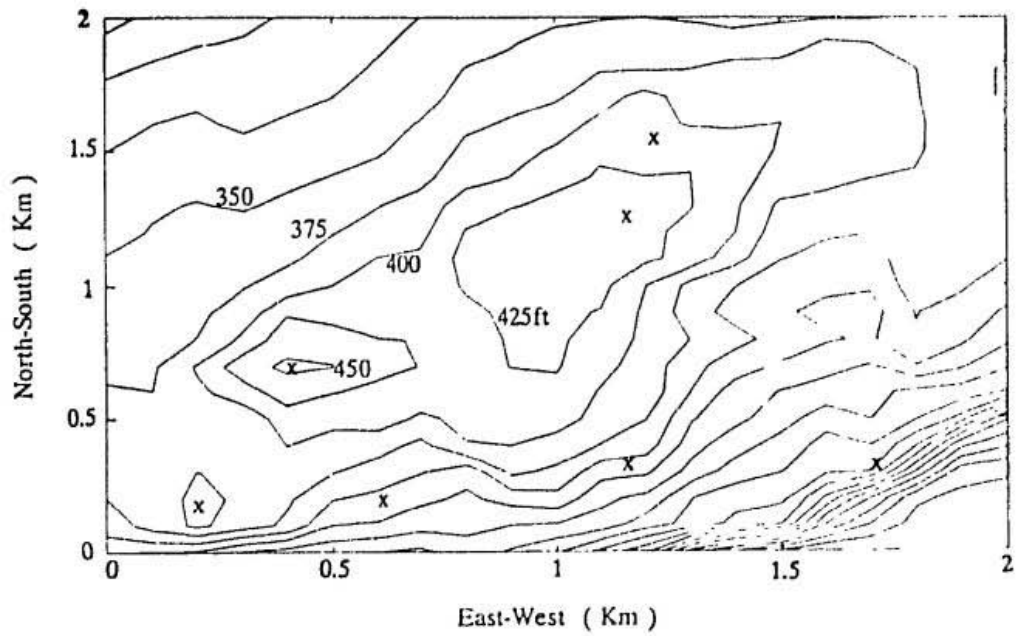

Figure 3.9: Contour from Modified Data Base

can be used as a reference. For the same area, Fig. 3.7 shows the contour from CRC data base. It can be seen that this figure is very different from Fig. 3.6. Fig. 3.8 represents the result from the augmented data base after the first step in the proposed procedure. Although this result provides a lot more details than that of CRC data base, comparing it with the reference, there are still some important features missed. By implementing the second step in proposed procedure, seven critical points in this area have been taken from the topographic map to correct the augmented data base. Fig. 3.9 shows the result of the second step from the modified data base. The locations of the points read from the map are marked by 'x'. Comparing Fig. 3.9 with Fig. 3.6 (i.e. the reference), it is clearly seen that Fig. 3.9 is much closer to the reference than Fig. 3.7. Therefore, the modified data base is much more accurate than CRC data base. It can be concluded that the proposed procedure for modifying CRC data base is an economical and practical way to obtain higher resolution and more accurate terrain data base. This is a major contribution of our research work in improving the propagation loss predictions as well as other applications.

3.3 Construction of Path Profiles

Terrain data bases are used to provide path profiles for propagation loss predictions. The construction of path profiles will be briefly discussed.

When the positions of transmitter and receiver are given, the transmission path is the line connecting these two points along the great circle. The length and the azimuth of this line can be obtained by solving the spheric triangle N-T_x-R_x in Fig. 3.10, while N is the north pole, and T_x, R_x denote the transmitter and the receiver.

If this path is within the data base area, the path profile can be constructed from the data base. In CRC method, discrete points on the path line are chosen by approximately 500 metres apart. Corresponding to each of these points, its closest four points in the CRC data base can be found, and the elevation is obtained by these four point linear interpolation. In this thesis, discrete points are taken with approximate 100 metres away from each other on a path line. For each of these points, nine closest points in the modified data base can be found and the elevation is obtained by complete quadratic interpolation as presented in the last section. The surface code is determined by weighted vote method. After every discrete point on a path line has obtained its elevation and surface code, the path profile from a data base is formed. The path profiles constructed from the modified data base are called modified path profiles. The construction of modified path profiles and the flow chart of this routine will be presented in detail in Chapter 5.

A path profile constructed from a terrain data base is not ready for use in propagation loss prediction calculations, because the effect of the effective earth's curvature needs to be taken into account. In this thesis, the effective earth radius factor is normally assumed as 4/3, unless otherwise noted. The heights of some trees and buildings should be also added to a path profile as stated in Chapter 2. Moreover, since the terrain features near transmitter and receiver are essential to propagation loss predictions, within 1 Km distances from transmitter and receiver more points with 50 m apart are interpolated. The path profile is now ready for use in the propagation loss prediction calculations.

Fig. 3.11 shows a path profile constructed from CRC data base with transmitter at 47°30'22" latitude, 52°50'47" longitude, and receiver at 47°30'22" latitude,

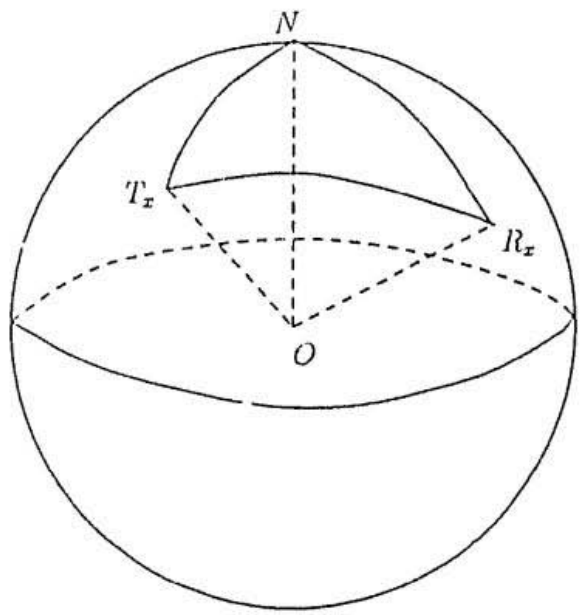

Figure 3.10: Spherical Triangle

52°38'13" longitude. Fig. 3.12 is the corresponding path profile constructed from the modified data base. These two profiles include the earth's curvature and the heights of some trees and buildings. Comparing these two profiles, at 8 Km distance from the transmitter, there is a hill missed in CRC profile. Around 4 Km distance, the modified path profile is discontinuous. This is caused by the surface type. In this case the surface type is tree, so the elevations of these points increase by 10 to 20 m. In the CRC profile, due to the 500 m spacing leads to the loss of a part of terrain which has no tree cover, so the elevations of this part of the CRC profile are all covered with trees. It is clearly demonstrated that the modified profile has much more detail and is more accurate than the CRC profile.

It can be seen that the propagation loss prediction results based on the modified data base will be different from those based on CRC data base. More accurate terrain data base provides more accurate path profiles, and the propagation loss predictions are therefore more accurate.

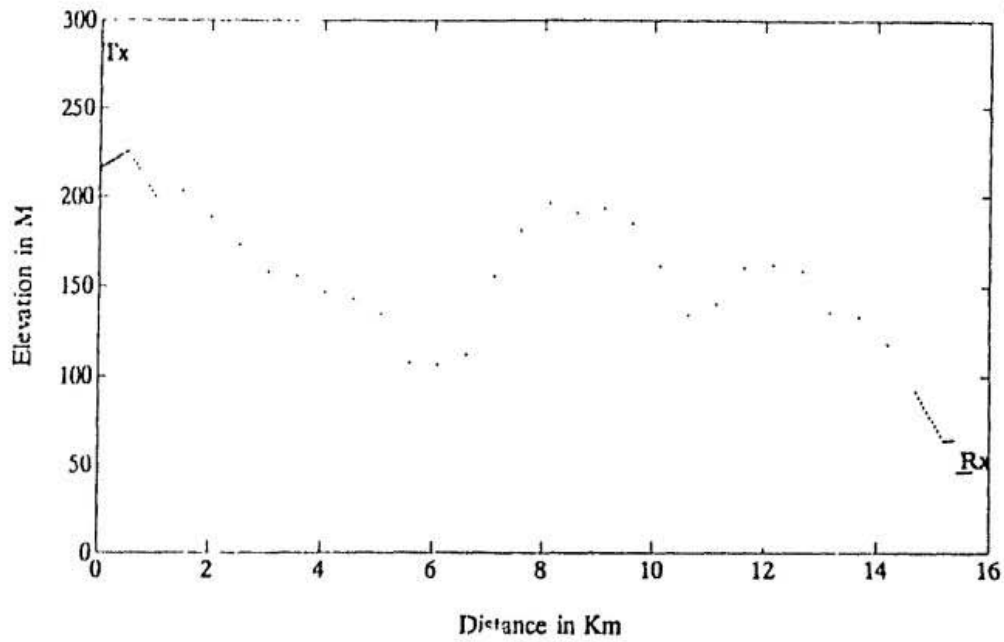

Figure 3.11: Path Profile from CRC Data Base

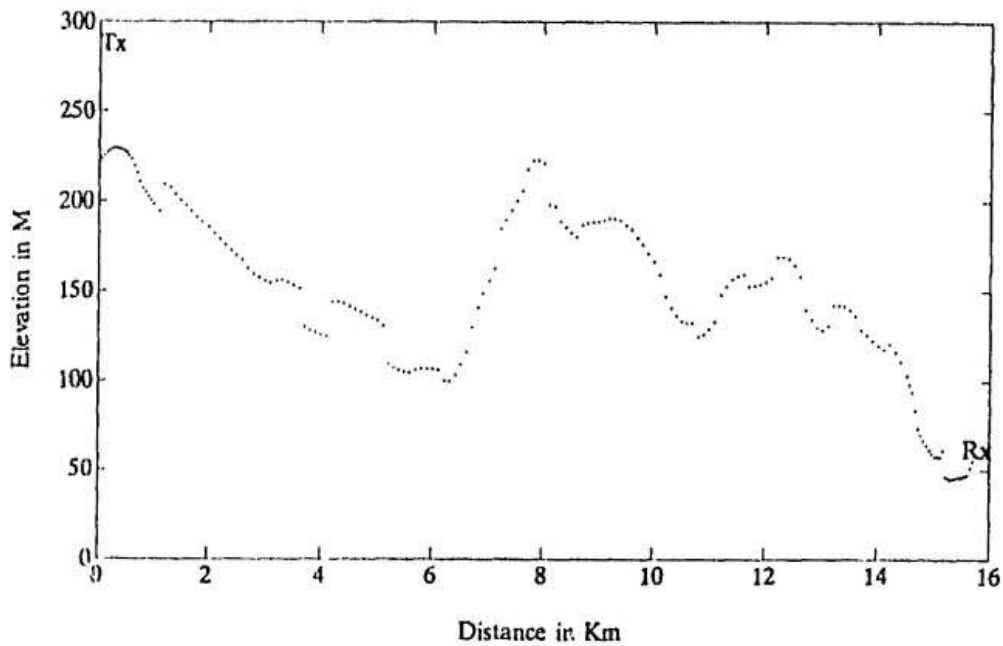

Figure 3.12: Path Profile from Modified Data Base

Chapter 4

Modification of Diffraction Loss Prediction

Since in land mobile radio communications, almost 95% of the radio links is non-line-of-sight, so diffraction loss is one of the main parts in the propagation loss. Diffraction losses over a knife edge, a rounded obstacle, and multiple obstacles were described in Chapter 2. In this thesis, all obstacles on path profiles are treated as rounded obstacles, and de Assis method for evaluating the diffraction loss over multiple rounded obstacles is applied. The following sections will discuss the effects of modified path profiles on diffraction loss, and the modifications to the diffraction loss prediction.

4.1 The Effects of Modified Profiles

As presented in Chapter 3, CRC terrain data base has been modified, and modified path profiles provide more details than CRC profiles. This modification has the significant effect on diffraction loss, since diffraction loss is entirely dependent on the parameters of path profiles. It is described in Chapter 2 that the diffraction loss over a single rounded obstacle is the function of H/R, α, the minimum effective

antenna heights of the transmitter and the receiver. H is the height of obstacle referred to the line of sight, R is the radius of first Fresnel zone. α is the function of frequency, R, and the radius of curvature of obstacle's crest r. If a hill in a path profile has its $H/R \geq$ -0.6, it will be considered as an obstacle to the propagation path. The diffraction loss over multiple rounded obstacles can be evaluated by de Assis method discussed in Chapter 2. The diffraction loss prediction for a given path profile can be implemented in three steps. The first step is to select important obstacles based on H/R. The second step is to determine the parameter r and calculate individual obstacle's diffraction loss. The last is to sum all the individual diffraction losses and correct the sum if some obstacles are closely spaced. In the diffraction loss calculation, the parameters related to the geometry of a path profile are, H, r, path length and locations of obstacles (which affect R), the ground elevations under the transmitter and the receiver (which affect H), the number of obstacles, and their spacings (which affect correction factor for the closeness). For a given transmission path, compared with the CRC path profile, the modified profile usually has more hills, and has different heights of hills, different radii of hills' crests, and different elevations under the transmitter and the receiver. Therefore, the hills which are selected as the obstacles to the propagation based on H/R may be different in these two profiles. And the parameters as H/R, r, the minimum effective antenna heights and correction factor may all be changed. So, the results of diffraction loss will be different.

Following is an example to demonstrate how a modified path profile causes a different diffraction loss. If only the first three prior obstacles are considered, Fig. 4.1 shows the CRC path profile (the same as in Fig. 3.11) and the three obstacles

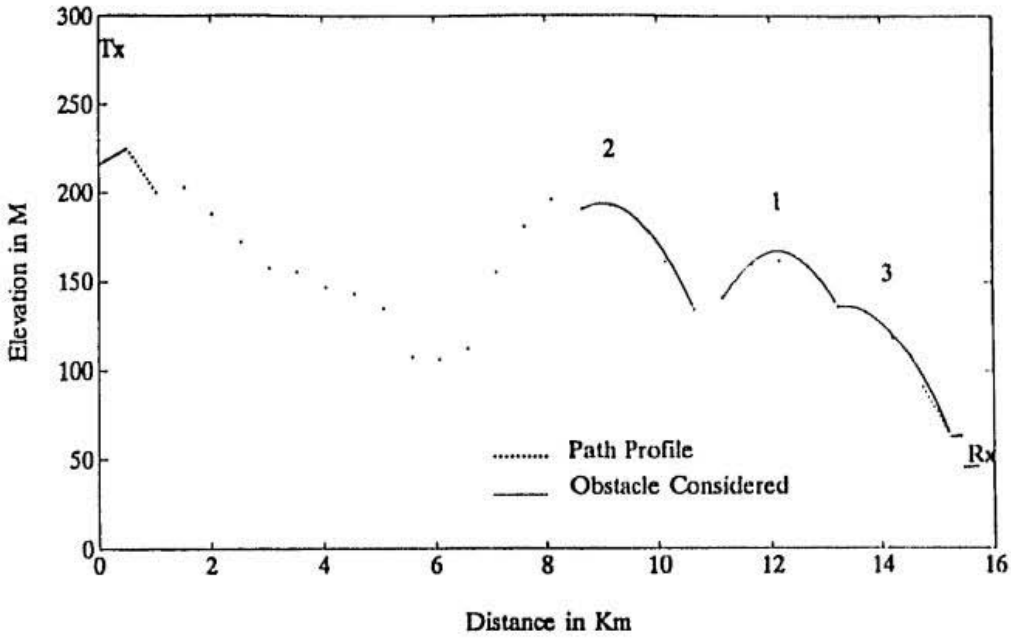

Figure 4.1: CRC Path Profile

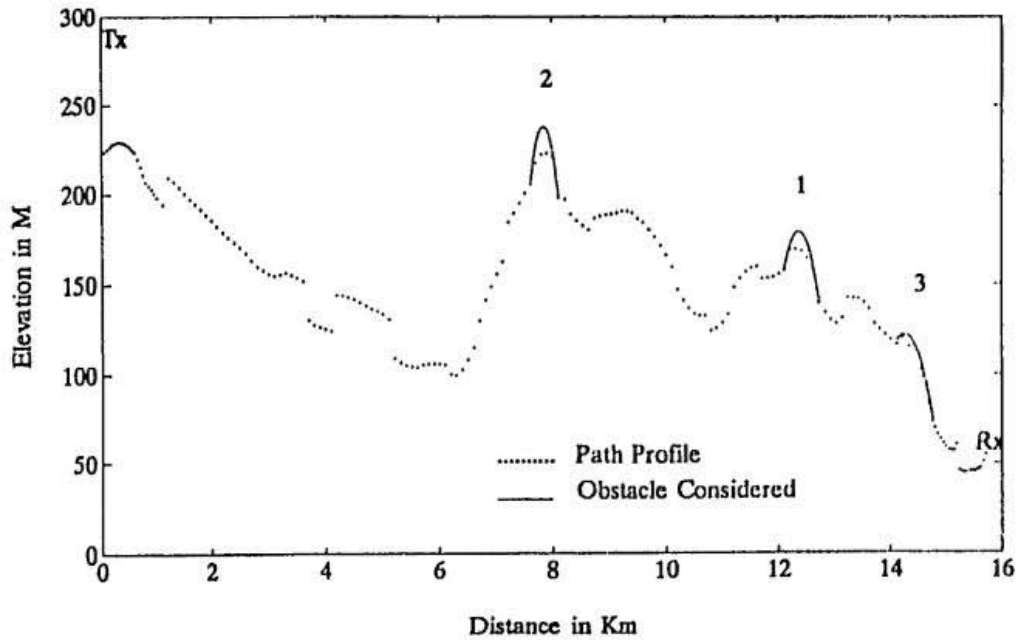

Figure 4.2: Modified Path Profile

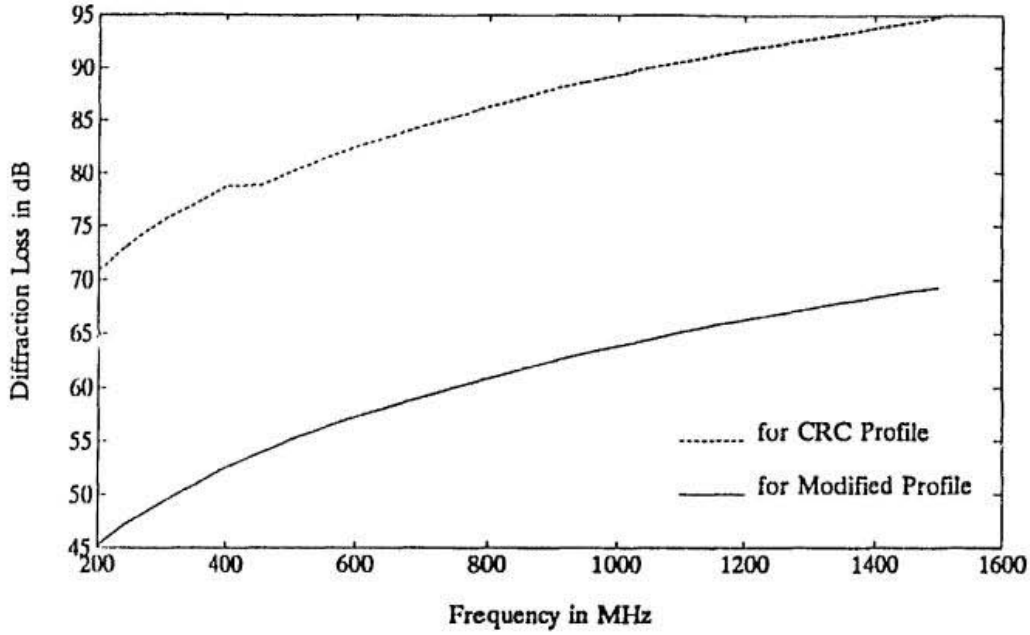

Figure 4.3: Diffraction Losses vs. Frequency

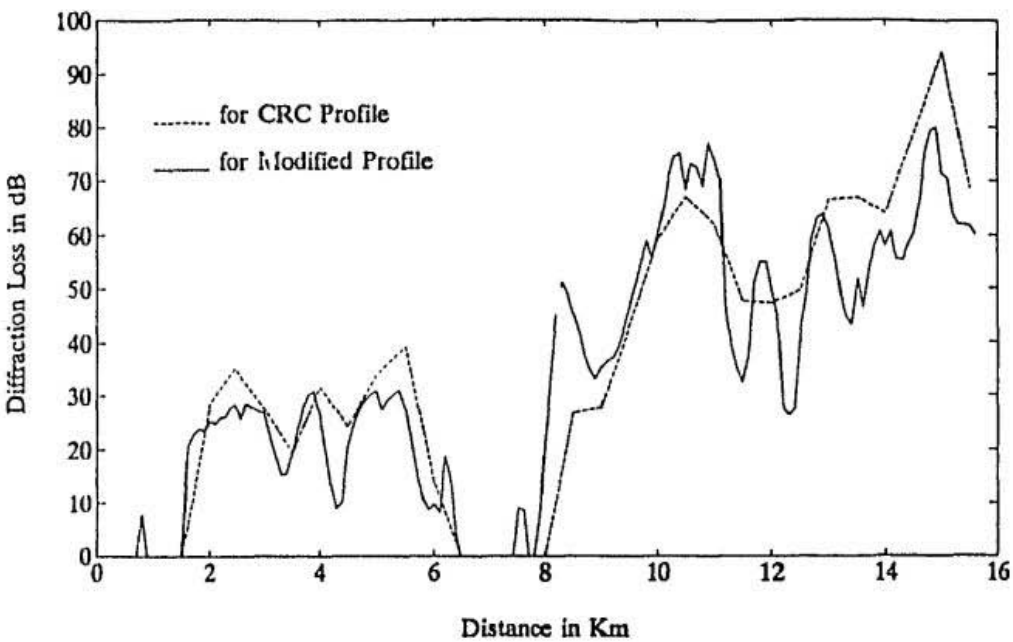

Figure 4.4: Diffraction Losses vs. Distance

with parabolic fittings and their priority numbers. Fig. 4.2 is the modified profile (the same as in Fig. 3.12) and three obstacles. In these two figures, the transmitter (T_x) is located at 47°30'22" latitude, 52°50'47" longitude, and the receiver (R_x) at 47°30'22" latitude, 52°38'13" longitude. It can be seen that the first prior obstacles in these two figures are in about the same locations, but their radii of the crests are very much different. This is because the 500 m spacing in CRC profile causes the loss of terrain details around 12 Km from the transmitter, so it considered a larger distance range for this obstacle. The same situation occurs to the third obstacle. In these two profiles, the second obstacles are selected at different locations and their radii of the crests are also very different. Since the CRC profile missed the top of a hill at about 8 Km distance from T_x, so the other hill at about 9 Km is selected. It can also be seen that the terrain elevations under the transmitter and the receiver in the modified profile are a little bit higher than those in the CRC profile. This is one of the reasons that result in change in H with respect to the line of sight. The results of diffraction loss over these two profiles versus frequency are given in Fig. 4.3, where the transmitter and receiver antenna heights are 61 m and 1.8 m. The diffraction loss for the CRC profile has about 25 dB more than that for the modified profile (only three obstacles are considered). In this example, H/R for the first and the third obstacles is not sizably changed in these two profiles. For the second obstacle, H/R in the modified profile is larger than that in the CRC profile, and this alone will cause a higher diffraction loss. However since for these three obstacles the radii of the crests in the modified profile are all less than those in the CRC profile, so the resultant diffraction loss is less. The difference between the diffraction losses for CRC and the modified profiles is different from

case to case. In different cases, modified profiles have different changes in these parameters, and the combined effects of all the parameter changings cause different results. For some transmission paths, diffraction losses for modified profiles are more than those for the corresponding CRC profiles, and for some others, they may be less. In the example shown above, if the receiver moves away from the transmitter along the path in Fig. 4.1 or Fig. 4.2, then for different locations of the receiver the parameters related to the geometry of profiles will be different. Fig 4.4 shows the diffraction losses against distance between transmitter and receiver for CRC profile and modified profile. The transmitter and receiver antenna heights are the same as before. Compared the two results in this figure, it is noticed that at about 8.5 Km distance the diffraction loss for the modified profile has about 20 dB more than that for the CRC profile because of the missed hill at 8 Km in the CRC profile. From this figure it can be seen that diffraction loss is very sensitive to the change in its path geometry. Since CRC data base has been modified, and modified path profiles are more accurate, the diffraction losses calculated based on them are more reliable than the results based on CRC profiles.

4.2 Determination of the Radius of Curvature of Obstacle's Crest

In the implementation of diffraction loss prediction for a path profile, the important step is to determine accurately the parameters related to the geometry of the path profile. Usually, first obtain the minimum effective antenna heights and draw the line of sight. Then determine H/R for every point and select the main obstacle which includes the point with maximum H/R ($\geq$ -0.6). Based on Deygout

method described in Chapter 2, H/R for other obstacles can also be obtained. Since the shape of obstacles (especially for hills) is generally close to parabolic curves, the parameter r is determined by a radius of curvature of the fitted parabola. In CRC method, the radii of curvature of hills' crests are obtained in two steps. First, find the beginning and the end points for all hills. By parabolic fitting to each set of consecutive three points, if the radius of curvature of the second point is negative, then this point is a turning point and considered as a begining of the next hill or an end point of the present hill. Second, determine the radius of each hill's top by three point parabolic fitting. The three points are the begining and the end points of a hill, and any point between these two points which makes a minimum radius of curvature. This minimum radius of curvature is taken as the radius of the hill's top. There is a problem in this method. If a hill is steep, the point which forms a minimum radius of curvature may not be near the top of the hill or even it is near, but the parabola may not be close to the top. Therefore, a minimum radius of curvature does not properly represent the radius of a hill's top. In this thesis, an improved method for determining the radius of obstacle's crest is proposed.

Since not all the hills in a profile are obstacles to the propagation path, it is unnecessary to find radii for all the hills. In the proposed method, only the radii of crests of hills which become obstacles are determined. It can be described by three steps. The first step is to find the range of an obstacle which is suitable for the parabolic fitting to its crest. When a point P_o (x_o, y_o) which has maximum H/R is found, the corresponding obstacle needs to be determined. On the left side and right side of P_o, search the begining and the end points of the obstacle by the same way as in the CRC method. These two points may not have the same distance to

point P_o. Usually the shape of an obstacle's crest has better symmetry than that of the whole obstacle's shape. To fit a parabola to the crest, take the closest point as one end of the fitting range, and on the other side of P_o obtain the point with equal distance as the other end. The second step is to do least-squares parabolic fitting to the points within the range determined in the first step. To fit an obstacle, let the expected parabola curve be

$$y(x) = a_0 + a_1 x + a_2 x^2. \tag{4.1}$$

Then the total error E_s between this curve and all the points within the fitting range is

$$E_s = \sum_{i=1}^{N} (y_i - \sum_{j=0}^{2} a_j x_i^j)^2 \tag{4.2}$$

where N is the total number of points (x_i, y_i) within the fitting range. Since for different obstacle the length of fitting range is different, so N is also different from one obstacle to another.

The minimum value of E_s is determined by

$$\frac{\partial E_s}{\partial a_j} = 0. \tag{4.3}$$

Substituting Eq. (4.2) to Eq. (4.3), it can be derived as:

$$\begin{aligned}
a_0 N + a_1 \sum_{i=1}^{N} x_i + a_2 \sum_{i=1}^{N} x_i^2 &= \sum_{i=1}^{N} y_i \\
a_0 \sum_{i=1}^{N} x_i + a_1 \sum_{i=1}^{N} x_i^2 + a_2 \sum_{i=1}^{N} x_i^3 &= \sum_{i=1}^{N} x_i y_i \\
a_0 \sum_{i=1}^{N} x_i^2 + a_1 \sum_{i=1}^{N} x_i^3 + a_2 \sum_{i=1}^{N} x_i^4 &= \sum_{i=1}^{N} x_i^2 y_i
\end{aligned} \tag{4.4}$$

Using Gaussian elimination or Cramer's rule, a_0, a_1, a_2 can be solved, therefore the

parabolic curve is determined.

The third step is to obtain the radius of curvature of obstacle's crest. For any function $f(x)$ the curvature is defined as

$$\kappa = \frac{y''(x)}{[1 + y'^2(x)]^{3/2}}, \tag{4.5}$$

and the radius of curvature is

$$r = \frac{1}{\kappa}. \tag{4.6}$$

For the parabolic function in Eq. (4.1), the radius of curvature at any point (x, y) can be derived as:

$$r(x) = \frac{[1 + (a_1 + 2a_2x)^2]^{3/2}}{2a_2}. \tag{4.7}$$

Since point P_o (x_o, y_o) may not be on the fitted parabola, let (x_o, y_{oc}) be its corresponding point on the parabola. Then the radius of curvature of the fitted parabola at point (x_o, y_{oc}), i.e. $r(x_o)$, is taken as the radius of the obstacle's crest.

Fig. 4.5 shows the least-squares parabolic fittings for three obstacles and the obtained radius values on the profile which is the same as in Fig. 4.2. The result of CRC three point parabolic fittings and the radii for the same obstacles is given in Fig. 4.6. It can been seen that the parabolic fittings in Fig. 4.5 is much closer to the obstacles than those in Fig. 4.6. The radii of curvature determined by the proposed method are therefore more accurate than those by CRC method. The diffraction losses calculated by the radii from the proposed method and from CRC method are shown in Fig. 4.7. The transmitter and receiver antenna heights are also 61 m and 1.8 m. In this case the difference on the diffraction loss is about 1.2 dB. For some other cases the difference can be more than that. Since the proposed method gives more accurate radius of curvature, the prediction results of diffraction

loss are improved.

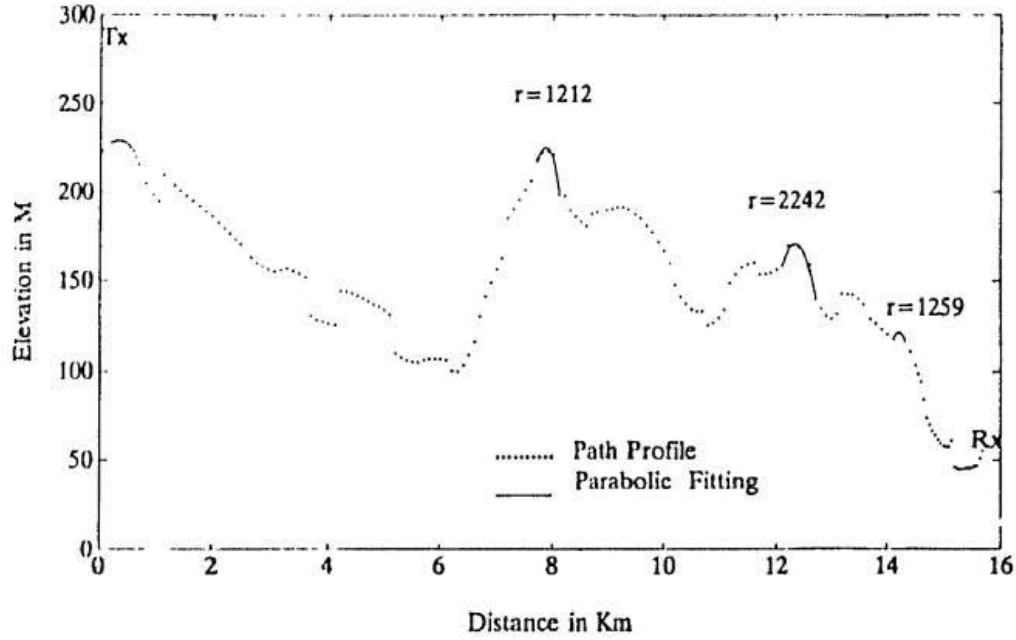

Figure 4.5: The Proposed Method for Radius

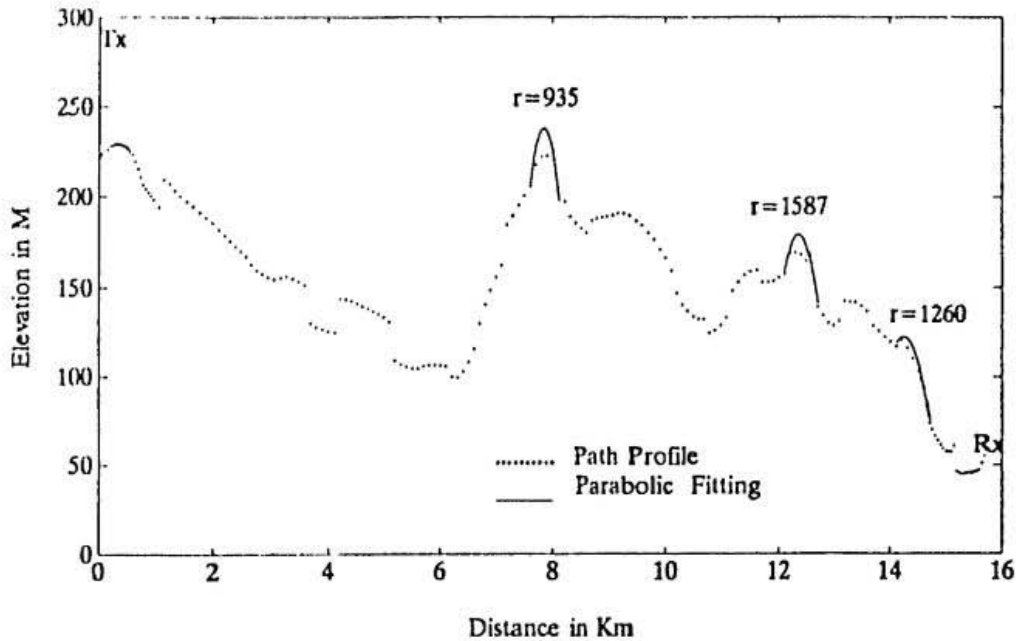

Figure 4.6: CRC Method for Radius

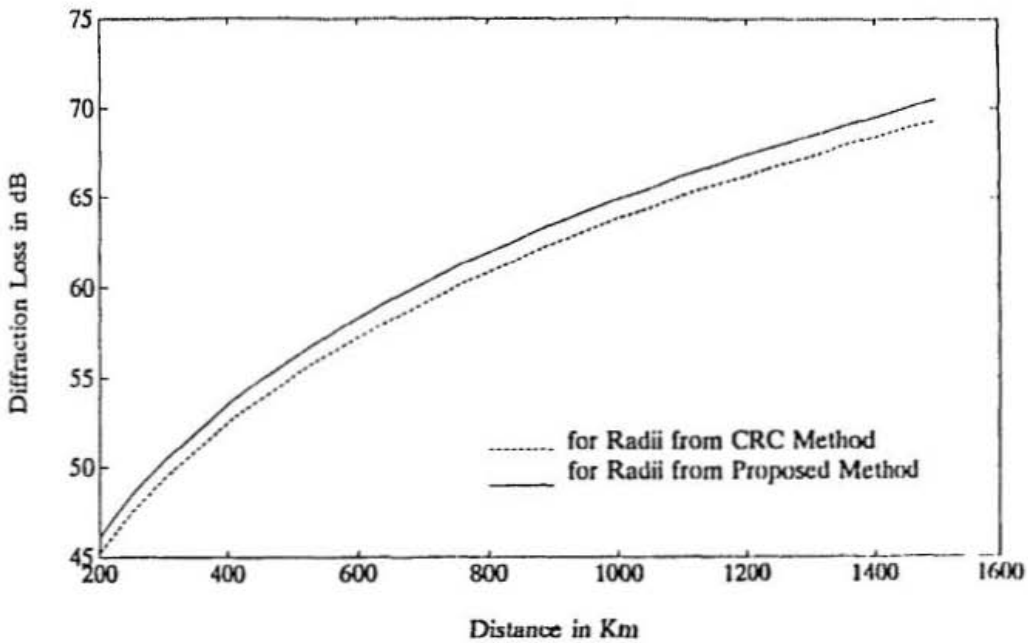

Figure 4.7: Diffraction Losses Based on the Radii from Two Methods

4.3 Correction Factor

Diffraction loss over multiple obstacles can be evaluated by Deygout's multiple knife edge method as presented in Chapter 2. In this method, the total diffraction loss is formed by summing all individual diffraction losses which are calculated using the parameters determined by a certain rule. M.S. de Assis applied Deygout multiple knife edge method to multiple rounded obstacles and found that this combination has good agreement with experiments [35]. However, Deygout method and de Assis methods do not include the consideration for the case when two obstacles are close to each other. In this case both these methods give excess total losses. A few correction factors have been developed [30]. Most of these conventional corrections use many empirical coefficients and are complicated for computer implementation. Recently, J. Deygout has published a correction factor for his multiple knife edge method [43]. In his paper, the results of this correction factor were compared with Millington's curves and found the difference never exceeds 1 dB. It was also compared with Giovaneli's measurements and it showed very good agreement [43]. Since this modification is given by a simple mathematical expression, it is easier for understanding and much more convenient for use. Based on de Assis' idea in dealing with rounded obstacles, in this thesis, this Deygout correction factor is introduced to handle multiple rounded obstacles. Deygout correction factor is stated in the following.

Fig. 4.8 shows the diagram of a transmission path consisting of two obstacles, where m_1 and m_2 are two obstacles, h_1 and h_2 are the height referred to the line of sight. m_1 is the main obstacle, and h' is the relative height of m_2. These obstacles are treated as knife edges. The correction factor takes into account the spacing of

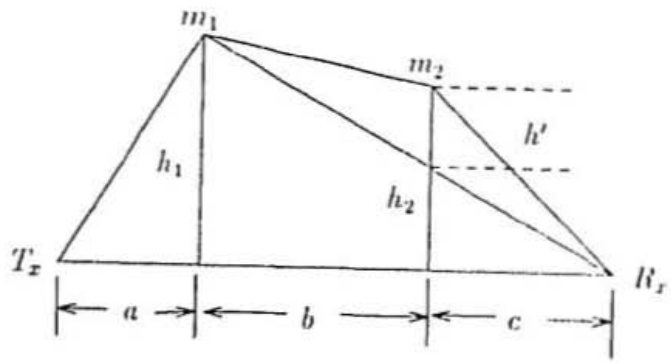

Figure 4.8: The Typical Transmission Path with Two Obstacles

the obstacles and their relative heights. The spacing is characterized by

$$\tan\beta = \sqrt{\frac{b(a+b+c)}{ac}}. \tag{4.8}$$

The radii of first Fresnel zone for these two obstacles are given by

$$R_1 = \sqrt{\frac{\lambda a(b+c)}{a+b+c}} \tag{4.9}$$

$$R_2 = \sqrt{\frac{\lambda c(a+b)}{a+b+c}}. \tag{4.10}$$

The parameters p and q describing the heights related to the first Fresnel zone size, are defined as

$$p = \frac{h_1}{R_1}\sqrt{2} \tag{4.11}$$

$$q = \frac{h_2}{R_2}\sqrt{2} \tag{4.12}$$

p will be always assigned to the main obstacle. For the particular case p=q=0, this is when both obstacles are on the line of sight, Deygout derives the correction factor from Millington's formula and nomograph [11] as:

$$C_{f_o} = 12 - 20\log(\frac{2}{1-\beta/\pi}). \tag{4.13}$$

And he admitted that this factor is valid for $p = q$ case, i.e. when the summits of the obstacles are located on the same ellipse. Then he gives more general formula for taking into accout the case when $q < p$. The final correction factor is:

$$C_f = [12 - 20\log(\frac{2}{1-\beta/\pi})](\frac{q}{p})^{2p}. \tag{4.14}$$

Therefore the total diffraction loss for the path shown in Fig.2.13 is expressed as:

$$L_d = L_m + L_s - C_f \tag{4.15}$$

where L_m is the diffraction loss by the main obstacle and L_s is that by the secondary one. In the calculation of the individual loss, parameter H/R for m_1 is h_1/R_1, for m_2 it is h'/R', where

$$R' = \sqrt{\frac{\lambda bc}{b+c}}. \tag{4.16}$$

It can be seen from the equations above that, when the distance b between m_1 and m_2 decreases, β decreases and the amount of correction increases. On the other hand, when the relative heights of these obstacles are close, q/p is close to 1, the amount of correction is more.

Following is an example of applying Deygout correction factor to de Assis method for multiple rounded obstacles. Fig. 4.9 is a modified path profile with the first three prior hills as the important obstacles, while the transmitter is at 47°22'35" latitude, 52°59'45" longitude, the receiver at 47°22'35" latitude, 52°37'5" longitude. Fig. 4.10 shows the diffraction losses for this profile calculated by de Assis method without correction and with Deygout correction factor. The transmitter and the receiver antenna heights are set at 61 m and 1.8 m. As shown in Fig. 4.10, the diffraction loss is improved by 5 dB with the Deygout correction.

4.4 The Number of Obstacles Considered

Usually, within well designed coverage areas for mobile radio systems, transmission paths may only have a couple of obstacles on the terrain. However, in site selections, trial transmission paths may encounter a lot more obstacles, especially in the hilly terrain. The de Assis method for multiple rounded obstacles does not have the limit on the number of obstacles. In the implementation of the de Assis method, CRC prediction program calculates the diffraction loss for maximum three

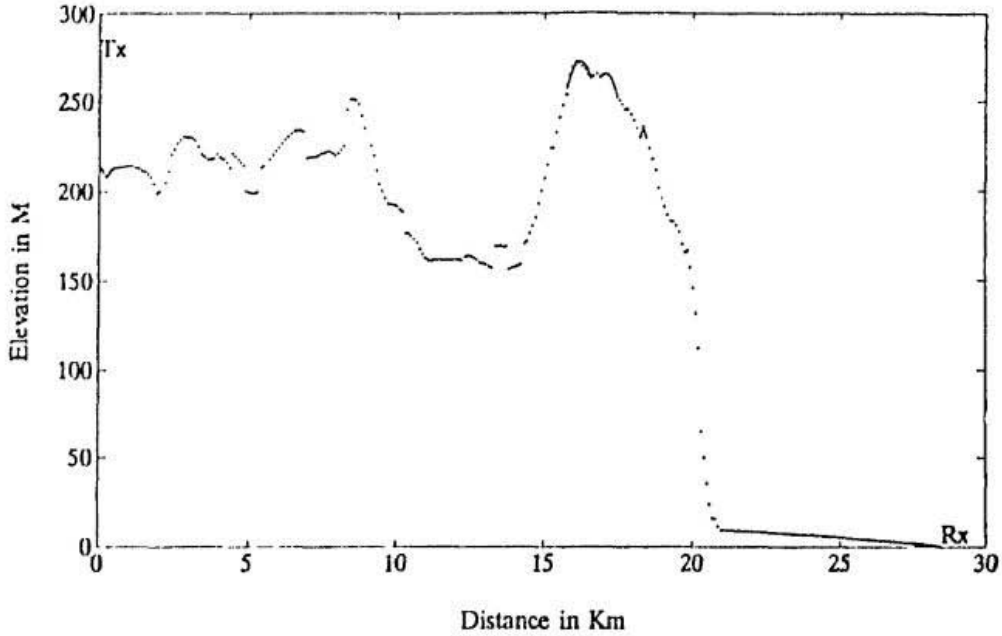

Figure 4.9: Modified Path Profile

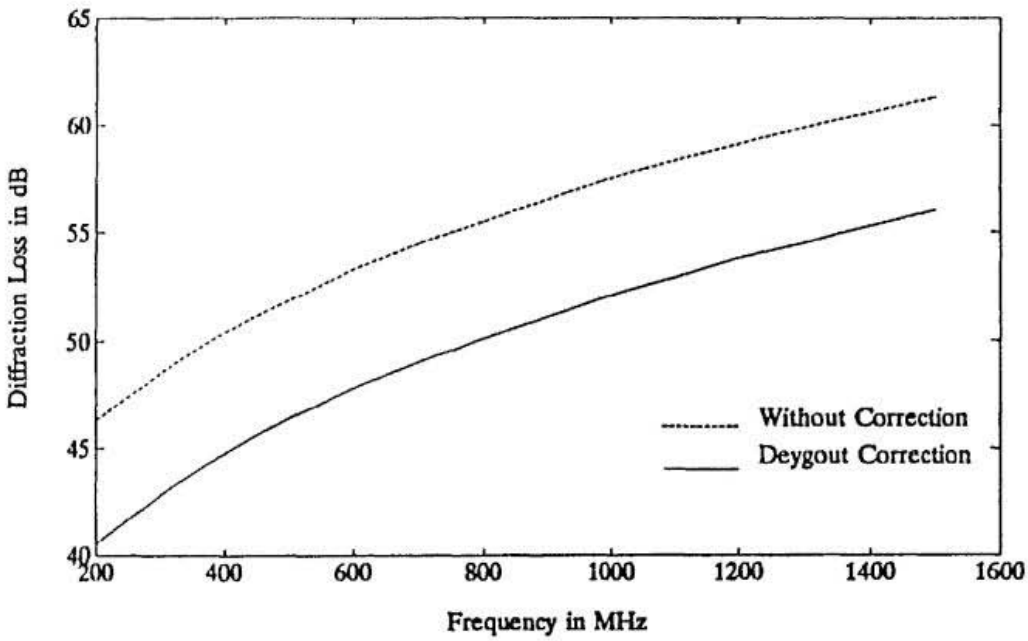

Figure 4.10: Diffraction Losses with Deygout correction and without correction

obstacles on a path profile. The consideration is that some obstacles are less important than others to the diffraction loss. In a transmission path, if the number of obstacles is not much more than three or the diffraction losses of the less important obstacles are neglectable compared with those of the first three prior obstacles, CRC method can give reliable results. However, in the reverse situations, consideration for only three obstacles may have sizeable effect on the accuracy of the prediction results. On the other hand, the priority of importance of obstacles on a path profile is determined by the parameter H/R only. This criterion in de Assis method is borrowed directly from Deygout multiple knife edges method. Diffraction loss over rounded obstacles not only depends on H/R, but also depends on the parameter r. Therefore, in a conservative manner and for achieving higher accuracy, all the obstacles in a path profile are considered in this thesis.

As an example, the effect of the number of obstacles taken into account in total diffraction loss is shown in the following. Fig. 4.11 is a modified path profile in which transmitter is tentatively put on a relatively low hill. The location of the transmitter is 47°30'22" latitude, 52°56'47" longitude, and the receiver is at 47°30'22" latitude, 52°38'13" longitude. The transmitter and receiver antenna heights are 61 m and 1.8 m. In this figure, there are total six obstacles (with parabolic fittings) and those with number 1, 2, 3 are the obstacles considered in CRC method for diffraction loss. The diffraction losses calculated by three obstacles and by all obstacles are shown in Fig. 4.12. In the curve of the diffraction loss for all obstacles, there is an irregular portion around 450 MHz. This is attributed to that the obstacle between obstacle 1 and obstacle 2 becomes non-obstacle when the frequency higher than 550 MHz. Since this obstacle is below the line connecting

obstacle 1 and obstacle 2, its H/R is less than 0. When the frequency increases, R decreases, and its H/R also decreases. When H/R < -0.6, it becomes non-obstacle, therefore the diffraction loss goes down a little bit. In Fig. 4.12, for low frequencies there are more than 20 dB difference between the diffraction losses, and for high frequencies there are more than 15 dB difference. This example shows that the two prediction results have sizeable difference. Therefore, it is recommended that in order to improve the accuracy of prediction results all possible obstacles in a path profile be considered.

4.5 Results of the Modified Diffraction Loss Prediction

As stated in the previous sections, several aspects of the diffraction loss prediction such as the radius of curvature of obstacle's crest, the correction factor, and the number of obstacles have been modified. Also, path profiles have been modified. The results given in each section above are caused by each aspect alone. The total results of these modifications on diffraction loss compared with the results of CRC method will be shown by following two examples. Fig. 4.13 shows the CRC path profile with T_x at 47°34'19" latitude, 52°53'17" longitude, R_x at 47°34'19" latitude, 52°42'0" longitude. Fig. 4.14 presents the modified profile. The transmitter and the receiver antenna heights are 61 m and 1.8 m. The diffraction losses predicted by CRC method based on the CRC profile and predicted by the modified method based on the modified profile are shown in Fig. 4.15. In this case, the modified diffraction loss versus frequency is about 10 to 15 dB less than the CRC result. Since the CRC profile misses the top of the hill near 10 Km distance from the transmitter,

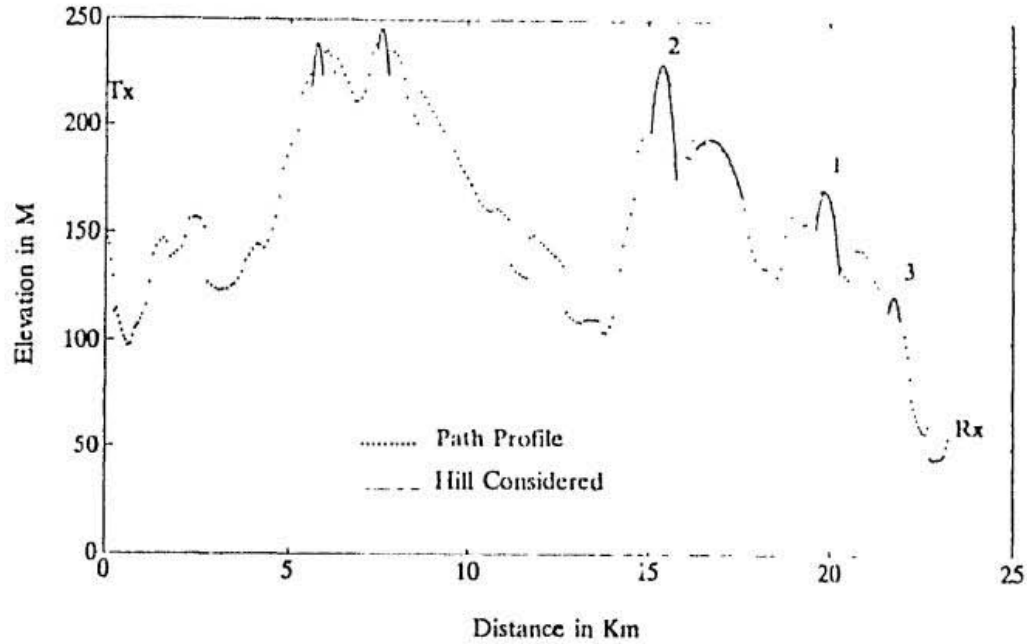

Figure 4.11: Modified Path Profile

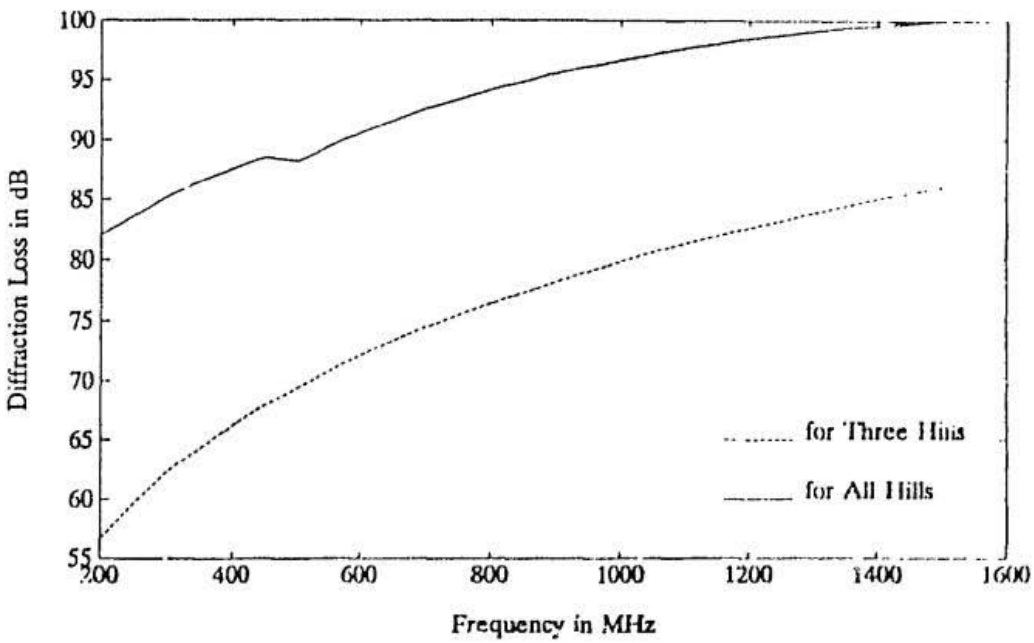

Figure 4.12: Diffraction Losses by Different Number of Obstacles

so the hill located around 6 Km distance is treated as the main obstacle. In the modified profile, the hill near 10 Km distance is the main obstacle. Since the radius of curvature of this main obstacle is much less than that of the main obstacle in the CRC profile, the modified prediction result is lower than the CRC result in this case. The other reason is that the elevations at the transmitter and the receiver in the modified profile are higher than those in the CRC profile, these decrease the parameter H. As the receiver moves away from the transmitter along the path shown in Fig. 4.13 and Fig. 4.14, the diffraction loss results are given in Fig. 4.16, where the frequency is 900 MHz. In another example, a CRC path profile is given in Fig. 4.17, where T_x is at 47°24'43" latitude, 52°48'25" longitude, R_x at 47°30'22" latitude, 52°48'25" longitude. Fig. 4.18 shows the modified profile. The antenna heights are the same as in the last example. The diffraction losses against frequency are shown in Fig. 4.19. The diffraction loss from the modified method based on the modified profile is about 6 dB less than that from CRC method based on CRC profile. In this case, the difference is mainly caused by the radii of curvature of the two obstacles located at 10 Km and 8.5 Km distance from the transmitter in the two profiles. Fig. 4.20 is the diffraction losses along the paths in Fig. 4.17 and Fig. 4.18 with the frequency as 900 MHz.

It is believed that the results obtained by the modified method are more reliable than those from CRC method, because of the much more accurate path profiles and the improvements in the three aspects of the diffraction loss prediction method.

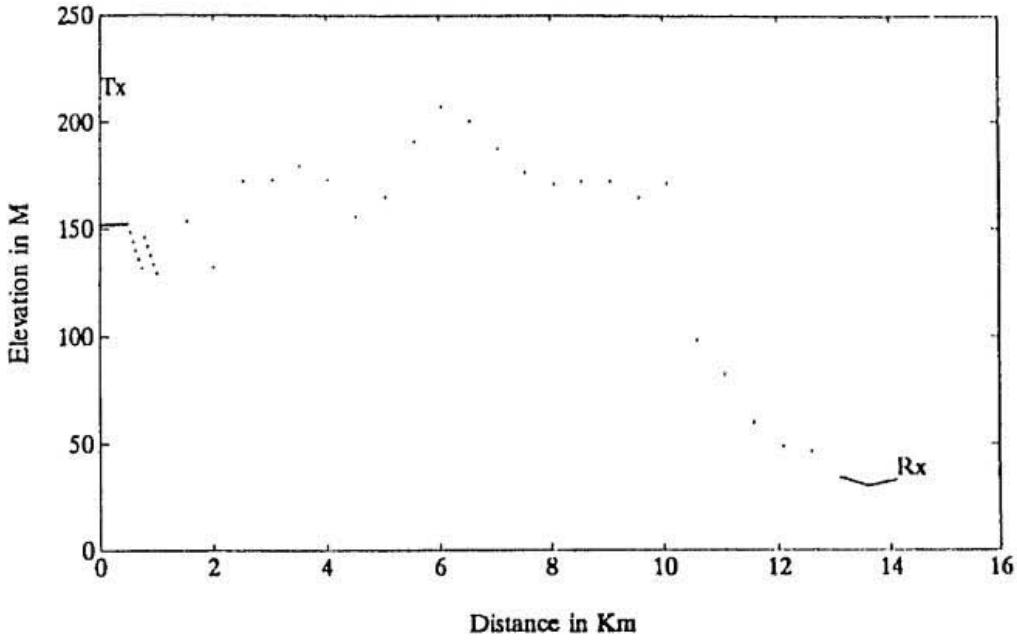

Figure 4.13: CRC Path Profile

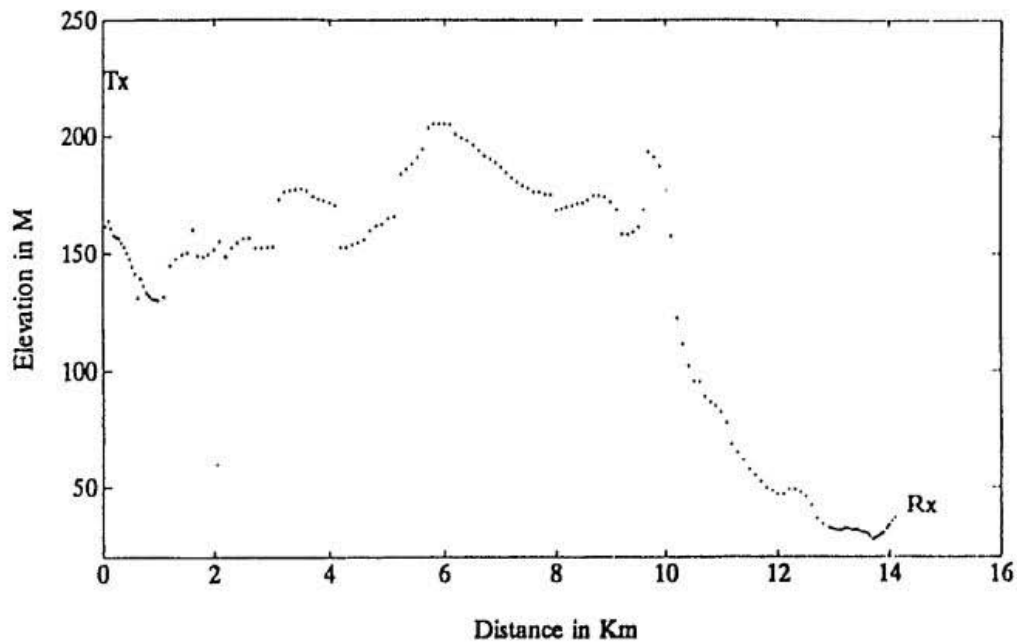

Figure 4.14: Modified Path Profile

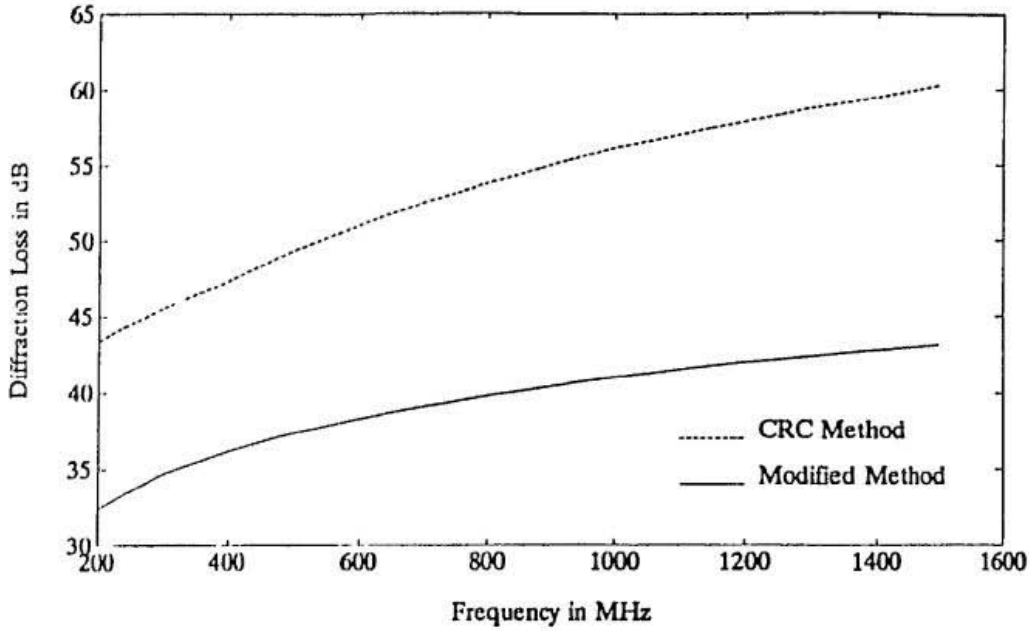

Figure 4.15: Diffraction Losses vs. Frequency

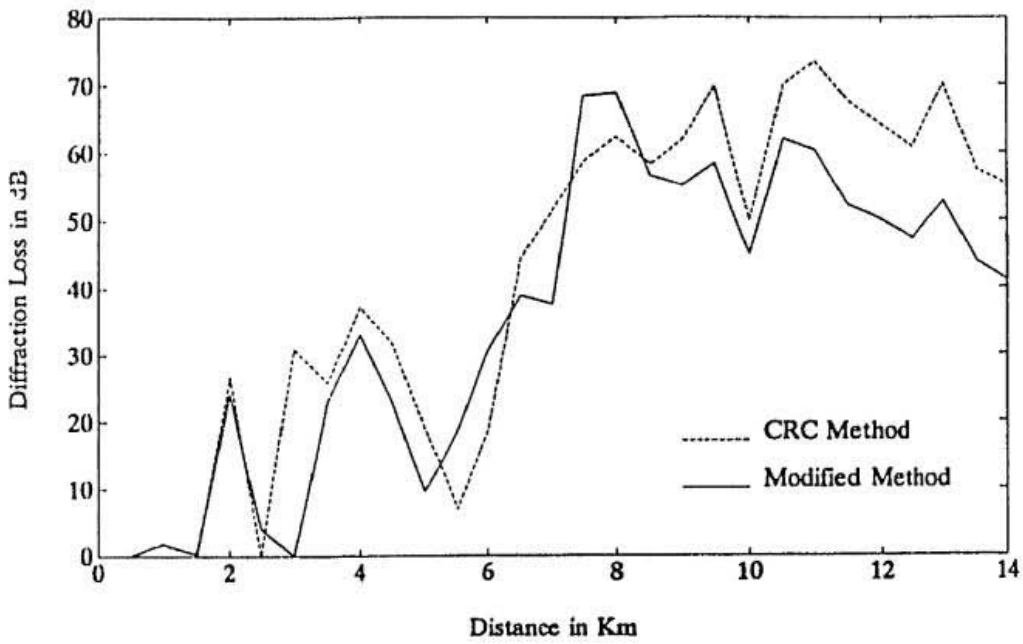

Figure 4.16: Diffraction Losses vs. Distance

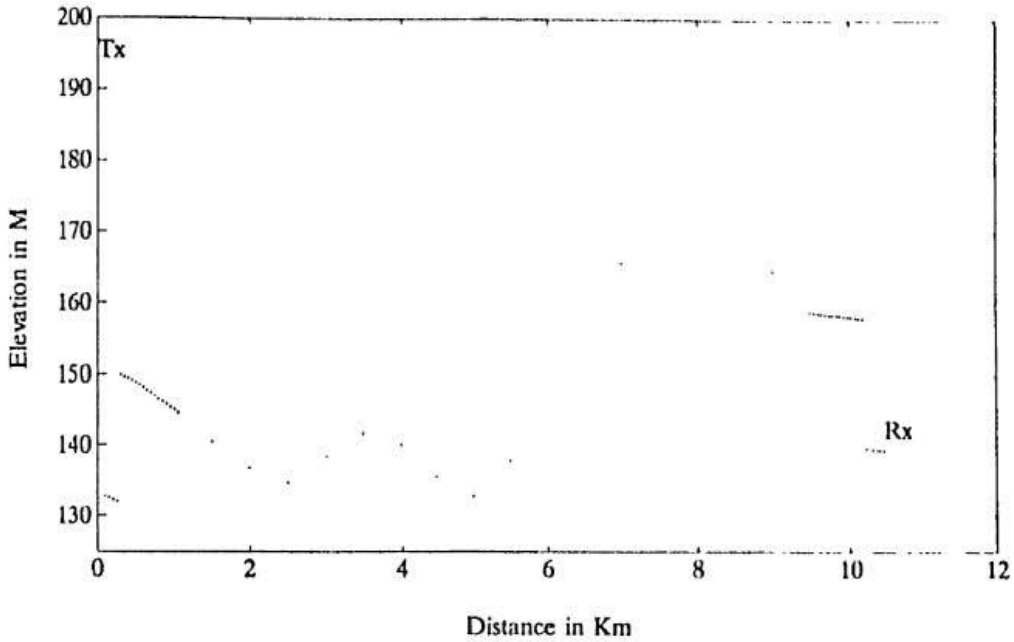

Figure 4.17: CRC Path Profile

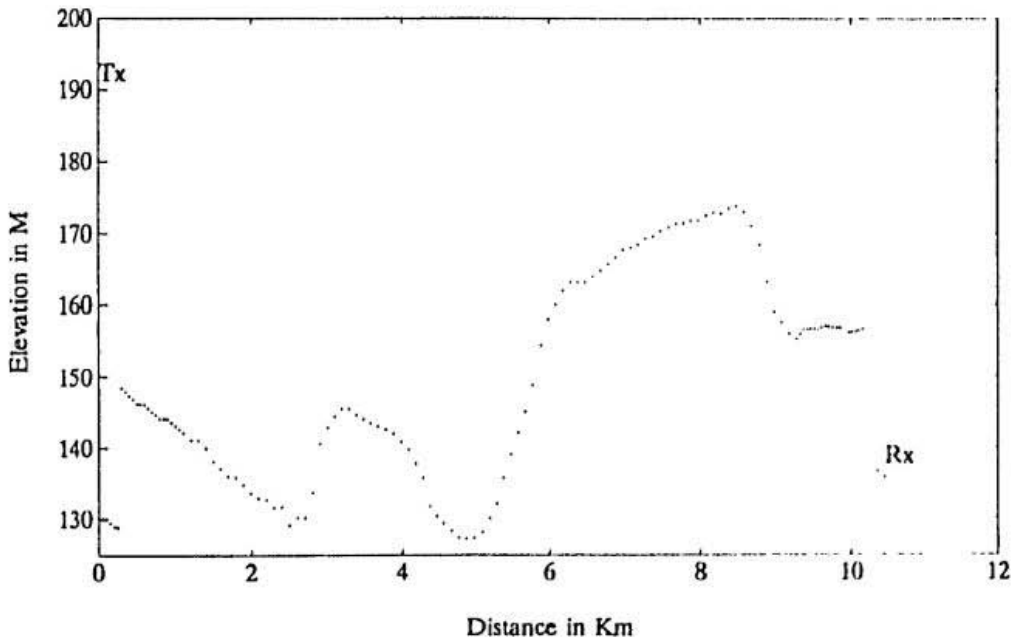

Figure 4.18: Modified Path Profile

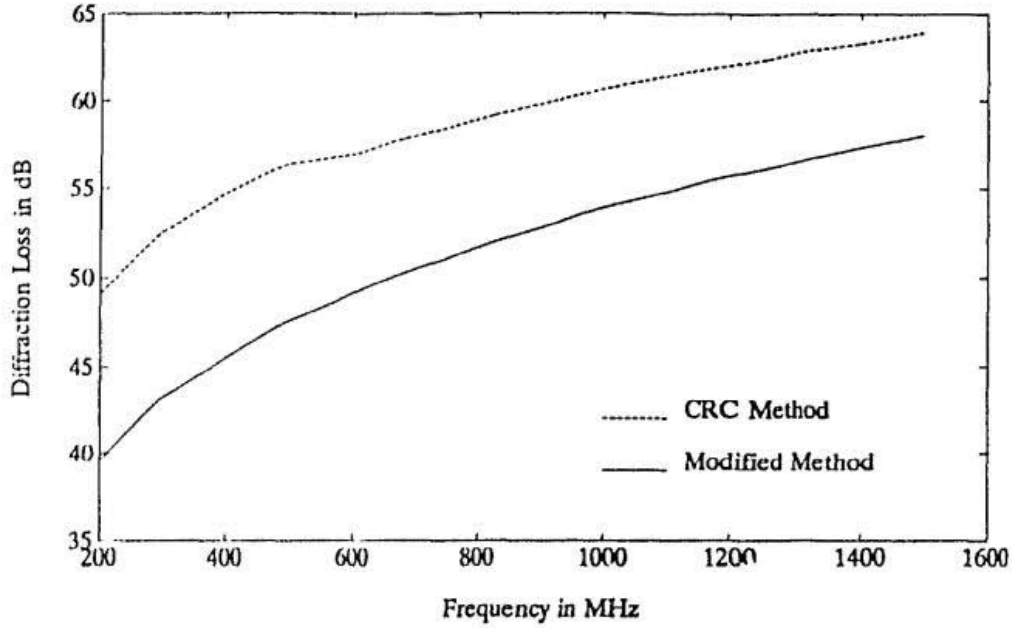

Figure 4.19: Diffraction Losses vs. Frequency

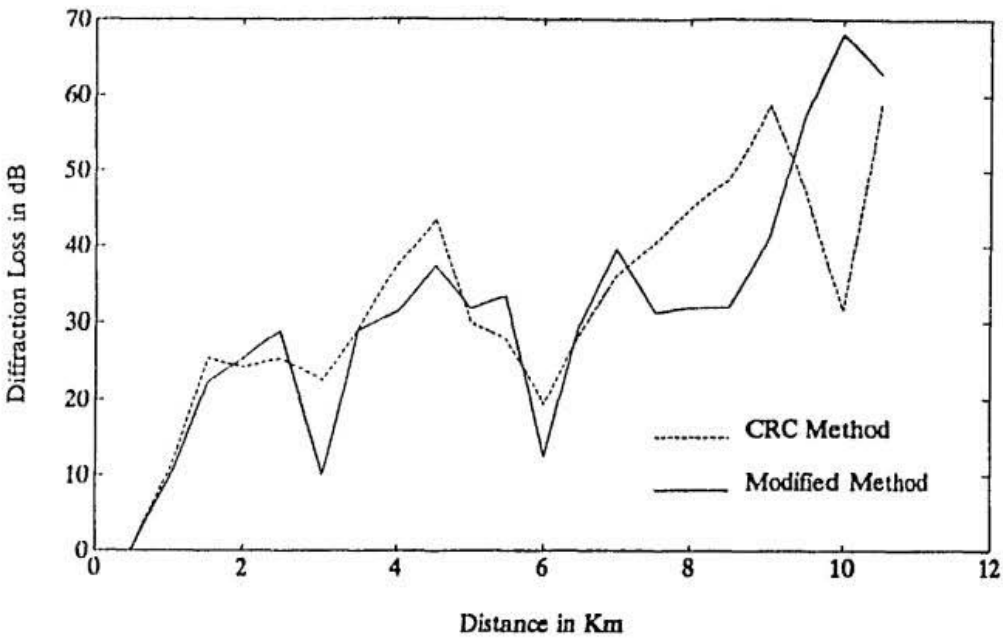

Figure 4.20: Diffraction Losses vs. Distance

Chapter 5

Total Propagation Loss Prediction

5.1 The Composition of Total Propagation Loss

VHF/UHF frequency bands are used in land mobile radio communications. Propagation in these frequency bands, for the most part, takes place via space waves. At these frequencies, groundwaves are attenuated very rapidly with distance, and skywaves pass readily through the ionosphere with little energy being reflected back to earth. Space waves are subject to absorption, reflection, refraction, and scattering by the troposphere and by the surface of the earth and obstacles in their paths. For the relatively short service ranges of the land mobile radio systems, the modes of propagation are usually free space propagation, reflection from the earth surface, diffraction over obstacles on the terrain, atmospheric refraction, scattering by the troposphere, and multipath propagation in urban areas. The total propagation loss (i.e. median transmission loss) considered in this thesis is composed of free space loss, diffraction loss, reflection loss, tropospheric scattering loss, urban loss, clutter loss, and season loss.

Free space loss is the basic loss for all the propagation paths. Atmospheric refraction of radio waves is taken into account by the effective earth radius. If the path profile has obstacles ($H/R \geq -0.6$), diffraction loss is predicted according to the modified method presented in Chapter 4. Otherwise reflection loss is calculated based on the method discussed in Chapter 2. Diffracted reflection waves are neglected. When transmission path is within urban or suburban area, urban loss due to high density of buildings is estimated by Hata model. Tropospheric scattering (troposcattering) loss is computed according to National Bureau of Standards Technical Note 101 which is briefly discussed in Chapter 2. For transmission paths extending slightly beyond line of sight, diffraction will be the dominant mode in most cases and scattering may be neglected. Conversely, for long paths (far beyond line of sight), the diffraction field may be hundreds of decibels weaker than the scattered field, and thus the diffraction mode can be neglected. In intermediate cases, such as for path length greater than 10 Km, both modes have to be considered and the results combined in the following manner [29]. If

$$x = L_d - L_s$$

where L_d is diffraction loss, L_s is scattering loss, let

$$B = \begin{cases} 2.6\exp(\frac{x}{5.2}) & x \leq 0 \\ x + 2.6\exp(-\frac{x}{5.2}) & x > 0 \end{cases} \tag{5.1}$$

Then the combined loss is :

$$L = L_d - B. \tag{5.2}$$

It can be seen that, if $L_d < L_s$, L depends on L_d more, otherwise depends on L_s more. Generally speaking, in land mobile communications which involve relatively

short paths, diffraction mode is more important than troposcattering mode, and it affects the total propagation loss more.

Along the transmission path, if there are trees or buildings near either the transmitting or receiving antenna within 250 m and the buildings are not part of an urban area, clutter loss should be calculated and added to the total loss. In mobile communications, time variability of the transmission power is not as important as location variability. However, for certain area sector transmission loss changes from season to season, year to year, therefore season loss is also added to the total loss.

The implementation of total loss prediction is discussed in the next section.

5.2 Program Flow Chart

CRC propagation loss prediction program basically consists of two kinds of predictions. One is for detailed path profiles which are constructed from the terrain data base or entered by user when there is no data base. The other is for non-detailed terrain with statistic features. In this thesis, the interest is in improving the accuracy of the prediction for detailed path profiles. The following flow charts are the implementation of the modified prediction methods. Fig. 5.1 is the flow chart of the main program. Since the output parameters can be the transmission loss (or called path loss, total propagation loss), field strength, and signal voltage, the input parameters are different for different output parameters. Generally the input parameters are latitude, longitude of transmitter, antenna heights of transmitter and receiver, frequency and polarization, atmospheric refractivity or K factor, clutter parameters if there is any, etc.. In a more convenient way, input

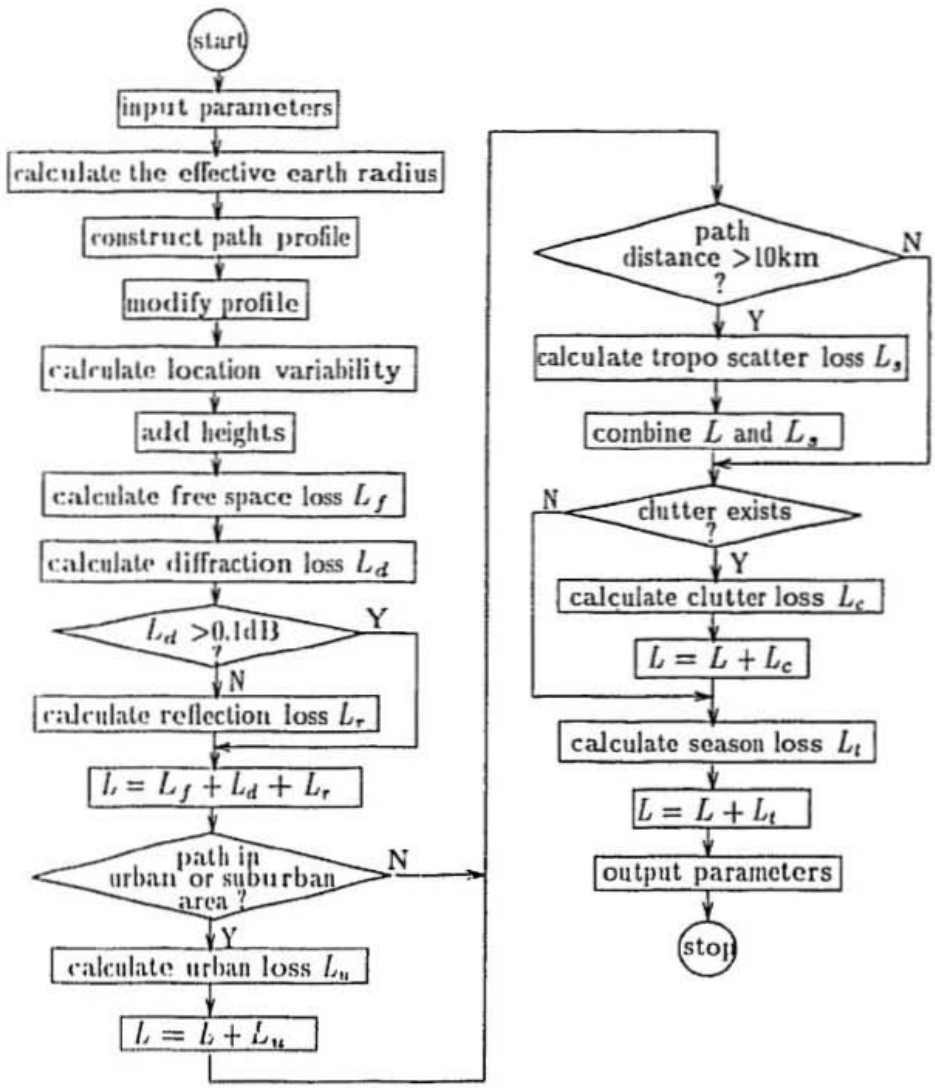

Figure 5.1: The Flow Chart of the Main Program

parameters are organized in the certain format as a separated input file. In Fig. 5.1, 'modify profile' takes into account the effective curvature of the earth to the path profile. 'add height' adds to the path profile the heights of those trees and buildings which are neither considered in clutter model nor in urban model. The conditions of various loss calculations are discussed in the last subsection. In the main program, each of these steps involves several subroutines. The flow charts of 'construct profile' and 'calculate diffraction loss L_d' are shown in the following.

In constructing profiles from the terrain data base, the Universal Transverse Mercator (UTM) coordinates are used. The earth surface is considered as a sphere which is divided into 60 zones with a 6° longitude interval. The procedure of obtaining a profile may be explained by using Fig. 5.2. T_x, R_x represent transmitter and receiver. The path length is obtained by solving the spherical triangle $N-T_x-R_x$, where N is the north pole. N_1, N_2 are the intersecting points of transmission path with zone boundaries. S_1, S_2, S_3 are the segments of T_x-N_1, N_1-N_2, N_2-R_x, respectively. The length of each segment is obtained by one of the spherical triangles such as $N-T_x-N_1$, $N-N_1-N_2$, and $N-N_2-R_x$. In each segment, locate the points with approximate 100 m interval. The elevations and surface codes of these points are required to be determined from the modified data base. Since the location of each of these points may not be right on the point in the data base, so the complete quadratic interpolation and the weight vote method are applied again to obtain the elevation and surface code. The flow chart for constructing the path profiles from the modified data base is given in Fig. 5.3, where NS is the total number of segments, NP is the number of the points P_i in each segment with an approximate 100 m interval, D_{1-9} are the corresponding closest nine points in the

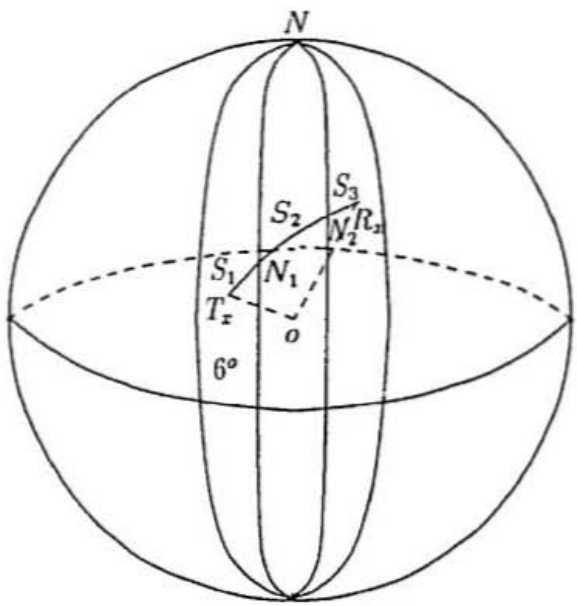

Figure 5.2: Construction of Path Profile

modified data base for each of P_i.

Fig. 5.4 is the flow chart of the modified diffraction loss prediction which is presented in Chapter 4. h_{mt}, h_{mr} are the minimum effective antenna heights of transmitter and receiver.

5.3 Results and Discussions

As the terrain data base has been modified, the evaluations of diffraction, reflection, tropospheric scattering, urban, and season losses are affected. Also the diffraction loss calculation has been modified, it will affect more in the predictions for relatively short transmission paths. The followings are the results of the modified program prediction system with respect to CRC prediction results. In the following six studied cases, the transmitter antenna height is 61 m (200 ft), the receiver antenna height is 1.8 m (6 ft), and the transmission paths are in Newfoundland area. In all the following path profiles, transmitter is always fixed at one end. For showing the relationship of losses versus frequency, receiver will locate at the other end. For examining losses versus distance, receiver will move along the paths. '(R_x)' in the figures denotes the receiver location fixed or moved. In the latter situation, the frequency is always set to 900 MHz and vertical polarized.

Case 1 represents the case that diffraction, tropospheric scattering, urban loss, season loss, and clutter loss are all involved. Fig. 5.5 shows a path profile constructed from CRC data base. The locations of the transmitter and receiver are the same as in Fig. 4.13 in Chapter 4, but in Fig. 5.5 the effective earth radius factor (K) is set to 1. There are very minor changes of elevations in this two figures due to the change of K factor. Fig. 5.6 shows the corresponding path profile

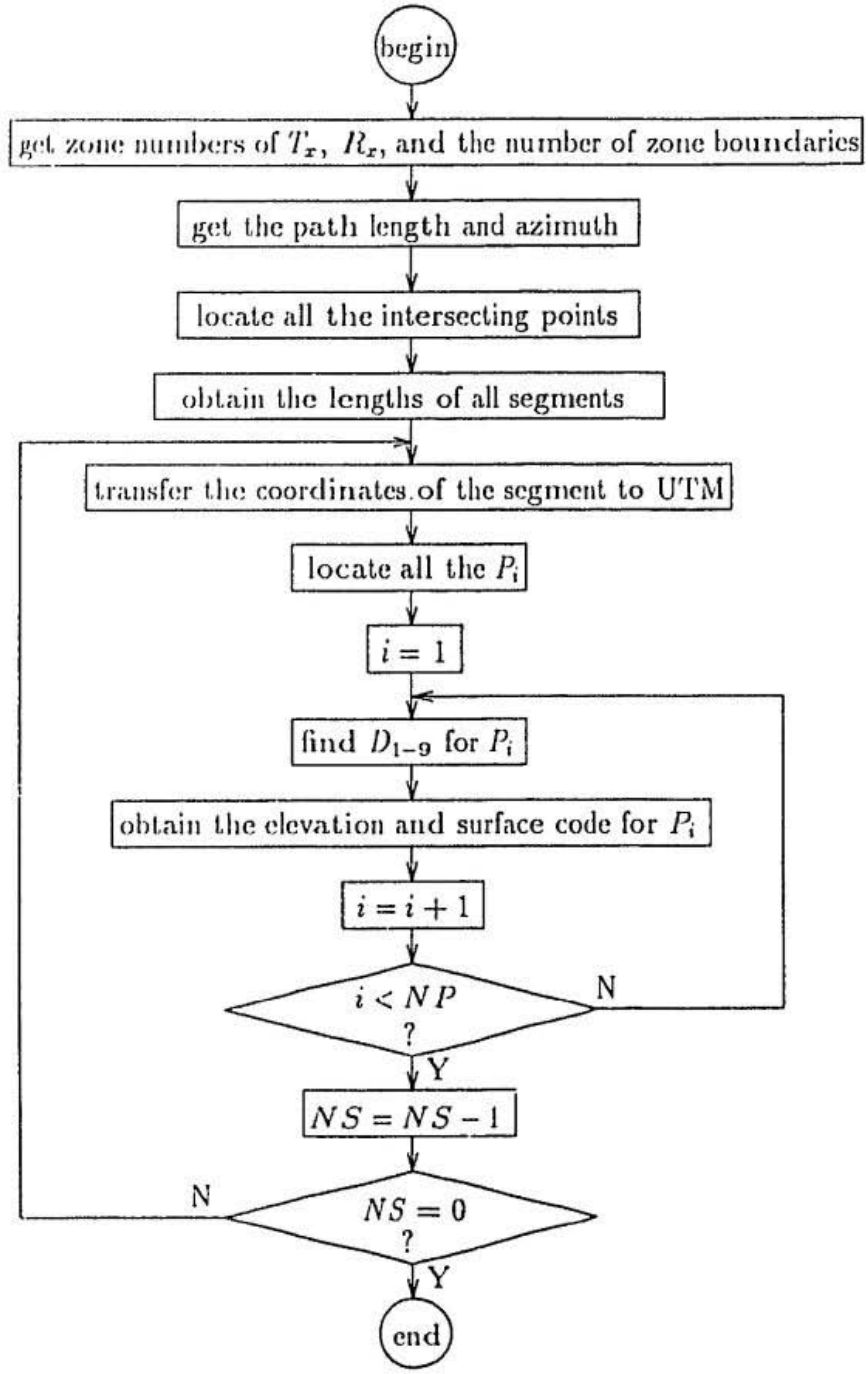

Figure 5.3: The Flow chart of Constructing Path Profile from the Modified Data Base

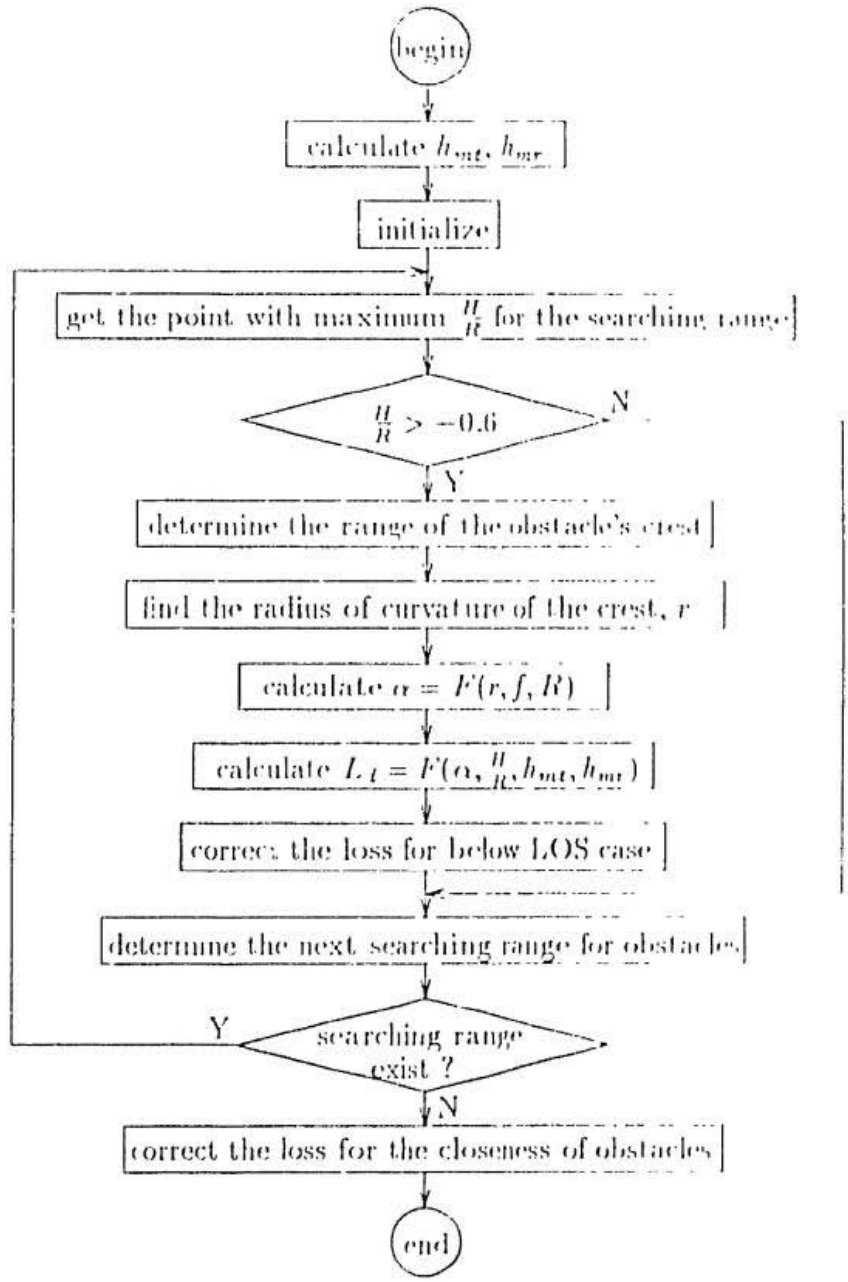

Figure 5.4: The Flow chart of the Modified Diffraction Loss Prediction

constructed from the modified data base. Based on the profiles in Fig. 5.5 and Fig. 5.6, the predicted propagation losses versus frequency are shown in Fig. 5.7. There is about 11 dB less loss for the modified result. In this terrain path, several kinds of losses occur. The following figures show the effects of the modifications on these losses. Fig. 5.8 is the diffraction losses with about 9 to 15 dB difference. These results are not exactly the same as in Fig. 4.15, because of the change in K factor. The tropospheric losses are given in Fig. 5.9. There is about 0.5 dB more for the modified result due to the modification of surface codes. Fig. 5.10 shows the urban losses with about 0.7 dB difference. Since the urban loss model is the empirical model, the results are affected only by surface codes. Fig. 5.11 shows the season losses. The difference is very minor which is caused by the modification of elevations near transmitter and receiver and surface codes. The clutter losses are included in this case, there are no difference in the two results, since all the parameters of the clutter are not provided by terrain data base, but they are the inputs of the prediction program. For the prediction of losses versus distance, Fig. 5.12 represents the total losses. Fig. 5.13 shows the diffraction losses. These results have very little changes compared with those in Fig. 4.16. Tropospheric losses are shown in Fig. 5.14, where for the distance less than 10 Km, the tropospheric scattering loss is set to 100 dB. Fig. 5.15 is the urban losses, and Fig. 5.16 is the season losses. This studied case shows that the modifications have the most effect on the diffraction loss.

In the Case 2, the diffraction is the dominant mode. The transmission path which is a relatively short path is the same as in Fig. 4.17 and Fig. 4.18. For convenience, these two profiles are repeated in Fig. 5.17 and Fig. 5.18. The pre-

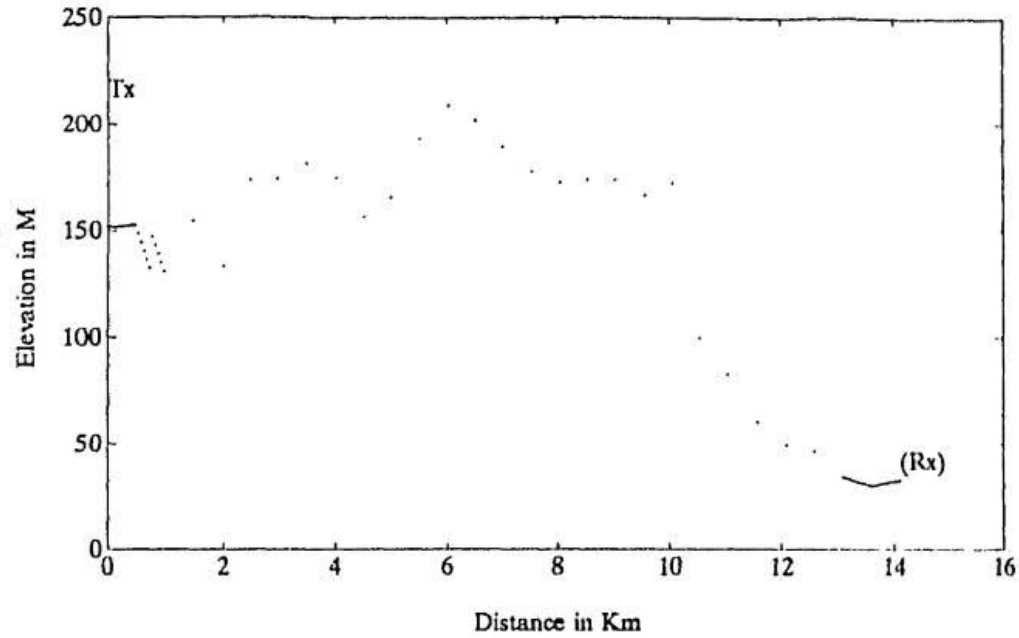

Figure 5.5: CRC Path Profile of Case 1

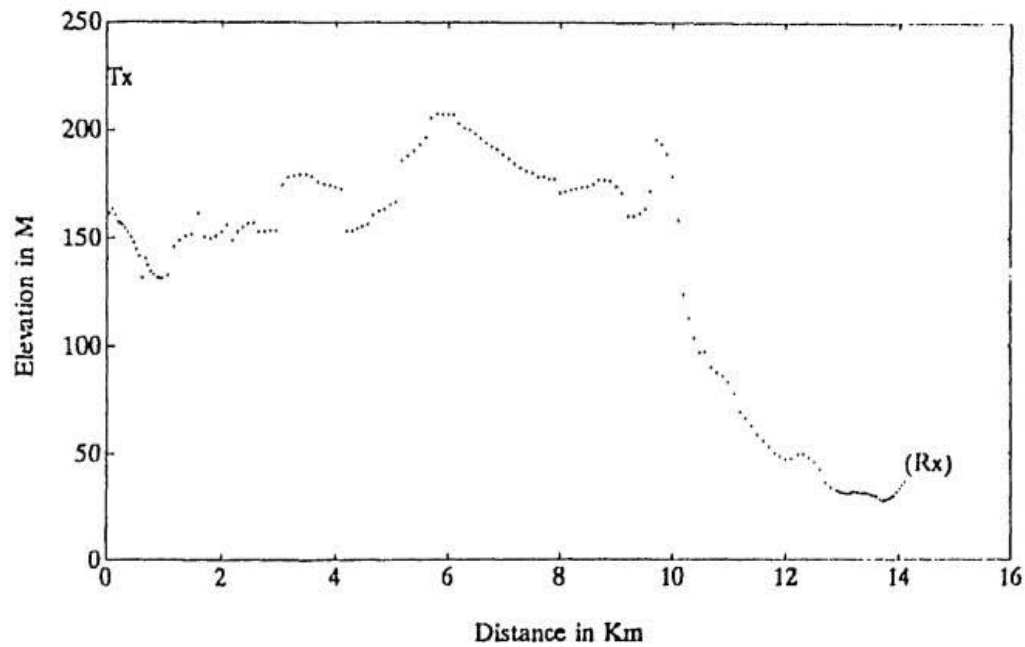

Figure 5.6: Modified Path Profile of Case 1

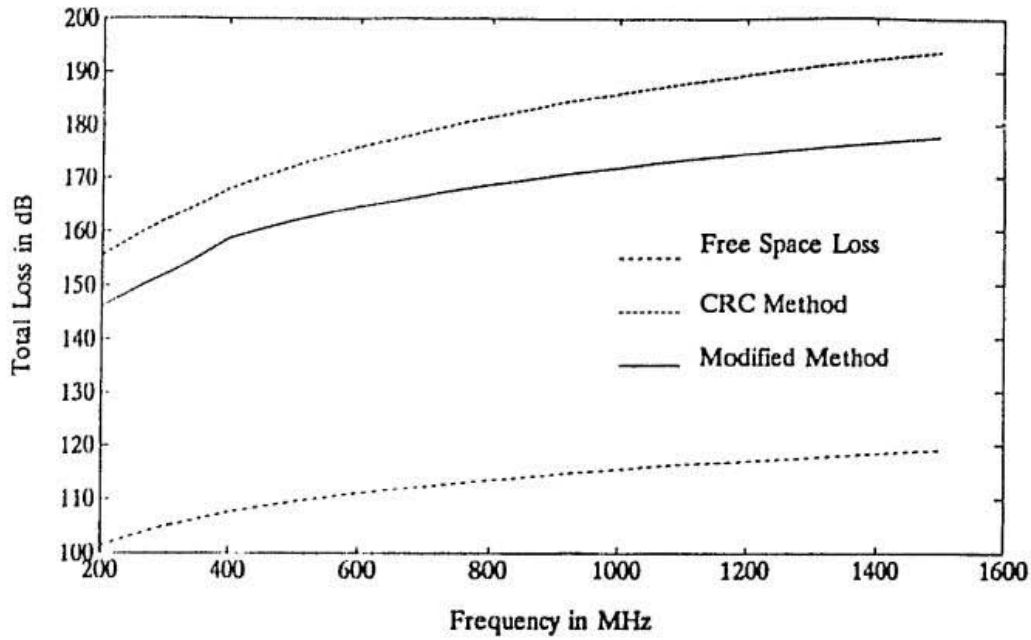

Figure 5.7: Total Losses vs. Frequency of Case 1

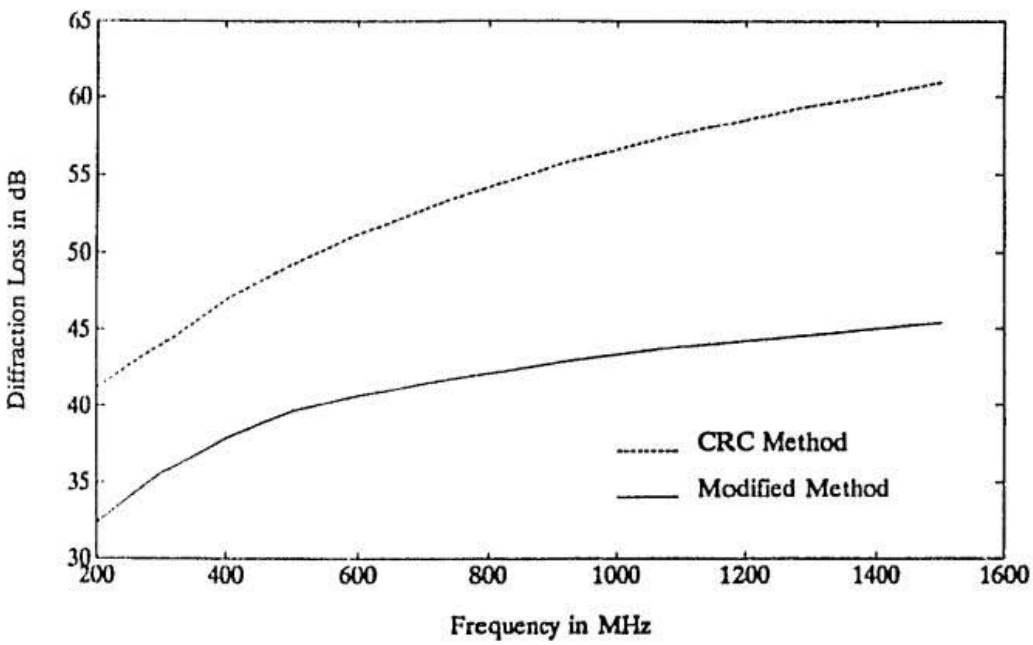

Figure 5.8: Diffraction Losses vs. Frequency of Case 1

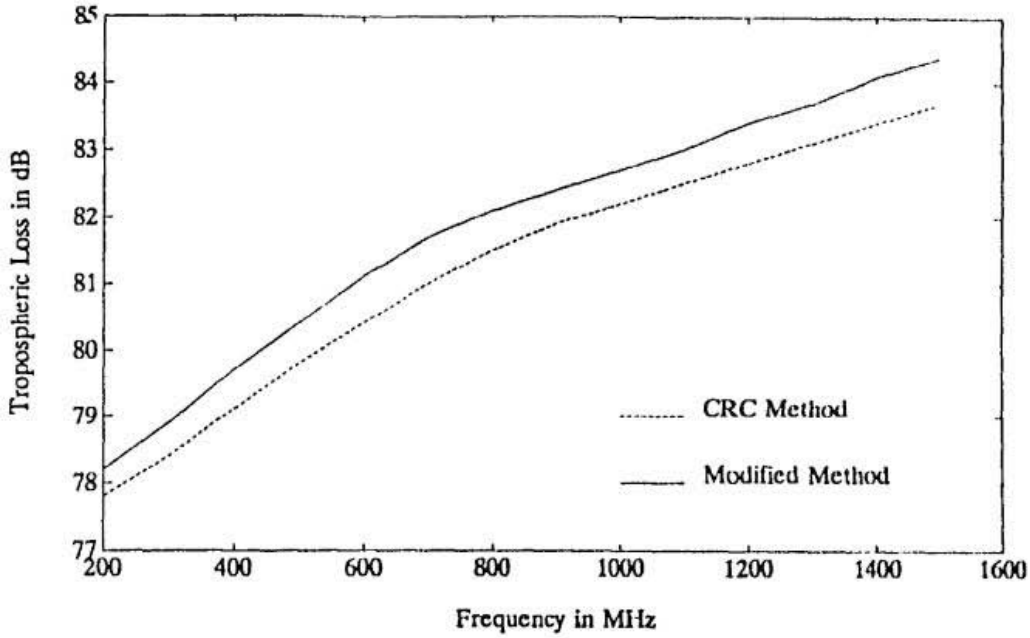

Figure 5.9: Tropospheric Losses vs. Frequency of Case 1

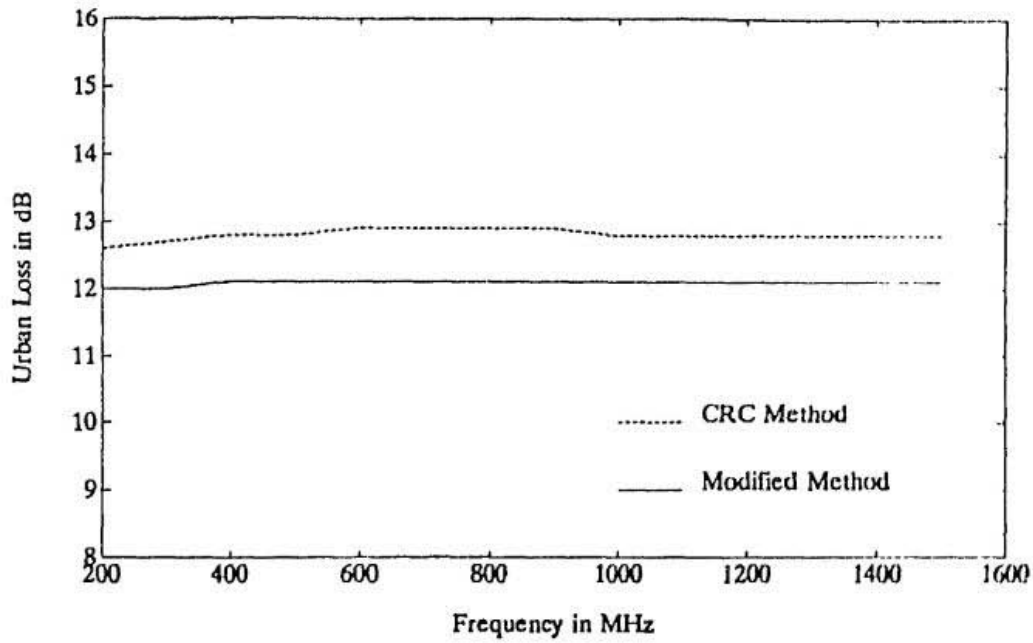

Figure 5.10: Urban Losses vs. Frequency of Case 1

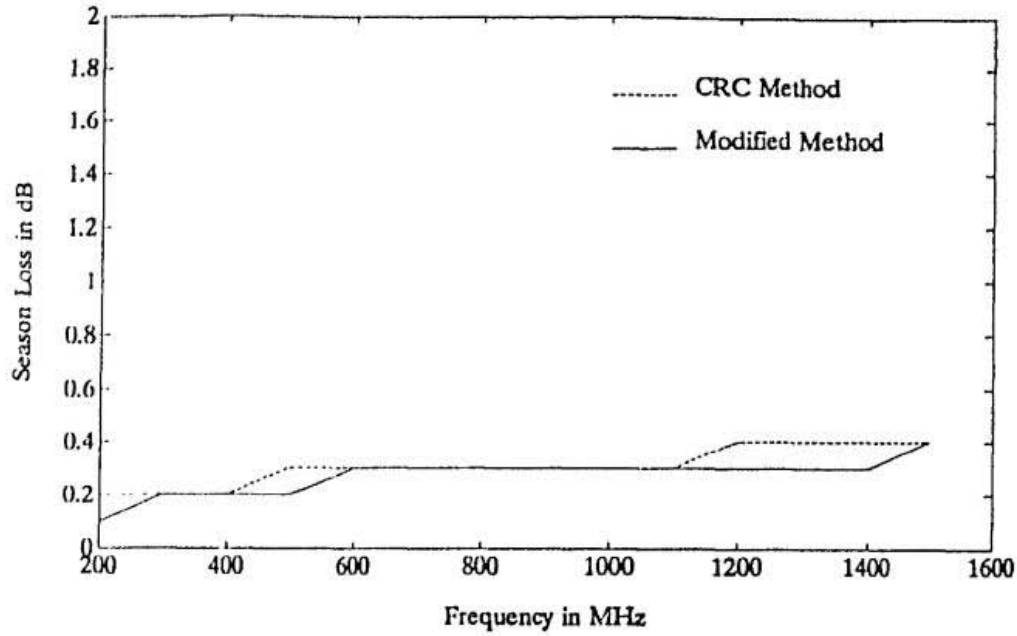

Figure 5.11: Season Losses vs. Frequency of Case 1

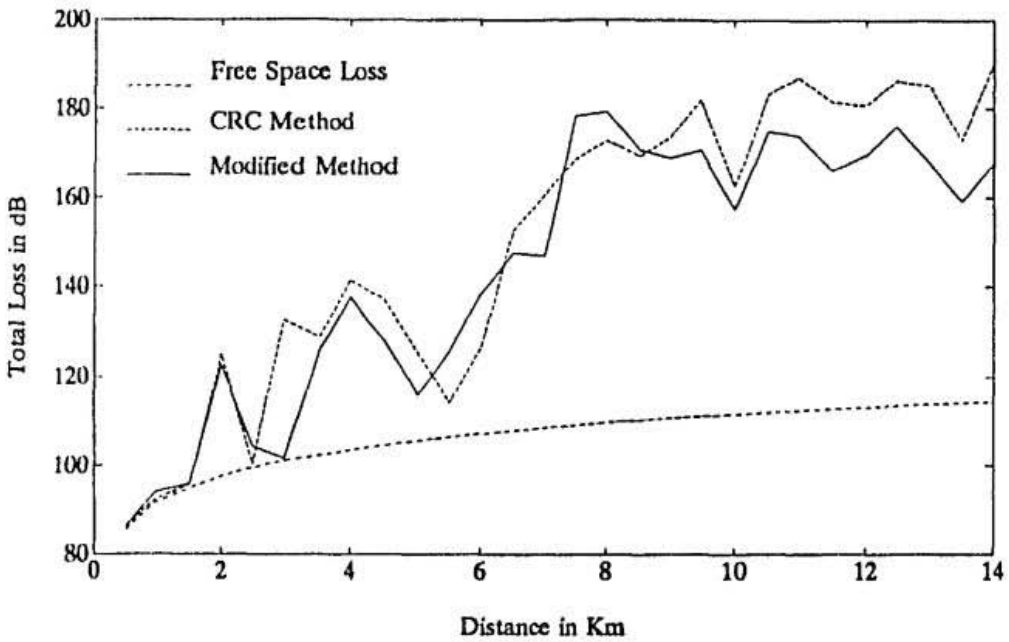

Figure 5.12: Totai Losses vs. Distance of Case 1

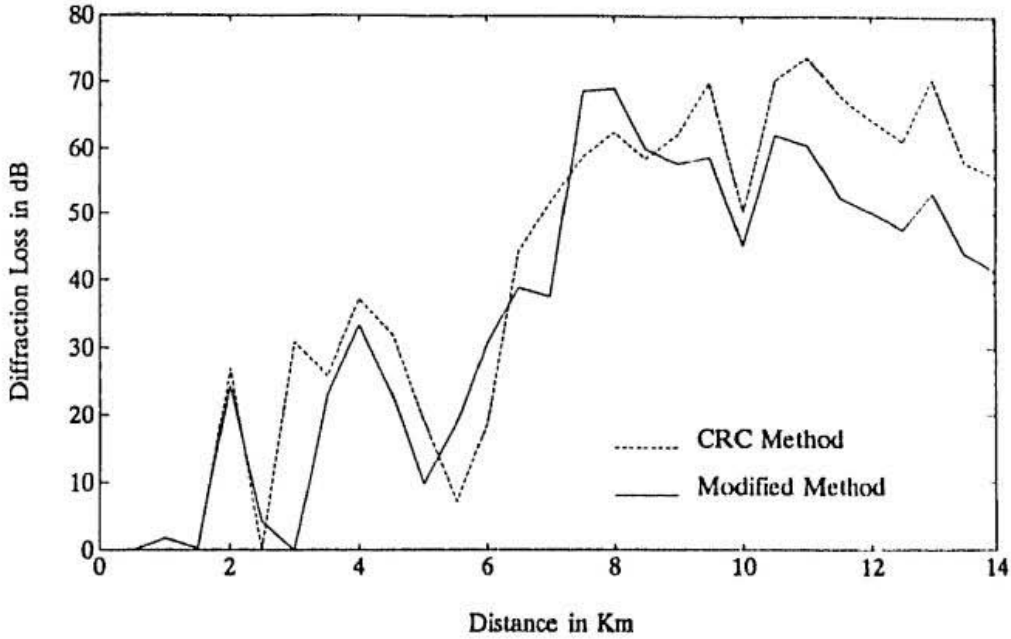

Figure 5.13: Diffraction Losses vs. Distance of Case 1

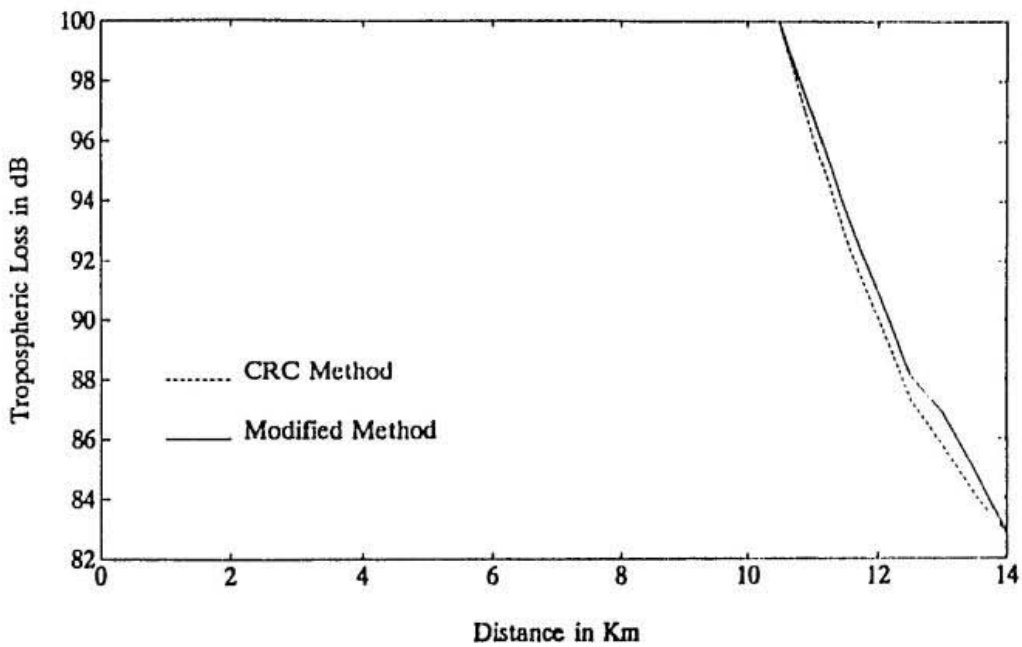

Figure 5.14: Tropospheric Losses vs. Distance of Case 1

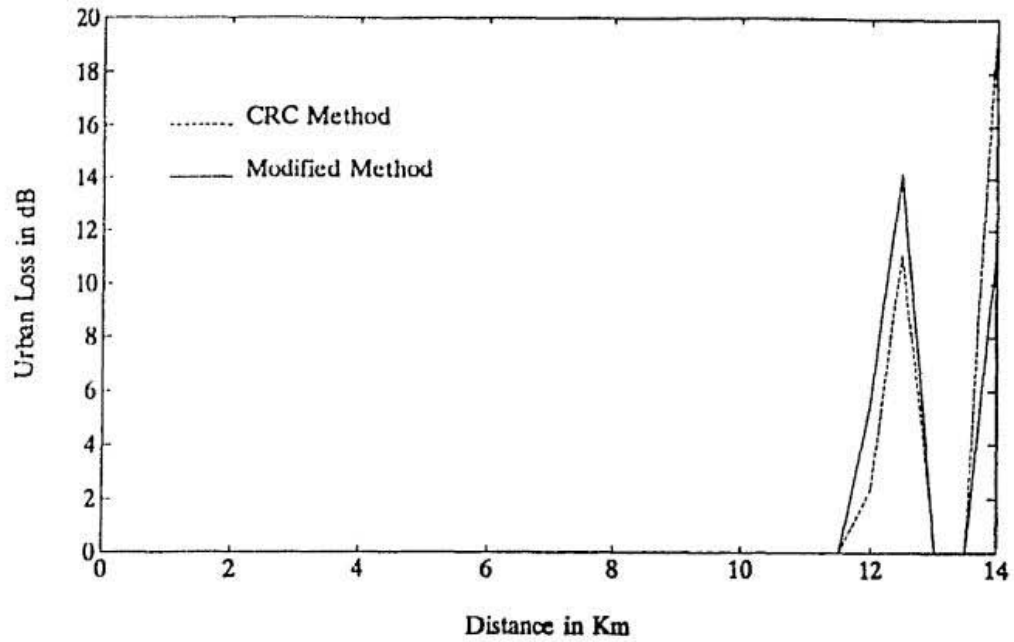

Figure 5.15: Urban Losses vs. Distance of Case 1

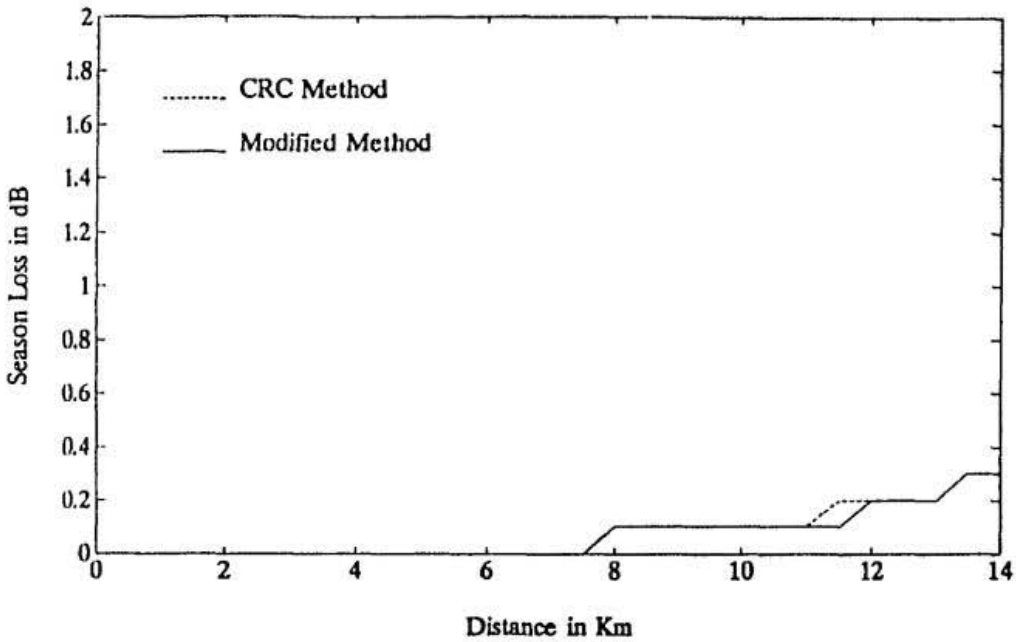

Figure 5.16: Season Losses vs. Distance of Case 1

dicted total losses against frequency are demonstrated in Fig. 5.19. The difference in this figure is caused by the difference in diffraction losses which can be referred to Fig. 4.19. The tropospheric scattering has neglectable contribution to the total loss. The total losses versus distance are shown in Fig. 5.20. In comparing with Fig. 4.20, the difference of these two figures is almost only the free space losses.

In the case 3, the path profiles are shown in Fig. 5.21 and Fig. 5.22. The transmitter is at 47°33'0" latitude, 52°54'45" longitude, and the other end is at 47°36'44" latitude, 52°57'55" longitude. In this path which crosses sea water, reflection from the earth surface is the dominant mode. The total losses versus frequency are shown in Fig. 5.23. The maximum difference is about 14.5 dB when the frequency is 700 MHz. Fig. 5.24 represents the total losses against distance. Within 2.5 Km distance from the transmitter, there is only free space losses. From 2.5 to 7 Km, the two results are very close. The two results have an explicit change at 7 to 7.5 Km due to the difference in the two profiles. Case 3 indicates that the modification on path profile also results in the modification of reflection losses.

In the case 4, the transmission path is a relative long path as shown in Fig. 5.25 and Fig. 5.26. T_x is located at 47°18'57" latitude, 52°47'54" longitude, and the other end is at 47°45'29" latitude, 52°48'36" longitude. If the receiver is fixed at the end, tropospheric scattering is the dominant mode. The total losses versus frequency are shown in Fig. 5.27. If the receiver moves along the path, within a distance of 43Km from T_x, diffraction mode prevails and at a further distance tropospheric mode dominates. The total losses versus distance is shown in Fig. 5.28.

For the case 5, the path profiles are shown in Fig. 5.29 and Fig. 5.30, with T_x

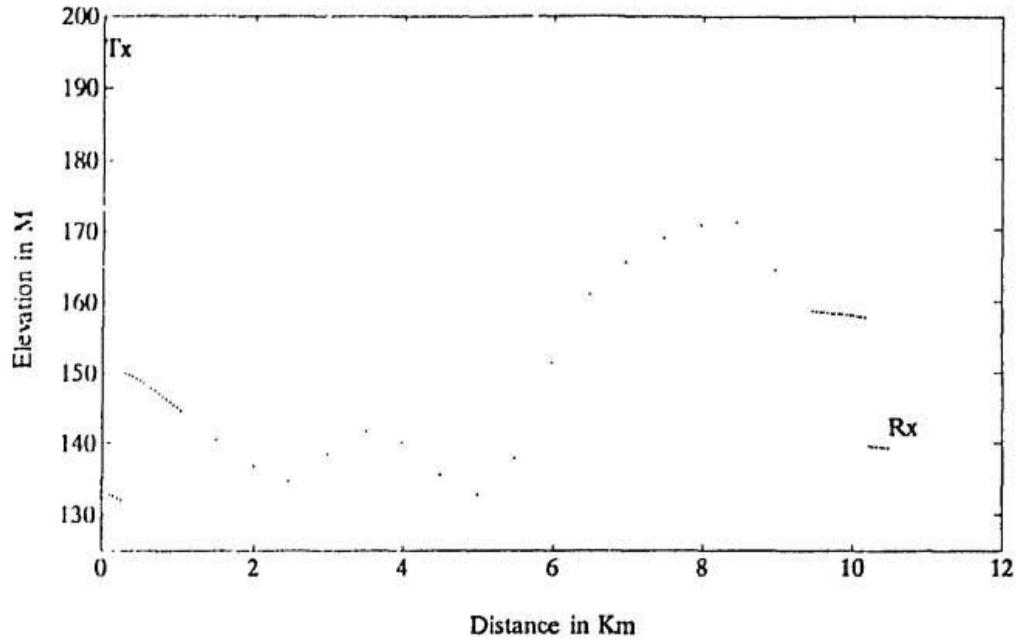

Figure 5.17: CRC Path Profile of Case 2

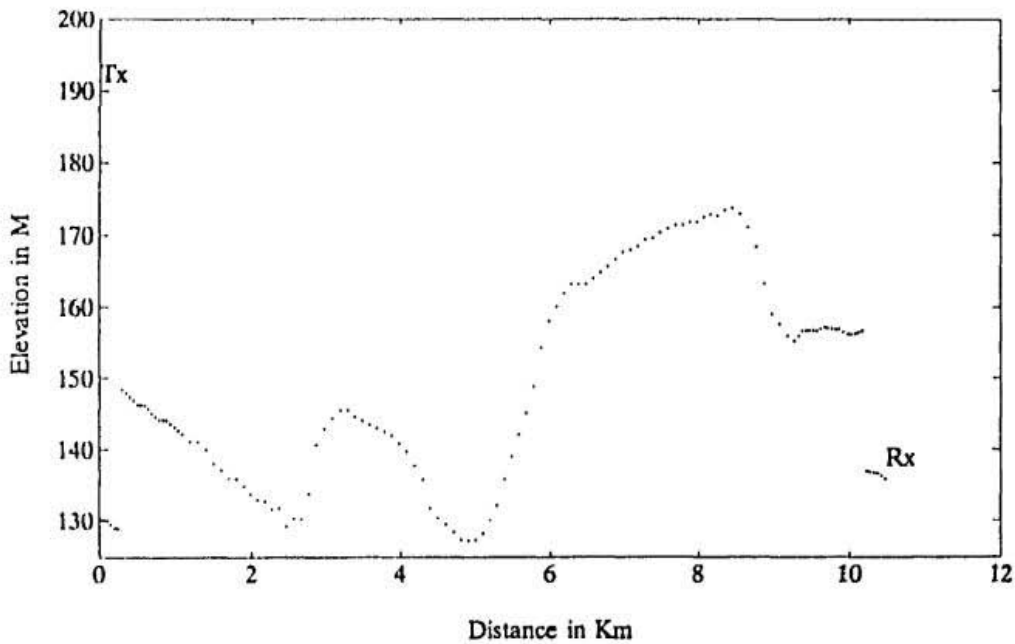

Figure 5.18: Modified Path Profile of Case 2

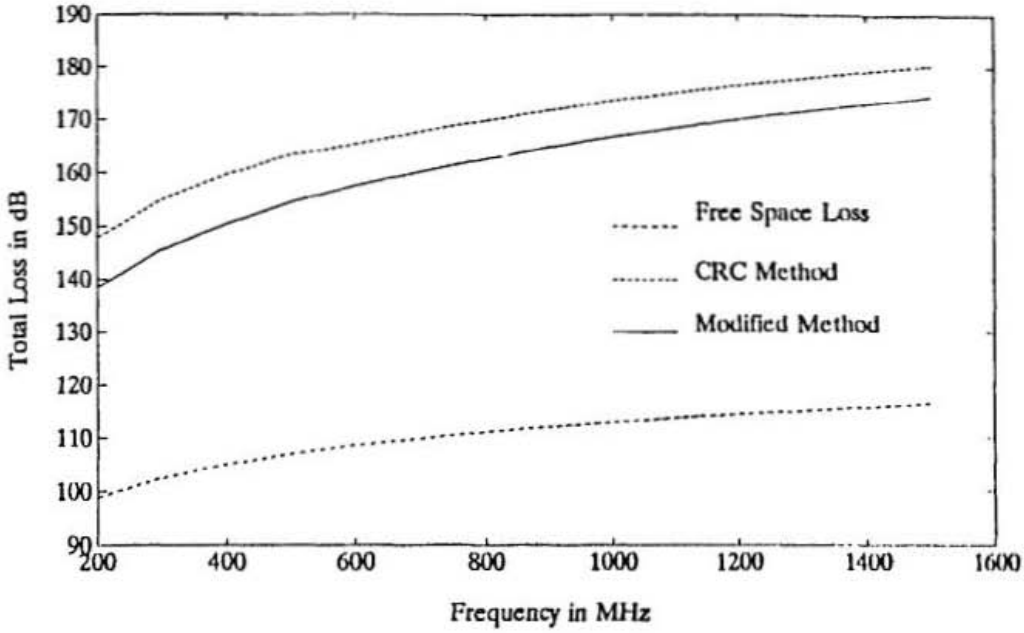

Figure 5.19: Total Losses vs. Frequency of Case 2

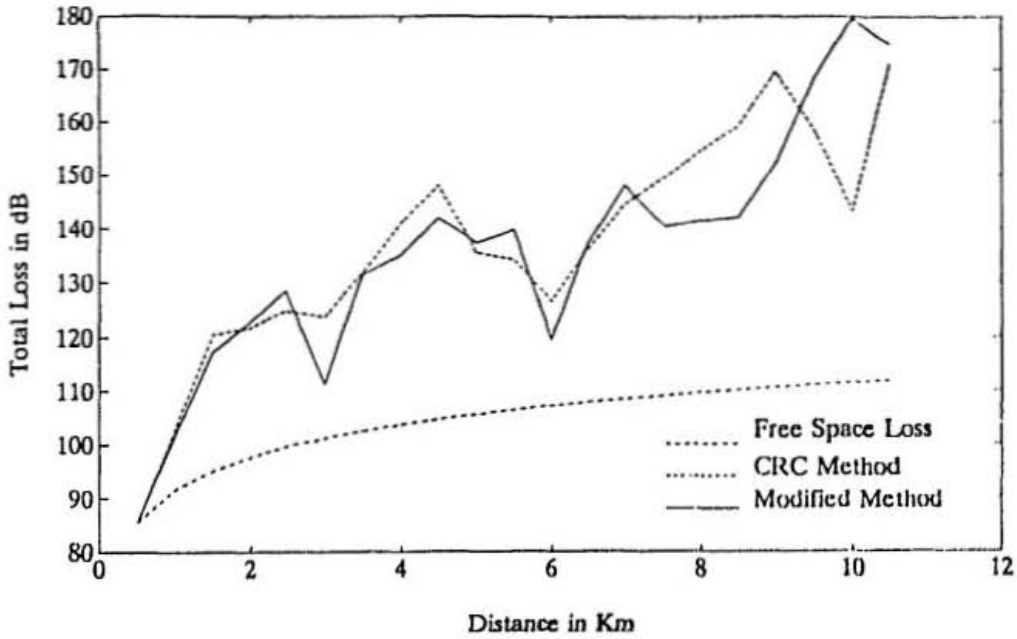

Figure 5.20: Total Losses vs. Distance of Case 2

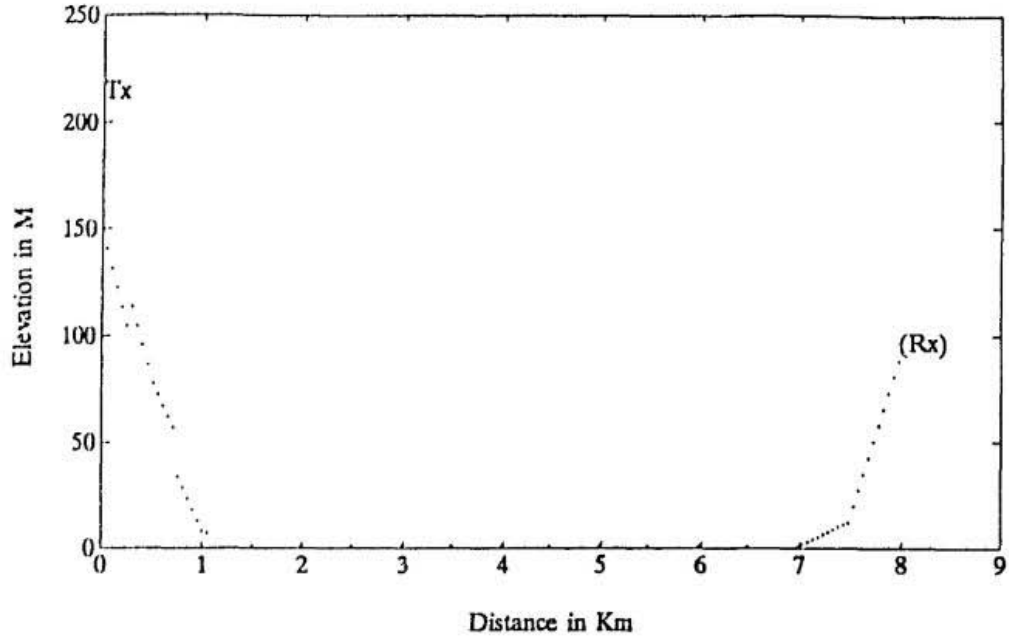

Figure 5.21: CRC Path Profile of Case 3

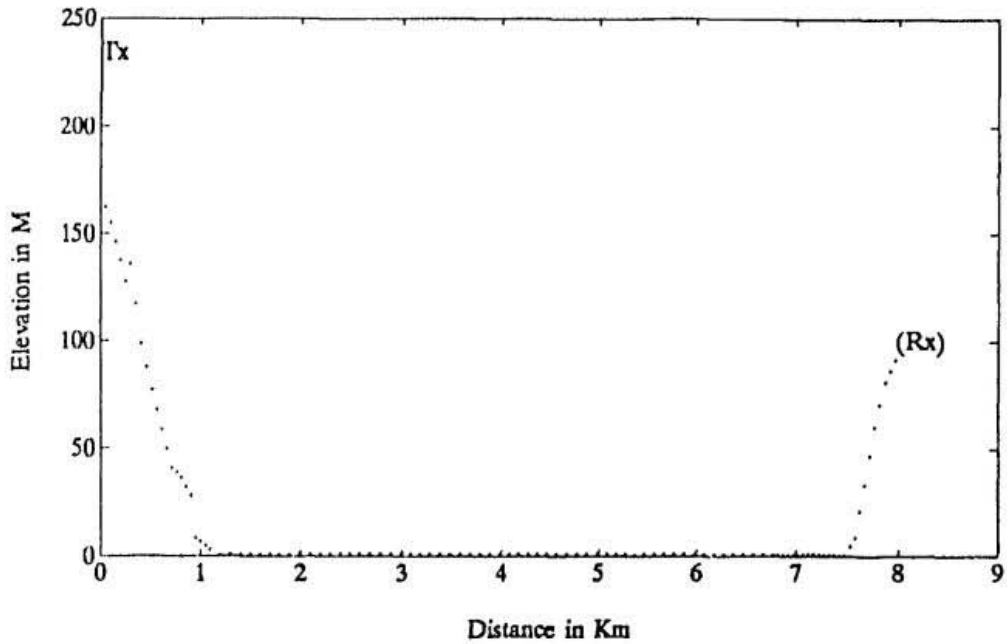

Figure 5.22: Modified Path Profile of Case 3

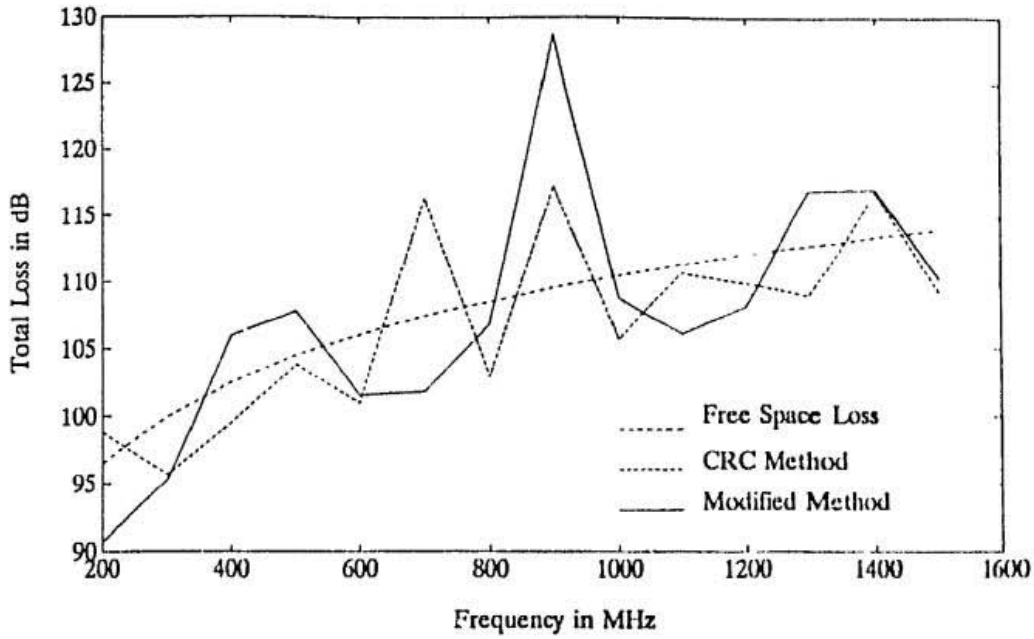

Figure 5.23: Total Losses vs. Frequency of Case 3

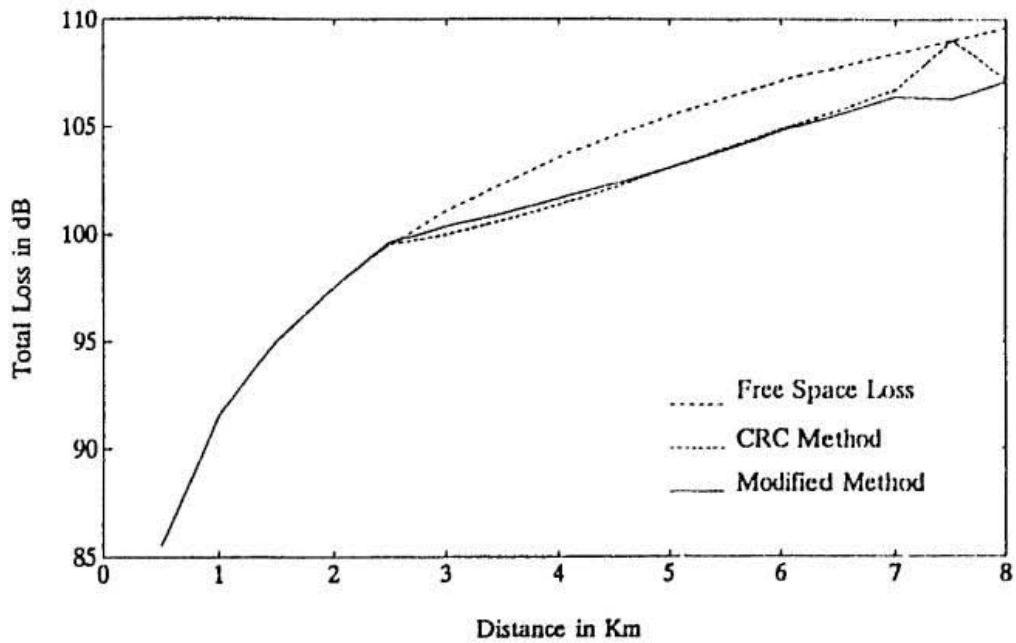

Figure 5.24: Total Losses vs. Distance of Case 3

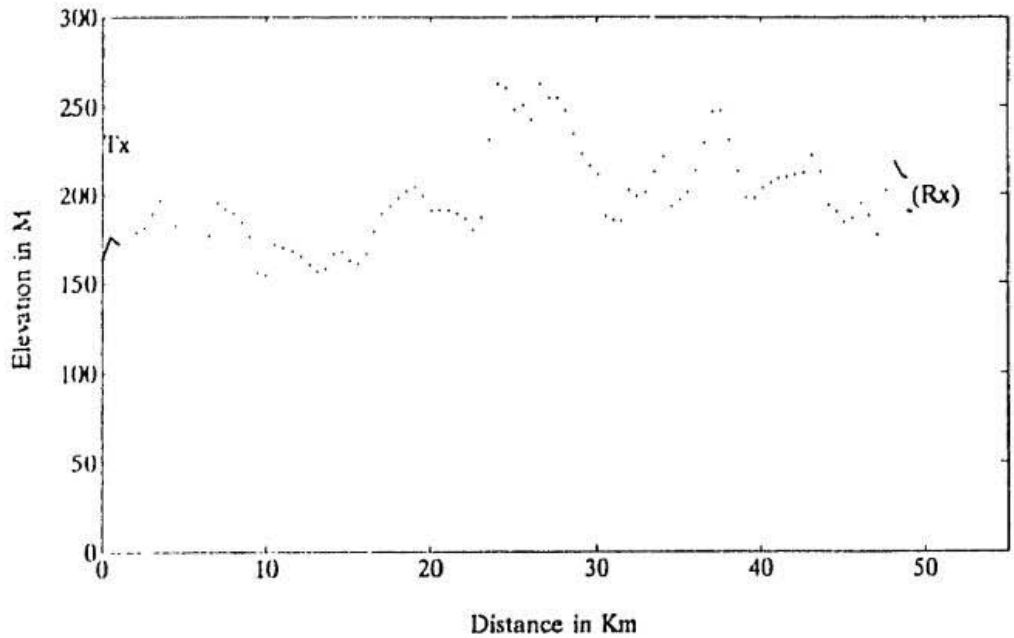

Figure 5.25: CRC Path Profile of Case 4

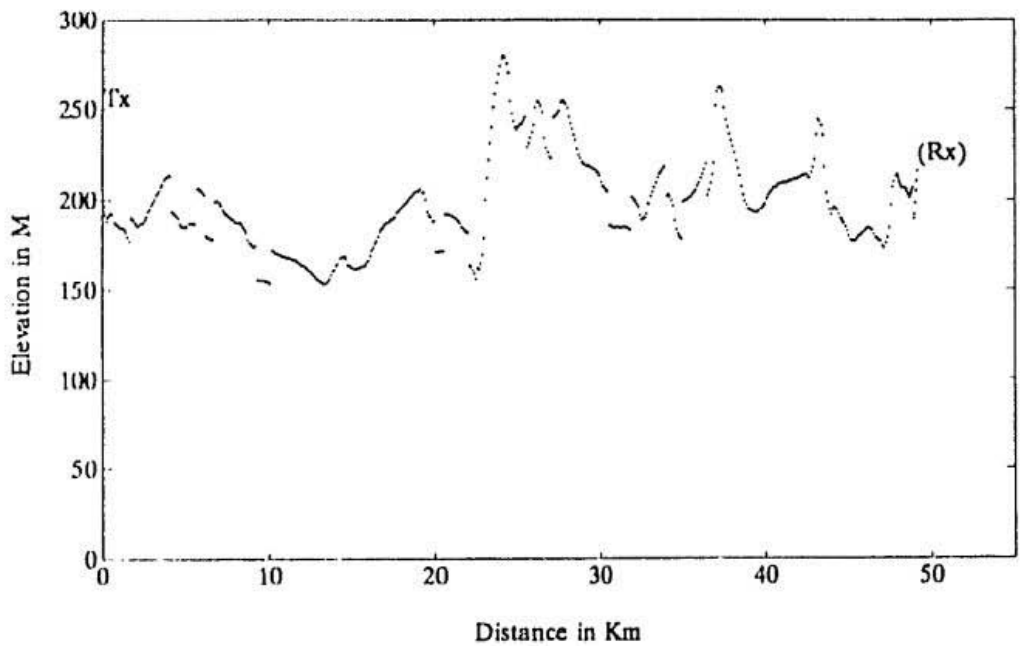

Figure 5.26: Modified Path Profile of Case 4

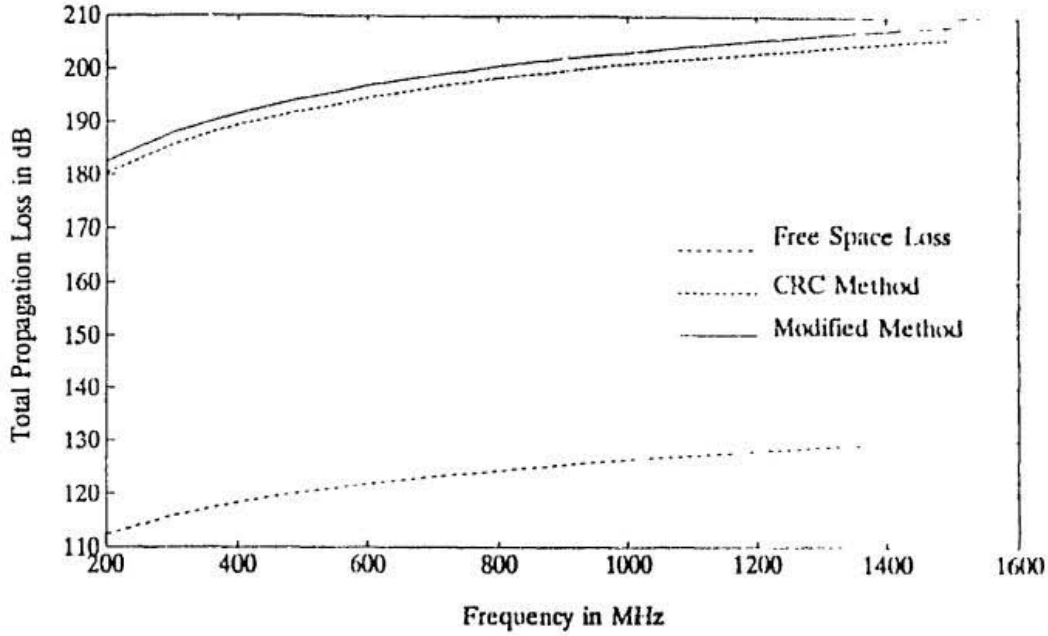

Figure 5.27: Total Losses vs. Frequency of Case 4

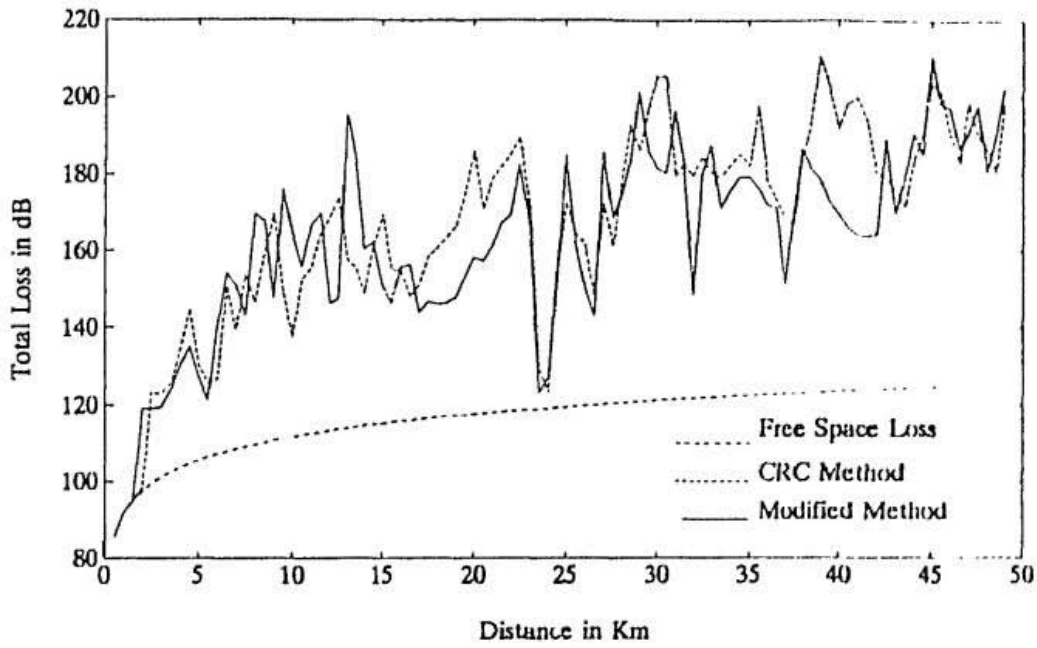

Figure 5.28: Total Losses vs. Distance of Case 4

at 47°34'20" latitude, 52°41'0" longitude, and R_x at 47°33'50" latitude, 52°45'20" longitude. This is a relatively short and regular terrain path in which urban loss and small diffraction loss are involved. The total losses versus frequency are shown in Fig. 5.31. They are almost the same. Fig.5.32 demonstrates the total losses against distance. It is clearly seen that the two results are almost the same due to the fact that the terrain is smooth and the 500 m spacing in CRC data base is sufficient.

The last case is an example of the signal coverage prediction. The transmitter is located at 47°35'20" latitude , 52°50'40" longitude which is the highest point available as the center of the coverage area of 15 Km radius. The transmitter power is 50 W and the omnidirectional transmitting antenna has a gain of 8 dBi. The transmission line losses in the transmitter and receiver are set to 2 dB. The receiving antenna is also omnidirectional and has a gain of 2.2 dBi. Fig. 5.33 shows the received signal voltage predicted by CRC method, and Fig. 5.34 shows the improved prediction result. In these figures, the sign '-' indicates the dead zone where the received signal is below the minimum specification. The sign '=' shows the area where the received signal level just barely meets the specification. The areas marked with the signs '+', '*', and '#' are the areas where the received signal strength is higher, much higher, and much much higher than the specification, respectively. Comparing these two results, in some area the signal predicted by the modified method is higher and in some area it is lower than that of CRC method. The maximum difference is about 28.8 dB at the location which 1.1 Km from the transmitter and 216° azimuth east.

Since the computer propagation loss prediction is completely based on the ter-

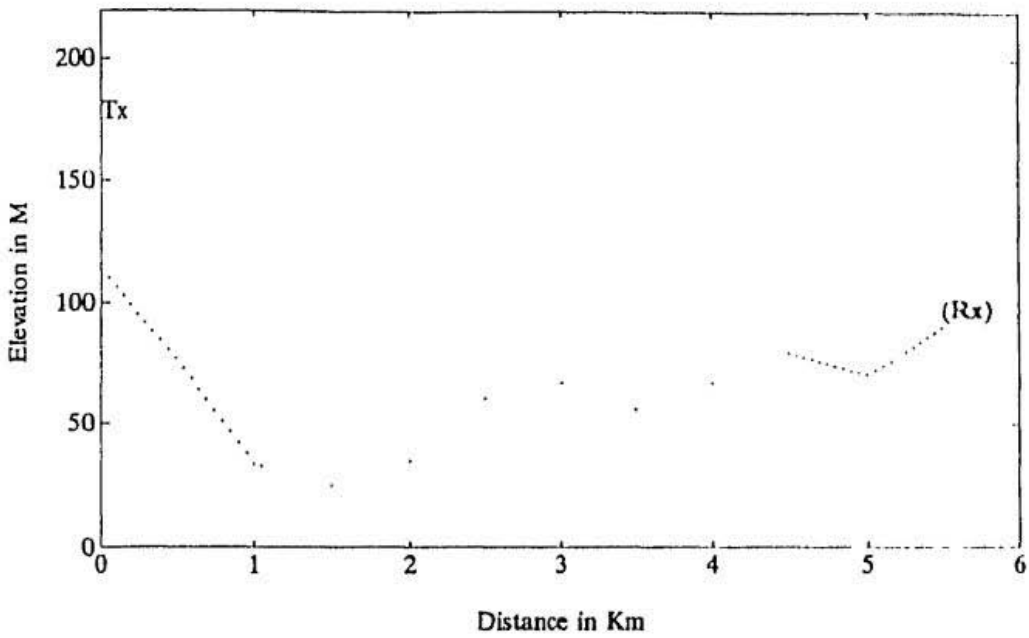

Figure 5.29: CRC Path Profile of Case 5

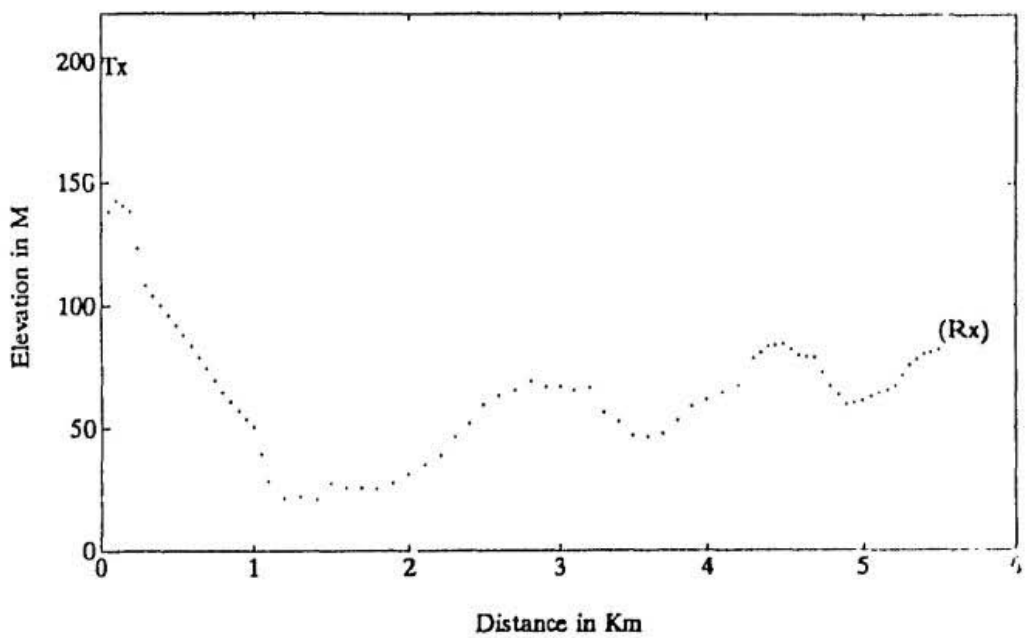

Figure 5.30: Modified Path Profile of Case 5

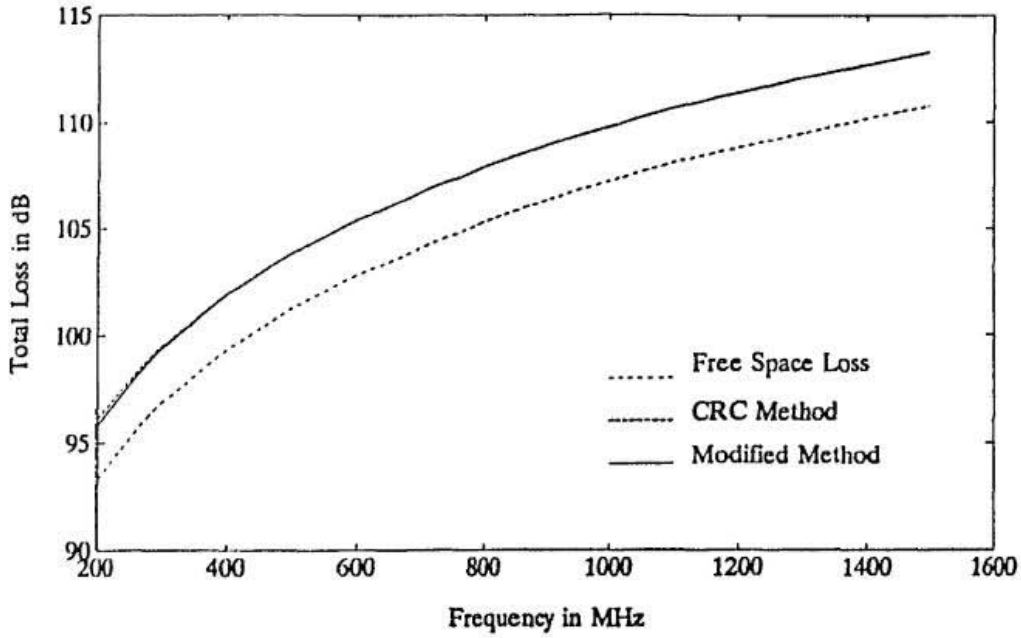

Figure 5.31: Total Losses vs. Frequency of Case 5

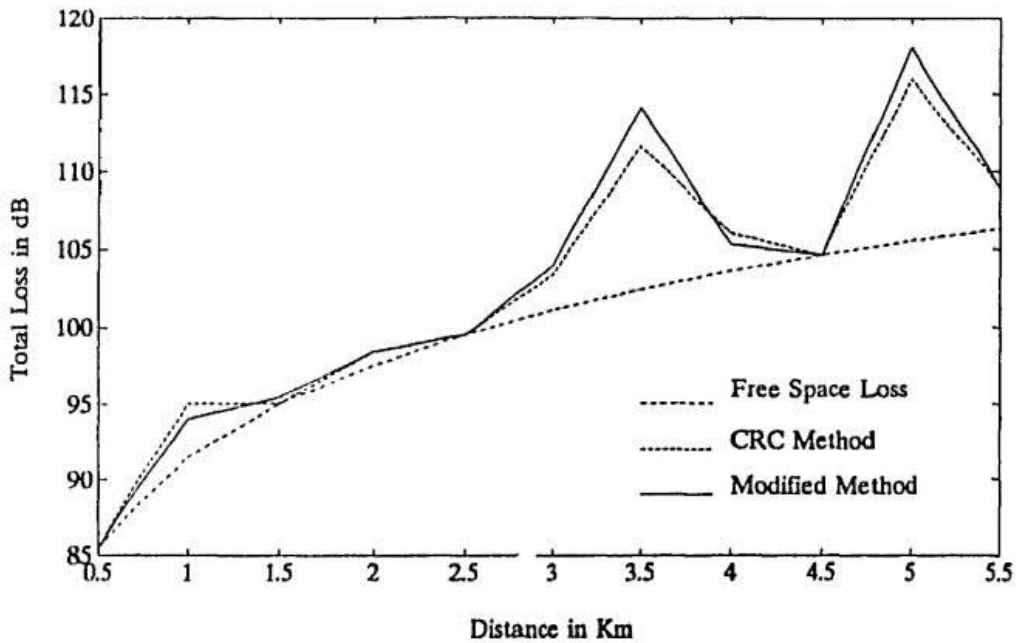

Figure 5.32: Total Losses vs. Distance of Case 5

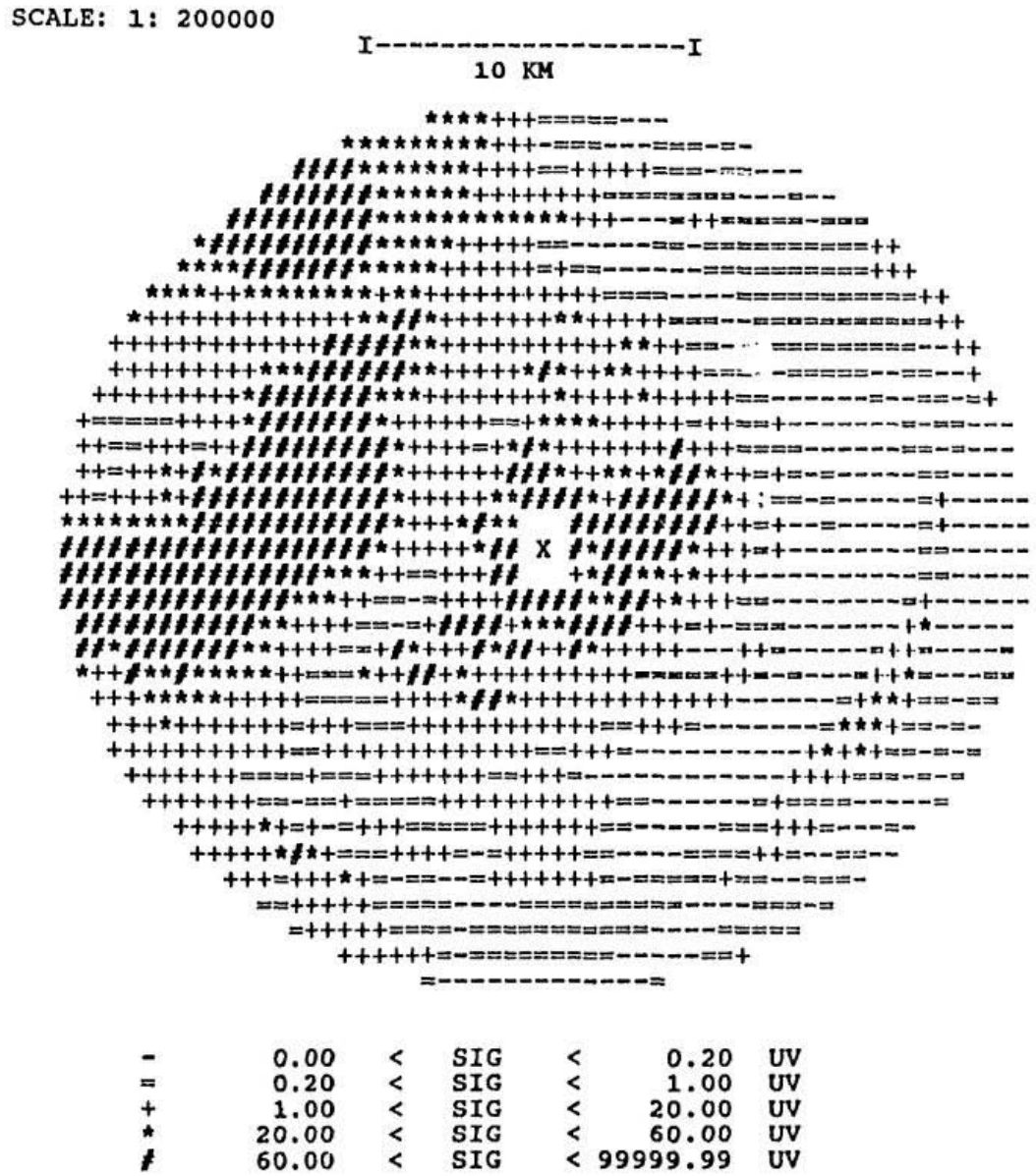

Figure 5.33: Signal Coverage Prediction by CRC Method

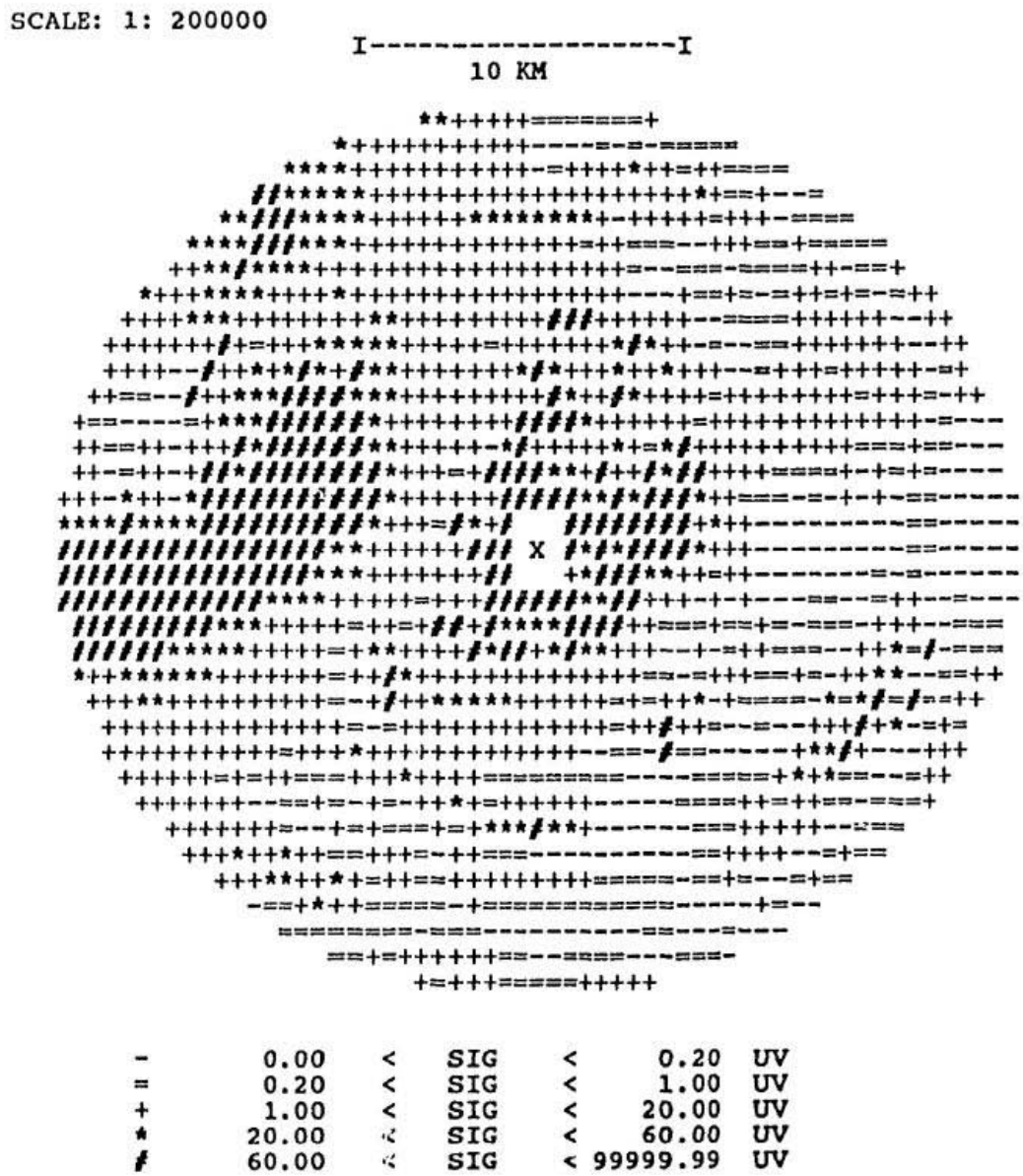

Figure 5.34: Signal Coverage Prediction by Modified Method

rain path profiles, more accurate profiles will produce more accurate results. In land mobile radio communications, diffraction mode is one of the main propagation modes, the improvement of the diffraction loss calculation will also increase the accuracy of total loss prediction. Therefore, the results of the modified prediction system should be more reliable.

Chapter 6

Conclusion and Recommendations

In land mobile radio communications, the propagation loss prediction is the central problem in the design and development of systems and networks as well as the planning of services. As the demand of mobile radio services rapidly increases such as in cellular systems, the cell is getting smaller and smaller, e.g. the micro-cell, to accommodate a larger number of subscribers. This is leading to the essential requirement that the propagation loss prediction must be more accurate. To improve the accuracy of the propagation loss prediction, In this thesis we have examined two major dependent parameters:

(i) the digital terrain data base;

(ii) the diffraction loss.

In the improvement of the terrain data base, we have proposed a procedure consisting of two steps. The first step is to augment CRC data base from 500 m spacing to 100 m spacing by using the complete quadratic method and the weighted vote method to interpolate elevations and surface codes. If our augmented data base is not checked with the actual important details of the topographic map,

we will proceed the second step. As discussed in chapter 3, in a smooth terrain the CRC data base and our results are agreed and are also checked with the actual topographic map. Of course, the second step is not required. However, in the rough terrain, the second step is then taken by reading critical points directly from the topographic map. These points are mostly the top of missed hill or the bottom of missed valley in the CRC and the augmented data base. In term of these important point data, the linear triangular method and the weighted vote method are used to correct the elevations and the surface codes, respectively. The second step will be repeated until the modified data base is checked with the actual topographic map. This high resolution and accurate data base provides a major contribution to the improvement of the propagation loss prediction which is an essential issue in land mobile communications. In addition, the accurate digitized map from this data base can also be used in many applications, such as the base station selection in cellular telephone networks, the site survey for microwave radio links, the earth station location and specially in any information and navigation systems, etc.. Generally speaking, the developed procedure can also be used to create any higher resolution data base from any other lower resolution data bases or even starting from the actual topographic map with an minimum effort in both time and labour.

For increasing the accuracy of diffraction loss prediction, the modified prediction method has been improved in three aspects: (a) the radius of curvature of the obstacle's crest; (b) the correction factor for the obstacles close to each other; (c) the number of obstacles considered in a path profile. On the other hand, since the diffraction loss prediction is entirely dependent on the terrain features, our modified path profiles have provided an essential tool to determine all parameters accurately.

Therefore, diffraction loss prediction is greatly improved.

Since the evaluations of reflection, urban, tropospheric scattering, and season losses are also dependent on the terrain features such as elevations and/or surface types, the modification of the terrain data base has provided the improvements to all these loss predictions. The CRC computer program prediction system has been modified to accept the modified data base and to construct the path profiles. It has also been modified to implement the improved diffraction loss prediction method and to calculate all the losses based on the modified path profiles. The improved total loss prediction results are presented in Chapter 5 by six studied cases. Case 1 showed generally that an usual path profile affects diffraction, tropospheric scattering, urban, season and clutter losses which form the total loss. Case 2 showed that for a short transmission path, the diffraction loss is a dominant component while in case 4, the tropospheric scattering is a dominant mode of propagation when the transmission path is relatively long. Case 3 showed the reflection mode is the dominant component when the earth surface is smooth such as water. In case 5, the terrain is regular, there is no significant difference between the CRC and our results. Case 6 is an example of the signal coverage prediction. It has been shown that our total propagation loss prediction result is rather close to the CRC result where the terrain is smooth, i.e. the path profiles are in a good agreement with each other. However, the difference of these two total loss prediction results is ranging from 3 dB to as much as 30 dB depending on how rough the terrain is. This discrepancy can well be explained by the terrain details missed in the CRC path profile with respect to our much more accurate path profile. For the future work, our results are supposed to be confirmed by the measured data.

Over all, by introducing a combination of various interpolation techniques, we have produced a high resolution and more accurate data base and path profiles. Coping with the modified diffraction loss prediction method leads to a major improvement of the total loss prediction. In consequence, our modified computer program prediction system will be a better tool in the design and development of land mobile radio systems and networks as well as the planning of services.

It is hoped that our research and investigation provide a more accurate result in the propagation loss prediction for the open and suburban areas. However, in the urban area where there are many buildings of various sizes, high population and most of all the great demand of radio telephone services, the urban loss prediction should be further improved. Researchers in Japan are developing a computer urban loss prediction system which employs a building data base [44]. This data base includes location and size of buildings. The theoretical prediction of urban loss is the future research direction, one may want to investigate.

Bibliography

[1] W.C.Y. Lee, *Mobile Communications Engineering*, McGraw-Hill, Inc., 1982.

[2] C. Burrows, *Radio propagation over plane earth - field strength curves*, Bell. Syst. Tech. J., 16, jan. 1937.

[3] J. Egli, *Radio propagation above 40 Mc over irregular terrain*, Proc. IRE, vol.45, pp. 1383-1391, 1957.

[4] J.P. Murphy, *Statistical propagation model for irregular terrain paths between transportable and mobile antennas*, AGARD Conf. Proc., no. 70, 1970, pp. 49-1-49-20.

[5] K. Allsebrook and J.D. Parsons, *Mobile radio propagation in British cities at frequencies in the VHF and UHF bands*, IEEE Trans. Veh. Technol., vol. VT-26, no. 4, pp. 313-323, 1977.

[6] Y. Okumura, E. Ohmori, T. Kawano, and K. Fukuda, *Field strength and its variability in VHF and UHF land-mobile radio-service*, Rev. Elec. Commun. Lab., vol. 16 no. 9-10, Sept.-Oct. 1968.

[7] M. Hata, *Empirical formula for propagation loss in land mobile radio services*, IEEE Trans. Veh. Technol., vol. VT-29, no. 3, pp. 317-325, 1980.

[8] K. Bullington, *Radio propagation at frequencies above 30 megacycles*, Proc.IRE, vol. 35,pp. 1122-1136, 1947.

[9] K. Bullington, *Radio propagation for vehicular communications*, IEEE Trans. Veh. Technol., VT-26, pp. 295-308, 1977.

[10] K.Furutsu, *On the theory of radio wave propagation over inhomogeneous earth*, J. Res. Nat. Bur. Stand., sec D, 67, pp. 39-62, 1963.

[11] G. Millington, R. Hewitt, and F.S. Immirzi, *Double knife-edge diffraction in field strength predictions*, Proc. Inst. Elec. Eng. Monogr., 507E. pp. 419-429, 1962.

[12] S.W. Lee, *Path integrals for solving some eletromagnetic edge diffraction problems*, J. Math. Phys., vol. 19, pp. 1414-1422, 1978.

[13] J.H. Whitteker,, *Near-field ray calculation for multiple knife-edge diffraction*, Radio Sci., vol. 19, pp. 975-986, 1984.

[14] G.A. Hufford, A.G. Longley, and W.A. Kissick, *A guide to the use of the ITS irregular terrain model in the area prediction mode*, NTIA Rep. 82-100, Apr. 1982.

[15] G.A. Hufford, *Memorandum to users of the ITS irregular terrain model*, Jan. 30, 1985.

[16] *Coverage Prediction for Mobile Radio Systems Operating in th 800/900 MHz Frequenct Range*, IEEE Vehicular Technology Society Committee on Radio Propagation, IEEE Trans. on Vehicular Technology, Vol. 37, No. 1, Feb. 1988.

[17] A.G. Longley, *Local variability of transmission loss-land mobile and broadcast systems*, OT Rep., May 1976.

[18] *Master Propagation System (MPS11); User's Manual.* (User's Manual available from NTIS under no. NTIS-PB83-178624. Computer program tape available under No. NTIS-PB83-173971.)

[19] A.G. Longley and P.K. Reasoner, *Comparison of propagation measurements with predicted values in the 20 to 10,000 MHz range*, ESSA Tech. Rep. ERL 148-ITS 97, Jan. 1970.

[20] J.F. Aurand and R.E. Post, *A comparison of prediction methods for 800 MHz mobile radio propagation*, IEEE Trans. Veh. Technol., vol. VT-34, No. 4, Nov. 1985.

[21] F.H. Palmer *The Communications Research Centre VHF/UHF propagation prediction program: an overview*, Can. Elec. Eng. J. Vol. 6, No. 4, 1981

[22] J.H. Whitteker,*Users guide to the C.R.C. VHF UHF propagation prediction program*, Communications Research Centre, Nov. 1990.

[23] H.L. Bertoni and J. Walfisch, *A theoretical model of UHF propagation in urban environments*, IEEE Trans. Antennas Propagat., vol. 36, pp. 1788-1796, 1988.

[24] S.Y. Seidel and T.S. Rappaport, *914 MHz Path loss prediction models for indoor wireless communications in multifloored buildings*, IEEE Trans. Antennas Propagat., Vol. 40, No.2, pp. 207-217, Feb. 1992.

[25] R.F. White, *Engineering Considerations for Microwave Communications Systems*, GET Lenkurt Incorporated, San Carlos, California, 1972.

[26] J.H. Whitteker, *Radio-wave Reflections from a Spherical Earth - Predictions at VHF and UHF*, CRC Technical Note No. 715, Nov. 1982, Ottawa.

[27] M.P.M. Hall, *Effects of the Troposphere on Radio Communication*, IEE Electromagnetic Wave Series 8, 1979.

[28] P. Beckmann and A. Spizzichino, *The Scattering of Electromagnetic Waves from Rough Surfaces*, Pergamon Press, Oxford, 1963.

[29] P.L. Rice, A.G. Longley, K.A. Norton and A.P. Barsis, *Transmission Loss Predictions for Tropospheric Communication Circuits*, NBS Technical Not 101, May 7, 1965.

[30] *CRC VHF/UHF Propagation Loss Prediction Programme*, CRC, Ottawa, Nov. 1990.

[31] J. Epstein and D.W. Peterson, *An experimental study of wave propagation at 850MC*, Proc. IRE, vol. 41, pp. 595-611, 1953.

[32] *Atlas of radio wave propagation curves for frequencies between 30 and 10000Mc/s*, Radio Research Laboratory, Ministry of Postal Services, Tokyo, Japan, pp. 172-179, 1957.

[33] J. Deygout, *Multiple Knife-edge diffraction of Microwaves*, IEEE Trans. Antennas Propagat., vol. 14, pp. 480-489, 1966.

[34] R.J. Holbeche, *Land Mobile Radio Systems*, Peter Peregrinus Ltd., 1985.

[35] M.S.de Assis, *A Simplified Solution to the Problem of Multiple Diffraction over Rounded Obstacles*, IEEE Trans. Antennas Propagat., Mar. 1971.

[36] P.L. Rice, *Some Effects of Building and Vegetation on VHF/UHF Propagation*, 1971 IEEE Mountain-West Electromagnetic Compatibility: Conference Record.

[37] T. Martin and Decker, *Private Communication.*

[38] F.H Palmer, *Report on the Great Lakes Propagation Measurement Program: Comparisons of the Canadian Data with the Predictions of FCC R-6602*, CRC Report No. 1332, Ottawa, Feb. 1980.

[39] A.G. Longley, *Location Variability of Transmission Loss - Land Mobile and Broadcat Systems*, OT Report 76-87 NTIS, May 1976.

[40] CCIR Report 239, Vol V .

[41] J.H. Whitteker, *The CRC Tropographic Data Base*, CRC Report No. 1353, Ottawa, Feb. 1982.

[42] J.H. Whitteker, *Users Guide To The CRC Tropographic Data Base*, CRC, Ottawa, Nov. 1990.

[43] J. Deygout, *Correction Factor for Multiple Knife-Edge Diffraction*, IEEE Trans. Antennas Propagat., vol. 39, no. 8, Aug. 1991.

[44] F. Ikegami, T. Takeuchi, and S. Yoshida, *Theoretical Prediction of Mean Field Strength for Urban Mobile Radio*, IEEE Trans. Antennas Propagat., vol. 39, no. 3, Mar. 1991.